Hamiltonian Dynamical Systems and Transport in a Coupled Standard Map

Sacha Carl BLUMEN, B.A. (UQ), A.Mus.A.
The Department of Mathematics
The University of Queensland
Qld. 4072, Australia.

Honours Thesis

Supervisor: Dr. C.A. Holmes.

November 17, 1997

Contents

List of Figures

Acknowledgement

I would like to acknowledge the constant support and faith of my supervisor, Dr. Cathy Holmes, in my work this year. I would like to thank the other Honours students for making the year a pleasant and stimulating one, and my family and friends for their encouragement.

Abstract

We review the theory associated with Hamiltonian (conservative) dynamical systems, and examine the transition to chaos in the standard (Chirikov-Taylor) map. Coupling together two standard maps, we obtain a two degree of freedom map which models the interaction of a laser with atoms in a magneto-optical trap. We analyse the affect of the coupling on the structure of the four dimensional phase space by examining the relationship between the coupling and the rate of transport through the phase space for a collection of trajectories. Numerical calculations confirm that an approximate power law relationship exists between the rates of the transport of collections of trajectories through phase space and the value of the coupling parameter.

The Arnol'd diffusion rate in our two degree of freedom map is calculated analytically and investigated numerically using the stochastic pump model of Lieberman [14]. Generally the rate of Arnol'd diffusion is much smaller than other forms of diffusion. In our two degree of freedom map the rate of Arnol'd diffusion is very low. For small stochasticity analytical results suggest it is much lower than in the coupled map considered by Froschle, Wang, and Wood [4, 5, 26, 27].

Chapter 1

Introduction

Sparked by the famous paper of Lorenz on numerical simulations of simplified fluid mechanics equations in the 1960's [15], the phenomenon of *chaos* has been studied in detail for several decades, and knowledge of its existence and effects has seeped into the general public's imagination.

Chaos has, of course, a well defined and precise meaning, and Arnol'd [1], Ruelle [24], and Scott [25] amongst others have examined chaos in dissipative systems. Chaos in Hamiltonian (conservative) systems has recieved its fair share of attention, with work undertaken by Dewar [3], Kolmogorov [10], MacKay [16], and Reichl [21] amongst others.

In this thesis we are concerned with investigating a Hamiltonian dynamical system: a model of the interaction of atoms with lasers in a magneto-optical trap. The equations that model this interaction are four coupled difference equations that may be obtained by coupling together two *standard maps.*

The standard map has been extensively studied [2, 13, 20, 21, 28], as has the coupled standard map introduced by Froschle [4, 5]. Knowledge of the standard map itself simplifies the analysis of the four dimensional coupled map. The coupling we consider is different from that considered by Froschle leading to some similar behaviour but also significant differences in the dynamics.

Our analysis starts in Chapter 2 with an introduction to Hamiltonian dynamics: starting with an identity and the variational principle we derive the Euler-Lagrange equations of motion and the Lagrangian. From the Lagrangian we derive the Hamiltonian, and Hamilton's equations of motion, and investigate aspects of Hamiltonian dynamics that makes it preferable to other formulations of dynamics.

We then proceed to investigate a special class of Hamiltonian dynamical systems: integrable systems, and their ability to undergo a transformation to a set of coordinates in which the description of their dynamics is particularly simple.

We then investigate a sub-class of dynamical systems: discrete time systems, or mappings. We examine the general classes of area preserving, twist, and perturbed twist maps, leading to the standard map. We review some of the work conducted on the standard map.

Examination of the standard map naturally leads to consideration of the celebrated KAM theorem (after Kolmogorov, Arnol'd, and Moser). We examine some supplementary number theory and converse KAM theory.

After this exhaustive review of the theory of Hamiltonian dynamical systems in general, and the standard map in particular, we introduce our four dimensional map that models the interaction of a laser with atoms in a magneto-optical trap.

The construction of this model reflects the current worldwide interest and research into the trapping and cooling of atoms and ions, a large part of which is directed to the study of mesoscopic manifestations of quantum effects. An introduction to the trapping and cooling of atoms in a magneto-optical trap may be found in Milburn [18].

There are any number of aspects of this four dimensional map that could be investigated: periodic orbits, the existence of two dimensional KAM tori, and rates of the transport of orbits through the four dimensional phase space are but a few of the possibilities for research. In Chapter 4 we focus on the relationship between rates of transport of collections of orbits through the phase space and various values of two parameters - the stochasticity parameter K and the coupling parameter b. We find what appears to be an excellent relationship between rates of transport through the phase space and b for each value of K.

In Chapter 5 we investigate Arnol'd diffusion, a form of transport through the phase space available to orbits in dynamical systems with more than two degrees of freedom. Arnol'd diffusion has been the subject of recent research, and we examine one research methodology, the stochastic pump model, and apply it, analytically, and numerically, to our map. It appears that Arnol'd diffusion is dramatically reduced for symmetric coupling of the form that occurs naturally through the modes of a trapped atom. Arnol'd diffusion is negligible compared to other forms of transport through the phase space and we may be able to ignore it.

Much of my understanding of this area, and of the work in this thesis, is attributable to Lieberman ad Lichtenberg [13], Reichl [21], an Honours thesis on a theoretical topic related to this thesis by Robins [22], and Zaslavsky et al [28]. Thanks go to my supervisor, Dr. Cathy Holmes, for her patience while the slow beginnings of awareness began to dimly illuminate my mind on the area of chaos in Hamiltonian dynamics.

Much of the value of this thesis lies in its drawing together of aspects of dynamics and chaos from various sources. While most of the work in Chapters 2 and 3 may be found in the cited sources, the material in Chapters 4 and 5 is original work based on the papers and works cited. This original work adds to our understanding of four dimensional maps and our four dimensional map in particular. Other items of note are my formulation of a more general statement of a theorem in expressions 2.67 and 2.68, the statement and proof of the Brouwer Fixed Point theorem (thus explicitly proving that every twist map has a fixed point), and the derivation of the Standard map with two different dynamical systems.

Our coupled map has only appeared recently in the literature [11], with respect to quantum behaviour. We consider the map with regards to classical behaviour. While the more commonly studied map of Froschle [4, 5, 8, 21, 22, 26, 27] models the time evolution of elliptic galaxies, our coupled map is of current interest in physics as it models the behaviour of atoms under laser forcing. We undertake original work on this map to determine the properties of transport through the four dimensional phase space under the forcing of the laser.

Chapter 2

Preliminaries

We start our work by giving an overview of Hamiltonian dynamical systems. We show how the Euler-Lagange equations can be derived from an identity and the variational principle, we proceed on through a discussion of Hamiltonian systems, canonical transformations, phase space, integrable systems, and Action-Angle variables, and introduce maps: discrete time dynamical systems. This Chapter draws together work from a large number of sources [7, 21, 22, 13].

2.1 Derivation of the Euler-Lagrange equations

In this section we explicitly derive the Euler-Lagrange equations of motion from a variational principle, from Goldstein [7].

The Euler-Lagrange equations of motion are derived from a variational principle: we take the state of the system at a particular time and cause a virtual, or infinitesimal, displacement of the system as a result of an arbitrary infinitesimal change of the co-ordinates δr consistent with the forces and constraints imposed on the system at time t, keeping t constant.

We begin with the identity

$$F_i = \dot{p}_i, \tag{2.1}$$

where F_i is the ith component of the force and p_i is the ith component of the momentum. Equation 2.1 may be rewritten

$$F_i - \dot{p}_i = 0. \tag{2.2}$$

For a system in equilibrium, the virtual work is identically 0

$$F_i.\delta r_i = 0, \tag{2.3}$$

which implies that

$$\sum_i F_i.\delta r_i = 0. \tag{2.4}$$

We have

$$(F_i - \dot{p}_i).\delta r_i = 0, \tag{2.5}$$

which implies that

$$\sum_i (F_i - \dot{p}_i).\delta r_i = 0. \tag{2.6}$$

We separate the applied and constraining forces

$$\sum_i (F_i^{app} - \dot{p}_i).\delta r_i + \sum_i F_i^{con}.\delta r_i = 0, \tag{2.7}$$

and only consider systems for which the virtual work of the forces of constraint vanish, and arrive at D'Alembert's principle:

$$\sum_i (F_i^{app} - \dot{p}_i).\delta r_i = 0. \tag{2.8}$$

Now we change from δr co-ordinates to generalised δq co-ordinates so that the virtual displacements of the generalised co-ordinates, δq^i, are independent, and we will have i independent expressions as follows

$$r_i = r_i(q^1, q^2, \ldots, q^n, t), \tag{2.9}$$

$$\delta r_i = \sum_j \frac{\partial r_i}{\partial q^j} \delta q^j. \tag{2.10}$$

We have the identity $v_i \equiv \dot{r}_i$, and thus

$$v_i = \sum_i \frac{\partial r_i}{\partial q^j} \dot{q}^j + \frac{\partial r_i}{\partial t}, \tag{2.11}$$

and the virtual work is

$$\sum_i F_i.\delta r_i = \sum_{i,j} F_i.\frac{\partial r_i}{\partial q^j} \delta q^j. \tag{2.12}$$

Defining Q^j to be the independent components of the generalised forces

$$Q^j = \sum_i F_i.\frac{\partial r_i}{\partial q^j}, \tag{2.13}$$

the virtual work becomes

$$\sum_i F_i.\delta r_i = \sum_j Q^j \delta q^j, \tag{2.14}$$

and given the following identity

$$\sum_i \dot{p}_i.\delta r_i = \sum_i m_i \ddot{x}_i.\delta r_i, \tag{2.15}$$

and expressing δr_i in terms of δq^j's, we obtain

$$\sum_i \dot{p}_i.\delta r_i = \sum_{i,j} m_i \ddot{x}_i.\frac{\partial r_i}{\partial q^j}\delta q^j. \tag{2.16}$$

Replacing the x_i's with r_i's we have

$$\sum_i m_i \ddot{r}_i.\frac{\partial r_i}{\partial q^j} = \sum_i \left(\frac{d}{dt}\left(m_i \dot{r}_i.\frac{\partial r_i}{\partial q^j}\right) - m_i \dot{r}_i.\frac{d}{dt}\left(\frac{\partial r_i}{\partial q^j}\right)\right), \tag{2.17}$$

then

$$\frac{\partial v_i}{\partial q^j} = \frac{d}{dt}\frac{\partial r_i}{\partial q^j} = \sum_k \frac{\partial^2 r_i}{\partial q^j \partial q^k}\dot{q^k} + \frac{\partial^2 r_i}{\partial q^j \partial t}, \tag{2.18}$$

and we have

$$\sum_i m_i \ddot{r}_i.\frac{\partial r_i}{\partial q^j} \equiv \sum_i \left(\frac{d}{dt}\left(m_i v_i.\frac{\partial v_i}{\partial \dot{q^j}}\right) - m_i v_i.\frac{\partial v_i}{\partial q^j}\right), \tag{2.19}$$

which implies

$$\sum_j \frac{d}{dt}\left(\frac{\partial}{\partial \dot{q^i}}\left(\sum_i \frac{1}{2} m_i v_i^2\right) - \frac{\partial}{\partial q^i}\left(\sum_i \frac{1}{2} m_i v_i^2\right)\right).\delta q^j = 0. \tag{2.20}$$

Associating the term $\sum_i \frac{1}{2} m_i v_i^2$ with the kinetic energy

$$T = \sum_i \frac{1}{2} m_i v_i^2, \tag{2.21}$$

our equation becomes

$$\sum_j \left(\left(\frac{d}{dt}\frac{\partial T}{\partial \dot{q^j}} - \frac{\partial T}{\partial q^j}\right) - Q^j\right)\delta q^j = 0. \tag{2.22}$$

Any virtual displacement δq^j is independent of δq^k, and the separate coefficients will vanish, that is, the δq^i's are independent, and we have n separate equations where n is the number of generalised co-ordinates:

$$\Rightarrow \frac{d}{dt}\left(\frac{\partial T}{\partial \dot{q^j}}\right) - \frac{\partial T}{\partial q^j} = Q^j. \tag{2.23}$$

Now assuming that the force $\mathbf{F}$ is conservative, that is, there exists a scalar potential Φ such that

$$\mathbf{F} = -\nabla\Phi, \tag{2.24}$$

we have

$$Q^j = \sum_i F_i . \frac{\partial r_i}{\partial q^j} = -\sum_i \nabla_i \Phi . \frac{\partial r_i}{\partial q^j}, \tag{2.25}$$

$$Q^j = -\frac{\partial \Phi}{\partial q^j}, \tag{2.26}$$

$$\frac{d}{dt}\left(\frac{\partial T}{\partial \dot{q}^j}\right) - \frac{\partial (T-\Phi)}{\partial q^j} = 0. \tag{2.27}$$

Φ is a function of position and not velocity, and thus

$$\frac{d}{dt}\left(\frac{\partial (T-\Phi)}{\partial \dot{q}^j}\right) - \frac{\partial (T-\Phi)}{\partial q^j} = 0. \tag{2.28}$$

We define the Lagrangian L

$$L = T - \Phi, \tag{2.29}$$

and thus arrive at the Euler-Lagrange equations

$$\frac{d}{dt}\left(\frac{\partial L}{\partial \dot{q}^j}\right) - \frac{\partial L}{\partial q^j} = 0. \tag{2.30}$$

As an example, let us examine a one degree of freedom system in which the potential is $\Phi(q) = -Bq^2 + q^4$, and the kinetic energy T is given by the usual formula $T = \sum_i \frac{1}{2} m (\dot{q}^i)^2$, where q is the position, $\dot{q}$ is the velocity, m is the mass of the particle, and B is a positive constant. This is a system which corresponds to the motion of a particle in a double well potential. The Lagrangian is

$$L = T + 2Bq - 4q^3, \tag{2.31}$$

and the Euler-Lagrange equations become

$$\frac{d}{dt}(m\dot{q}) - (2Bq - 4q^3) = 0, \tag{2.32}$$

or

$$m\ddot{q} = 2q(B - 2q^2). \tag{2.33}$$

2.2 Hamilton's equations of motion

The Hamiltonian formulation of a problem is often desirable as its representation in the appropriate phase space is volume preserving under evolution of the system; that is, a particular volume of the phase space will evolve into another region of the phase space with identical volume. In this section we draw on material in [7, 13, 22].

A Hamiltonian system with N degrees of freedom may be represented by a twice differentiable, real valued scalar function of N configuration co-ordinates and N conjugate momentum co-ordinates and possibly time. A Hamiltonian which is not dependent on time

$$H = H(p_1, p_2, \ldots, p_N, q^1, q^2, \ldots, q^N), \tag{2.34}$$

is said to be autonomous while one which is dependent on time

$$H = H(p_1, p_2, \ldots, p_N, q^1, q^2, \ldots, q^N, t), \tag{2.35}$$

is correspondingly non-autonomous.

We can define the Hamiltonian, given the Lagrangian, as follows

$$H(p, q, t) = \sum_i \dot{q^i} p_i - L(\dot{q}, q, t), \tag{2.36}$$

where $\dot{q} = f(q, p)$, then

$$dH = \sum_i \frac{\partial H}{\partial q^i} dq^i + \sum_i \frac{\partial H}{\partial p_i} dp_i + \frac{\partial H}{\partial t} dt,$$

$$= \sum_i \left(p_i - \frac{\partial L}{\partial \dot{q^i}} \right) d\dot{q^i} + \sum_i \dot{q^i} dp_i - \sum_i \left(\frac{d}{dt} \right) \frac{\partial L}{\partial \dot{q^i}} - \frac{\partial L}{\partial t} dt. \tag{2.37}$$

Setting

$$p_i = \frac{\partial L}{\partial \dot{q^i}}, \tag{2.38}$$

we have

$$\dot{p_i} = -\frac{\partial H}{\partial q^i}; \dot{q^i} = \frac{\partial H}{\partial p_i}, \tag{2.39}$$

where p_i and q^i are the sets of generalised momentum and position co-ordinates.

It is interesting to note that we can find a particle's trajectory in phase space by Hamilton's principle:

Defining the action S as a functional on trajectories in phase space $(p(t), q(t))$, by

$$S = \int_{t_0}^{t_1} [p.\dot{q} - H(p, q, t)]dt, \tag{2.40}$$

where $t_0 \leq t \leq t_1$, and $q(t_0), q(t_1)$ are given, Hamilton's principle states that the true path taken by a trajectory in phase space is the path that makes S stationary:

$$\delta S = \int_{t_0}^{t_1} [\delta p.\dot{q} + p.\delta\dot{q} - \frac{\partial H}{\partial p}.\delta p - \frac{\partial H}{\partial q}.\delta q]dt = 0. \tag{2.41}$$

We can show that the representation of the evolution of the Hamiltonian system in phase space is volume preserving by Liouville's Theorem.

Theorem 2.1 Preservation of Phase-Space volumes in Hamiltonian systems

Given that a flow Ξ_t is a one parameter group of transformations of phase space

$$\Xi_t : (p(0), q(0)) \to (p(t), q(t)), \tag{2.42}$$

where $p(t)$ and $q(t)$ are solutions of the differential equation $\dot{\xi} = \zeta(\xi)$ from the initial conditions $p(0), q(0)$, and given that $v(t, \mathcal{A})$ is the volume of the image of $\Xi_t(\mathcal{A})$, where $\mathcal{A}$ is a volume in phase space, then if $\mathrm{div}\zeta = 0, \Xi_t$ preserves volume for all t, that is $v(t_\alpha, \mathcal{A}) = v(t_\beta, \mathcal{A})$ for all $\alpha, \beta \in \mathbb{R}$.

For a Hamiltonian system

$$\mathrm{div}\zeta(\xi) = \sum_{n=1}^{N} \left(\frac{\partial}{\partial q^i} \left(\frac{\partial H}{\partial p_i} \right) - \frac{\partial}{\partial p_i} \left(\frac{\partial H}{\partial q^i} \right) \right) \equiv 0, \tag{2.43}$$

and the conditions for Liouville's theorem are satisfied; thus we have preservation of phase space volume under evolution of the system.

2.3 Canonical Transformations

A canonical transformation is a transformation from one set of generalised canonical co-ordinates (p, q), to another set of generalised canonical co-ordinates (P, Q) such that Hamilton's equations of motion (equation 2.39), are satisfied and volumes under the transformation are maintained. In this section we draw on material from [13].

If we initially take the Hamiltonian and Hamilton's equations of motion with generalised co-ordinates (p, q)

$$H = H(p, q), \tag{2.44}$$

$$\dot{q^i} = \frac{\partial H}{\partial p_i}, \dot{p_i} = -\frac{\partial H}{\partial q^i}, \tag{2.45}$$

and make a canonical transformation to the generalised co-ordinates (P, Q), where

$$P = P(p, q), Q = Q(p, q), \tag{2.46}$$

and where the determinant of the Jacobian is unity (that is, volumes are preserved under the transformation)

$$\begin{vmatrix} \frac{\partial P}{\partial p} & \frac{\partial P}{\partial q} \\ \frac{\partial Q}{\partial p} & \frac{\partial Q}{\partial q} \end{vmatrix} = 1,$$

or,

$$\frac{\partial P}{\partial p}\frac{\partial Q}{\partial q} - \frac{\partial P}{\partial q}\frac{\partial Q}{\partial p} = 1, \tag{2.47}$$

then the flow is area-preserving upon transformation from (p, q) co-ordinates to (P, Q) co-ordinates, and we have satisfied Hamilton's equations of motion:

$$\mathbf{H} = \mathbf{H}(P, Q), \tag{2.48}$$

$$\dot{Q^i} = \frac{\partial \mathbf{H}}{\partial P_i}, \dot{P_i} = -\frac{\partial \mathbf{H}}{\partial Q^i}. \tag{2.49}$$

While there is no mathematical reason to prefer any set of canonical co-ordinates to any other, analysis of Hamiltonian systems may be simplified by use of carefully chosen sets of pairs of canonical co-ordinates, one of the most common and useful pairs being Action-Angle co-ordinates. We will examine Action-Angle co-ordinates as a system of co-ordinates in which the analysis of dynamical systems may be particularly simplified in a succeeding section.

2.4 Generating Functions

We can make a canonical transformation between two sets of generalised canonical co-ordinates by means of a generating function [13]. As an example, let us take a Hamiltonian in one set of generalised momentum and position co-ordinates (p, q) and transform it to a Hamiltonian in another set of canonically conjugate co-ordinates (P, Q).

Taking the Lagrangian as

$$L(\dot{q}, q, t) = \sum_i \dot{q^i} p_i - H(p, q, t), \tag{2.50}$$

we have (by the variational principle)

$$\delta \int_{t_1}^{t_2} \left(\sum_i \dot{q^i} p_i - H(p,q,t) \right) dt = 0, \tag{2.51}$$

which is true for the Hamiltonian in either (p,q) or (P,Q) generalised co-ordinates. If we equate equation 2.51 for the two sets of generalised co-ordinates, the integrands must differ by at most a complete differential, thus

$$\sum_i p_i \dot{q^i} - H(p,q,t) = \sum_i P_i \dot{Q^i} - \mathbf{H}(P,Q,t) + \frac{d}{dt} F_1(q,Q,t), \tag{2.52}$$

where $F_1 = F_1(q,Q)$ is an arbitrary function of an 'old' and 'new' generalised position co-ordinates.

We have

$$\frac{d}{dt} F_i = \sum_i \frac{\partial F_1}{\partial \dot{q^i}} \frac{dq^i}{dt} + \sum_i \frac{\partial F_1}{\partial Q^i} \frac{d\dot{Q^i}}{dt} + \frac{\partial F_1}{\partial t}. \tag{2.53}$$

and taking

$$p_i = \frac{\partial F_1}{\partial q^i}, P_i = -\frac{\partial F_1}{\partial Q^i}, \tag{2.54}$$

we obtain

$$\mathbf{H}(P,Q,t) = H(p,q,t) + \frac{\partial}{\partial t} F_1(q,Q,t). \tag{2.55}$$

We can also define other generating functions as functions of pairs of other 'old' and 'new' co-ordinates

$$F_2 = F_2(q,P,t), \tag{2.56}$$

$$F_3 = F_3(p,Q,t), \tag{2.57}$$

$$F_4 = F_4(p,P,t). \tag{2.58}$$

2.5 Canonical transformations from non-autonomous to autonomous Hamiltonians

A feature of the representation of an autonomous Hamiltonian with N degrees of freedom in a $2N$ dimensional phase space is that trajectories do not cross (in addition to the preservation of phase-space volumes under evolution of the system). We

find that in the general case of a non-autonomous Hamiltonian with N degrees of freedom, trajectories may intersect in the $2N$ dimensional phase space. This complicates our analysis and in general negates the aspect of Hamiltonian systems of the preservation of phase space volumes under evolution of the system.

We are thus motivated to find a formulation of the original system in which trajectories do not intersect, that is, we wish to find an autonomous Hamiltonian equivalent to any certain non-autonomous Hamiltonian. If we can make such a transformation, then we need only ever consider autonomous Hamiltonians in analysing Hamiltonian dynamical systems. In this section we draw on material from [13, 20].

Given a non-autonomous Hamiltonian, we can make a canonical transformation to an autonomous Hamiltonian in the following manner. We integrate equation 2.51 with respect to a new variable β

$$\delta \int \left(\sum_{i=1}^{N} p_i \frac{dq^i}{d\beta} - H \frac{dt}{d\beta} \right) d\beta = 0. \tag{2.59}$$

Let us set $P_i = p_i, Q^i = q^i$, for $i = 1, \ldots, N$. We then have

$$H(P, Q) = H(p_1, p_2, \ldots, p_n, -H, q^1, q^2, \ldots, q^n, t), \tag{2.60}$$

and we have a new form of the variational equation

$$\delta \int \sum_{i=1}^{N+1} P_i \frac{dQ^i}{d\beta} d\beta = 0, \tag{2.61}$$

where $-H$ and t are treated like any other momentum and position co-ordinates in an extended $2N + 2$ dimensional phase space, with the flow being parametrised by β.

The Hamiltonian $\mathbf{H} = H(p, -H, q, t)$ describing this may be obtained by a generating function

$$F_2 = \sum_{i=1}^{N} P_i q^i + P_{N+1} t. \tag{2.62}$$

Using

$$\mathbf{H}(P, Q, t) = H(p, q, t) + \frac{\partial}{\partial t} F_2(q, P, t), \tag{2.63}$$

we find that

$$\mathbf{H}(P, Q) = H(p, q, t) - H, \tag{2.64}$$

where the canonical equations have the form

$$\frac{dP_i}{d\beta} = -\frac{\partial \mathbf{H}}{\partial Q^i}, \frac{dQ^i}{d\beta} = \frac{\partial \mathbf{H}}{\partial P_i}. \tag{2.65}$$

This new Hamiltonian is autonomous, and, as $i = N + 1$ in the generating function F_2 yields $\mathbf{H} = c$ (constant), we find that a non-autonomous Hamiltonian with N degrees of freedom is equivalent to an autonomous Hamiltonian with $N+1$ degrees of freedom, and thus we can represent the evolution of the system of the non-autonomous Hamiltonian as trajectories in the phase space of an autonomous Hamiltonian. Trajectories in the transformed Hamiltonian's $2N + 2$ dimensional phase space do not intersect, and in addition, we have preservation of phase space volumes under evolution of the system.

2.6 Phase Space

Given a dynamical system with M independent variables, we can represent the state of the system by a point in an M-dimensional configuration space generated by M mutually orthogonal axes corresponding to the M independent variables. In an autonomous Hamiltonian system with N degrees of freedom we have

$$H = H(p_1, p_2, \ldots, p_N, q^1, q^2, \ldots, q^N), \tag{2.66}$$

and thus we can represent states of the system by points in a $2N$ dimensional phase-space corresponding to the N position co-ordinates and the N momentum co-ordinates.

We can extend this idea of representing the state of the system by points, to representing the evolution of the system, by a curve or trajectory, in the $2N$ dimensional phase space.

Let us take two initial points in phase space, x_α, x_β and evolve the system from those points in some variable, say time τ (we can evolve the system with respect to another variable but time is the easiest to consider). We obtain two trajectories in phase space corresponding to the evolution of the system from the two initial points: $\gamma_\alpha, \gamma_\beta$, respectively.

Let us now allow the trajectories to evolve as $\tau \to -\infty$, and $\tau \to \infty$ and denote the trajectories obtained by $\Gamma_\alpha, \Gamma_\beta$, respectively.

We find that either

$$\Gamma_\alpha = \Gamma_\beta, \tag{2.67}$$

or

$$\Gamma_\alpha \cap \Gamma_\beta = \emptyset. \tag{2.68}$$

In the first case the trajectories are identical, and in the second they are wholly disjoint. We thus have a situation that trajectories in phase space will not intersect unless they are identical under evolution of the trajectory in time ($\tau \to -\infty$, and $\tau \to \infty$).

This is a consequence of the theorem of the existence and uniqueness of solutions of ordinary differential equations, which is stated from Glendinning [6] without proof.

Theorem 2.2 Local existence and uniqueness

Suppose $\dot{x} = f(x,t)$ and $f : \mathbb{R}^N \times \mathbb{R} \to \mathbb{R}^N$ is continuously differentiable. Then there exists maximal $t_1 > 0$ and $t_2 > 0$ such that a solution $x(t)$ with $x(t_0) = x_0$ exists and is unique for all $t \in (t_0 - t_1, t_0 + t_2)$.

2.7 Poisson Brackets

A useful notion in dynamics is that of the Poisson bracket, which we define as follows

$$[u,v] = \sum_i \left(\frac{\partial u}{\partial q^i}\frac{\partial v}{\partial p_i} - \frac{\partial v}{\partial q^i}\frac{\partial u}{\partial p_i} \right), \tag{2.69}$$

where u, v are arbitrary functions of the generalised co-ordinates. Now

$$[q^i, H] = \sum_k \left(\frac{\partial q^i}{\partial q^k}\frac{\partial H}{\partial p_k} - \frac{\partial H}{\partial q^k}\frac{\partial q^i}{\partial p_k} \right) = \frac{\partial H}{\partial p_i}, \tag{2.70}$$

thus

$$\dot{p_i} = [p_i, H], \tag{2.71}$$

and

$$\dot{q^i} = [q^i, H]. \tag{2.72}$$

Let

$$z = [q^1, q^2, \ldots, q^N, p_1, p_2, \ldots, p_N], \tag{2.73}$$

and then

$$\dot{z} = [z, H]. \tag{2.74}$$

We say that x, y are in involution if the poisson bracket $[x,y]$ vanishes ($[x,y] = [y,x] = 0$). Poisson brackets have a number of interesting properties:
i) $[u,v] = -[v,u]$,

ii) $[[u,v],w]+[[w,u],v]+[[v,w],u]=0$, (the Jacobi identity)
iii) $[u+av,w]=[u,w]+a[v,w]$,
iv) $[uv,w]=u[v,w]+[u,w]v$.

Given an arbitrary function $\Upsilon=\Upsilon(q,p,t)$, where we have $\dot{q},\dot{p}$ given by Hamilton's equations of motion, the time rate of change of Υ is given by

$$\frac{d\Upsilon}{dt}=\sum_i\left(\frac{\partial\Upsilon}{\partial q^i}\frac{\partial H}{\partial p_i}-\frac{\partial\Upsilon}{\partial p_i}\frac{\partial H}{\partial q^i}\right)+\frac{\partial\Upsilon}{\partial t}=[\Upsilon,H]+\frac{\partial\Upsilon}{\partial t}. \tag{2.75}$$

For an autonomous Hamiltonian,

$$\frac{\partial\Upsilon}{\partial t}=0, \tag{2.76}$$

and if $[\Upsilon,H]=0$, Υ commutes with H, and Υ is a constant of the motion. If we choose $\Upsilon(q,p,t)$ to be one of the momentum variables, p_i (which is not explicitly dependent on time), and if the Hamiltonian is independent of position ($\frac{\partial H}{\partial q^i}=0$), then we find that

$$\frac{dp_i}{dt}=0, \tag{2.77}$$

and therefore p_i is a constant of the motion.

The notion of constants of the motion is of prime importance in determining the integrability of a system.

2.8 Integrability

A Hamiltonian system with N degrees of freedom is said to be integrable if there exist N global constants of the flow.

The N global constants of the motion $\alpha_1,\alpha_2,\ldots,\alpha_N$ are all in involution with each other, that is

$$[\alpha_i,\alpha_j]=0, \tag{2.78}$$

for all $i,j\in 1,\ldots,N$. The N global constants of the motion may be expressed as N real valued scalar functions of position and/or momenta.

Integrable systems are important in Hamiltonian dynamics as given an integrable system with a small perturbation, we may be able to show that a portion of the motion in the phase space remains regular by applying the celebrated KAM Theorem, which will be detailed in Chapter 3.

An integrable Hamiltonian system with N degrees of freedom may be expressed, via a canonical transformation, as N independent sets of Action-Angle variables.

Action-Angle variables have the form

$$\dot{I} = 0, \tag{2.79}$$

$$\dot{\theta} = \omega(I). \tag{2.80}$$

2.9 Action-Angle Variables

We can make a canonical change of variables to Action-Angle variables as a consequence of the Arnol'd-Liouville Theorem [17].

Theorem 2.3 Arnol'd-Liouville theorem for continuous systems

Given a continuous dynamical system with N degrees of freedom in which the volume and orientation of regions in phase space is maintained,
i) if there exist N independent integrals of the motion $I_i, i \in 1, \ldots, N$, all of which are in involution; and
ii) if the surfaces I_i =constant are compact,
then the trajectories in the phase space of the system lie on a collection of $N-$dimensional tori which foliate the phase space, and there is a canonical change of co-ordinates whereby the trajectories can be expressed in Action-Angle co-ordinates:

$$I = a(\text{constant}),$$

$$\theta = \omega(I)t + \theta_0.$$

In a dynamical system each constant of the motion restricts the flow of trajectories to a $2N-1$ dimensional surface in the $2N$ dimensional phase space. In an integrable system there are N constants of the motion and the intersection of these N surfaces is an N dimensional surface upon which the trajectories lie. Each trajectory is either periodic and stable or quasiperiodic, depending on whether the winding number is rational or irrational [21]. The concept of the winding number is introduced in chapter 3.

In an integrable system with 2 degrees of freedom the trajectories lie on 2-tori which foliate the phase space.

The trajectories of an integrable system with 2 degrees of freedom may be imagined to evolve on a 2 dimensional torus constructed from action-angle variables $(J_1, J_2, \theta_1, \theta_2)$ as shown in figure 2.1.

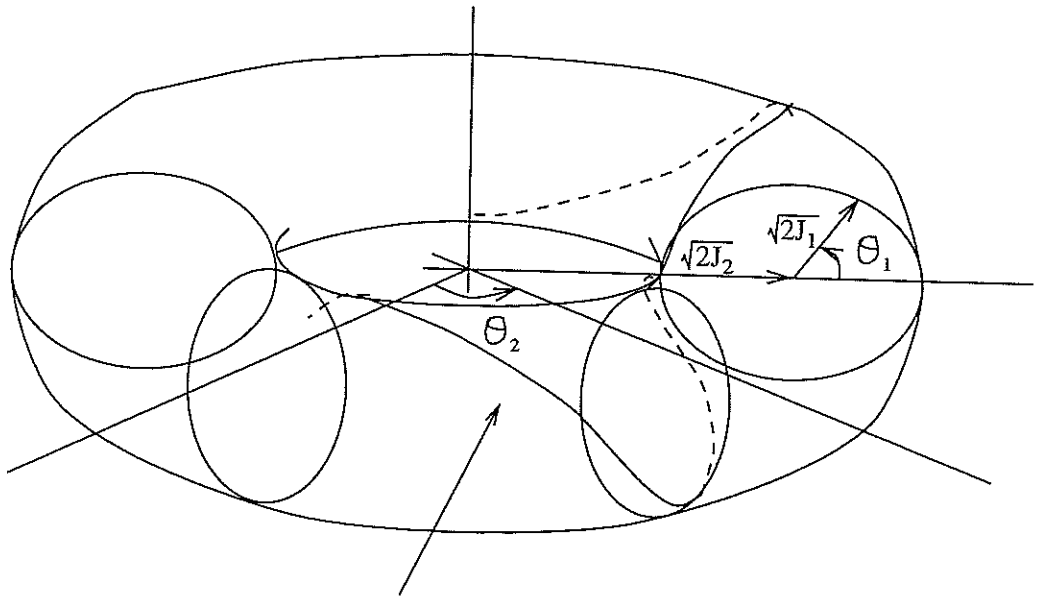

Figure 2.1: 2-torus on which a trajectory evolves in an integrable Hamitonian system with 2 degrees of freedom

As an example of this canonical change of co-ordinates let us examine an integrable Hamiltonian with 2 degrees of freedom and its transformation to Action-Angle co-ordinates [7, 13, 21].

The Hamiltonian for a system describing the relative motion of a moon of mass m_1 orbiting a planet of mass m_2 is given by

$$H = \frac{p_r^2}{2\mu} + \frac{p_\phi^2}{2\mu r^2} - \frac{k}{r} = E, \tag{2.81}$$

where (p_r, p_ϕ) and (r, ϕ) are the relative momenta and positions, respectively, of the two bodies in polar co-ordinates, E is the total energy of the system, $\mu = \frac{m_1 m_2}{m_1 + m_2}$, and $k = Gm_1m_2$ (G is the gravitation constant).

We introduce the Hamilton-Jacobi equation [13] in a general form as follows:

$$H\left(\frac{\partial F_2}{\partial q}, q\right) = E, \tag{2.82}$$

where F_2 is known as Hamilton's characteristic function.

In this system the Hamilton-Jacobi equation may be written

$$H = \frac{1}{2\mu}\left(\left(\frac{\partial W}{\partial r}\right)^2 + \frac{1}{r^2}\left(\frac{\partial W}{\partial \phi}\right)^2\right) - \frac{k}{r} = E = \alpha. \tag{2.83}$$

The variables in equation 2.87 may be separated by assuming a solution in the form

$$W = W_r(r) + W_\phi(\phi). \tag{2.84}$$

The second term in equation 2.87 is the only term that involves ϕ, so we have

$$\frac{\partial W_\phi}{\partial \phi} = \alpha_\phi. \tag{2.85}$$

We then have

$$H = \frac{1}{2\mu}\left(\left(\frac{\partial W}{\partial r}\right)^2 + \frac{\alpha_\phi^2}{r^2}\right) - \frac{k}{r} = E, \tag{2.86}$$

which may be rewritten

$$\left(\frac{\partial W}{\partial r}\right)^2 + \frac{\alpha_\phi^2}{r^2} = 2\mu\left(E + \frac{k}{r}\right). \tag{2.87}$$

We convert this to Action-Angle variables $(J_1, J_2, \theta_1, \theta_2)$ as follows

$$J_1 \equiv J_\phi = \oint p_\phi d\phi = \oint \frac{\partial W_\phi}{\partial \phi} d\phi, \tag{2.88}$$

$$J_2 \equiv J_r = \oint p_r dr = \oint \frac{\partial W_r}{\partial r} dr. \tag{2.89}$$

That is

$$J_1 \equiv J_\phi = \oint \alpha_\phi d\phi, \tag{2.90}$$

$$J_2 \equiv J_r = \oint \sqrt{2\mu\left(E + \frac{k}{r}\right) - \frac{\alpha_\phi^2}{r^2}}\, dr. \tag{2.91}$$

Expressing our original Hamiltonian in terms of Action variables, we have

$$H = \frac{-\mu k^2}{2(J_1 + J_2)^2} = E. \tag{2.92}$$

We find that Hamilton's equations of motion are satisfied:

$$\dot{\theta}_i = \frac{\partial H}{\partial J_i} = \omega_i(J_1, J_2), \tag{2.93}$$

$$\dot{J}_i = -\frac{\partial H}{\partial \theta_i} = 0, \tag{2.94}$$

for $i \in 1, 2$.

Performing simple integrations, we find

$$\theta_i = \omega_i t + d_i, \tag{2.95}$$

$$J_i = c_i, \tag{2.96}$$

where c_i, d_i are constants obtained from the initial conditions. We note that the Action (J_i) is constant.

We thus have variables (Action-Angle variables) in which the description of the evolution of trajectories in integrable systems is particularly simple. There is much work in this field of research that is devoted to finding the canonical transformations that transforms a system's original variables to Action-Angle variables, as this is often a non-trivial exercise. The often stated example of transforming from momentum and position variables for a nonlinear pendulum to Action-Angle variables is a good example of the difficulty of finding such canonical transformations.

2.10 Maps

In this thesis we are primarily concerned with discrete dynamical systems, or maps.

A mapping is a transformation of phase space $\mathcal{B} : \mathbb{R}^N \times \mathbb{R}^N \to \mathbb{R}^N \times \mathbb{R}^N$, and we denote the image of a point α_0 under the mapping by $\alpha_1 = \mathcal{B}(\alpha_0)$.

We define the orbit of a point $\alpha_0 \in \mathbb{R}^N \times \mathbb{R}^N$ to be the ordered collection of points

$$[\alpha_0, \alpha_1, \alpha_2, \ldots, \alpha_m, \ldots] = [\alpha_0, \mathcal{B}(\alpha_0), \mathcal{B}^2(\alpha_0), \ldots, \mathcal{B}^m(\alpha_0), \ldots], \tag{2.97}$$

where $\mathcal{B}^a(\alpha_0) = \mathcal{B}(\mathcal{B}^{a-1}(\alpha_0)) = \mathcal{B}(\mathcal{B}(\ldots(\mathcal{B}(\alpha_0))\ldots)), \alpha_0 \in \mathbb{R}^N \times \mathbb{R}^N$, and where are there a many $\mathcal{B}$'s.

A map derived from a Hamiltonian flow is symplectic, that is to say, volumes and orientation are preserved under the map. Alternatively we can say that the map preserves the symplectic 2-form ω, represented in canonical co-ordinates by the $2N \times 2N$ matrix

$$\omega = \begin{pmatrix} 0 & -I_n \\ I_n & 0 \end{pmatrix},$$

where 'preserves' means that the tangent space map M is governed by

$$M^T \omega M = \omega,$$

where

$$M = \left(\frac{\partial \alpha_1^i}{\partial \alpha_0^j} \right), \tag{2.98}$$

and M^T denotes the transpose of the matrix M. It is interesting to note that

$$|\omega| = |M^T||\omega||M| = |M|^2|\omega|, \tag{2.99}$$

which implies that $\det M = \pm 1$, and thus the mapping is volume-preserving. Since M is real, the eigenvalues come in complex conjugate pairs, and they come in reciprocal pairs. This implies that $\det M = 1$, and thus the map is orientation preserving.

As we may consider discrete dynamical systems as special cases of continuous systems, the Arnol'd-Liouville theorem applies to discrete dynamical systems.

Theorem 2.4 Arnol'd-Liouville theorem for discrete time systems

Given a symplectic mapping $\mathcal{B} : \mathbb{R}^N \times \mathbb{R}^N \to \mathbb{R}^N \times \mathbb{R}^N$, and

a) if there exist N independent integrals of the motion $I_i, i \in 1, \ldots, N$ all of which are in involution ($[I_i, I_j] = 0, \forall i, j \in 1, \ldots, N$) and

b) if the surfaces $I_i =$ constant are compact,

then the trajectories of $\mathcal{B}$ lie on a collection of $N-$ dimensional tori which foliate the $2N$ dimensional phase space, and there is a canonical change of co-ordinates such that $\mathcal{B}$ may be expressed in the form of Action-Angle variables:

$$\begin{aligned} I' &= I, \\ \theta' &= \theta + \Omega(I). \end{aligned}$$

A map that satisfies the conditions of this theorem is said to be integrable in the sense of Liouville [13].

2.11 Poincaré Sections

Taking a Poincaré section of a non-autonomous continuous dynamical system can yield information about the effect of perturbation on the system not readily apparent in the tangle of trajectories that generally appears in the system's phase space. Before we examine what a Poincaré section is, let us firstly consider a special case of the Poincaré section, the stroboscopic map.

2.11.1 Stroboscopic map

Let us take a Hamiltonian system with N degrees of freedom

$$H(p_i, q^i) = H_0(p_i, q^i) + \epsilon H_1(p_i, q^i, t), \tag{2.100}$$

where

$$\epsilon H_1(p_i, q^i, t_0) = \epsilon H_1(p_i, q^i, t_0 + m\tau), \tag{2.101}$$

$i \in 1, \ldots, N$, ϵ is a small paramater (generally $0 < \epsilon \ll 1$), τ is the period of the perturbation, and $m \in \mathbb{N}$.

Instead of representing the evolution of this non-autonomous system in a $2N+1$ dimensional phase space, we take the (p_i, q^i) co-ordinates of the trajectory whenever $t = m\tau, m \in \mathbb{N}$ and project those co-ordinates onto the $2N$ dimensional phase space. Instead of entire trajectories filling the phase space, we have a collection of points derived from 'snapshots' of the system at times $t = m\tau, (m \in \mathbb{N})$.

We generalise the idea of the stroboscopic map to the Poincaré section.

2.11.2 Poincaré sections

It is possible to reduce the analysis of a Hamiltonian system with N degrees of freedom in a $2N$ dimensional phase space to the study of a Poincaré section in a $2N-2$ dimensional phase space.

The Poincaré section is generated in the following manner:
In an autonomous integrable Hamiltonian with N degrees of freedom trajectories are restricted to lie in a surface of dimensionality $2N-1$. We project out a single generalised co-ordinate p_N and examine the co-ordinates (p_i, q^i) of the trajectory when it successively intersects a $2N-2$ dimensional surface generated by $q^N = c$ (constant). Volumes in the cross-section are preserved under evolution of the system, and we find that the trajectories of this integrable system will lie on a unique surface with dimensionality less than $2N-2$. If this system was not integrable we find that the trajectories will fill the $2N-2$ dimensional cross section.

A figurative illustration of the idea of the Poincaré section is found in figure 2.2.

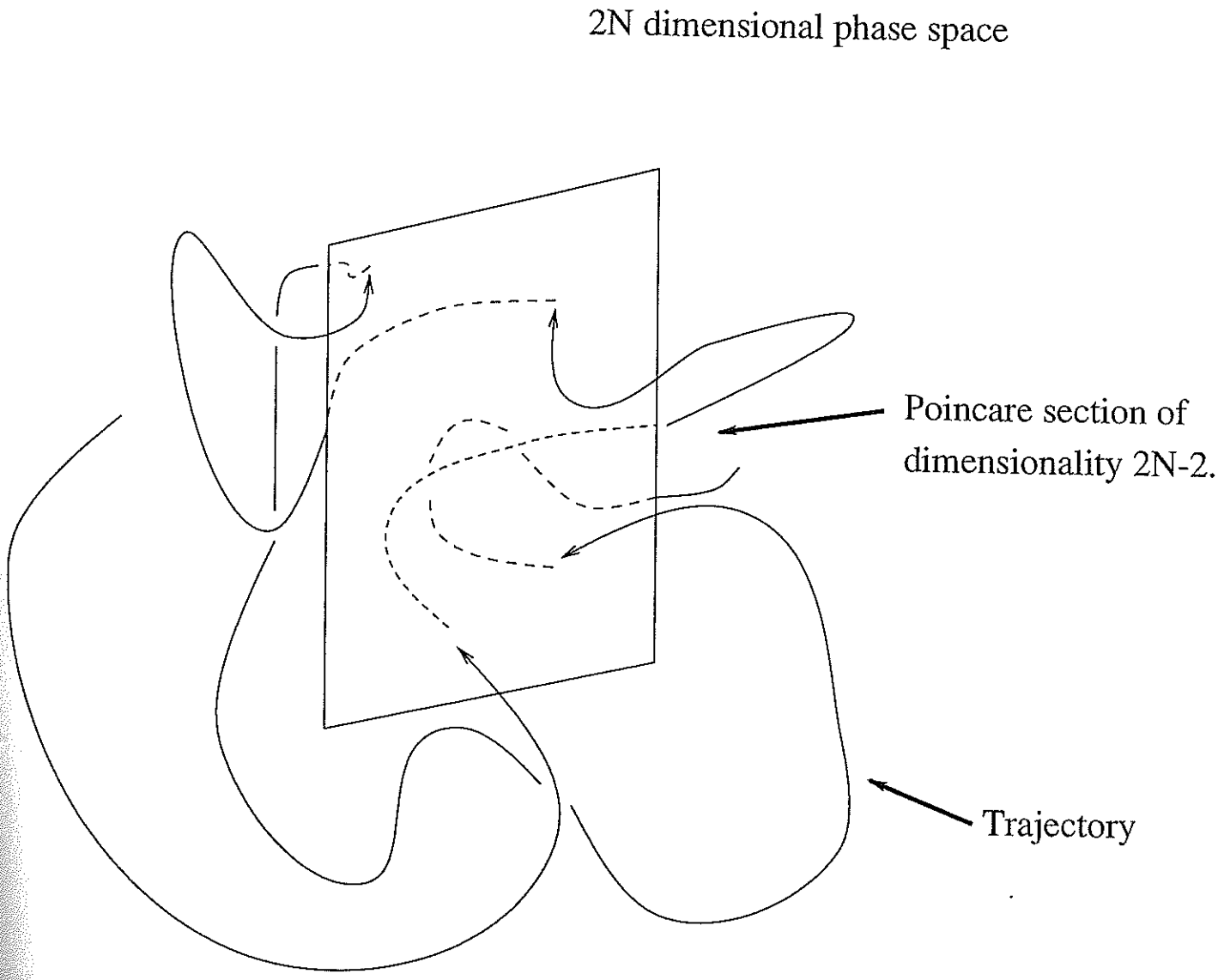

Figure 2.2: An illustration of the idea of the Poincaré section

Chapter 3

The Standard Map and KAM Theory

3.1 Maps

As introduced in Chapter 2, a map is a dynamical system which evolves in discrete units of time. Examples of maps include those representing the Poincaré section of a continuous dynamical system, and the standard map, which many nonlinear dynamical systems can to some degree be reduced to to facilitate their study [21, 13]. Maps are particularly easy to examine given the availability of computers which can easily generate phase space diagrams that reveal much detail about the global and local dynamics of such systems. Here we examine the standard map.

The standard map is a Poincaré section map that describes the behaviour of a rotor with one degree of freedom driven by a time periodic, position dependent kick modelled by a dirac delta function. It is a one-parameter nonlinear map that describes the local behaviour of trajectories in the separatrix region in nonintegrable dynamical systems, and is, therefore, an important map to study.

Here we derive the standard map from two directions - by firstly examining the Duffing system, and then looking at the Hamiltonian for a kicked rotor.

First we will give an overview of area preserving maps.

3.2 Area Preserving Maps

Let our map be of the form

$$I_{n+1} = I_{n+1}(I_n, \theta_n), \tag{3.1}$$

$$\theta_{n+1} = \theta_{n+1}(I_n, \theta_n). \tag{3.2}$$

The Jacobian is as follows

$$\mathcal{J} = \begin{pmatrix} \frac{\partial I_{n+1}}{\partial I_n} & \frac{\partial I_{n+1}}{\partial \theta_n} \\ \frac{\partial \theta_{n+1}}{\partial I_n} & \frac{\partial \theta_{n+1}}{\partial \theta_n} \end{pmatrix}.$$

If $\det\mathcal{J} = 1$ the map is area preserving, and we can think of the map as a canonical transformation from one time step to the next. This canonical transformation implies that there exists a generating function

$$F = F(\theta_n, \theta_{n+1}), \tag{3.3}$$

which we note is an F_1 generating function.

From the generating function we can obtain the iterates of the map

$$I_n = -\frac{\partial F}{\partial \theta_n}, \tag{3.4}$$

$$I_{n+1} = \frac{\partial F}{\partial \theta_{n+1}}. \tag{3.5}$$

3.3 Twist Maps

Twist maps are two dimensional area preserving maps which can be derived from a Poincaré section of a continuous system evolving on a torus, with the additional requirement of the twist condition.

Consider a Poincaré section of the $(J_1, J_2, \theta_1, \theta_2)$ torus in figure 2.1 generated by plotting the trajectories position in the (J_1, θ_1) plane every occasion that the trajectory passes through a certain given θ_2 angle, say $\theta_2 = \Psi$.

If we are dealing with an integrable system, the point will lie on a circle of radius $\sqrt{2J_1}$. Let $\dot{\theta}_2 = \omega_2 = \omega_2(J_1, J_2)$, and then the time between successive intersections between the trajectory and the $\theta_2 = \Psi$ plane will be $\tau = \frac{2\pi}{\omega_2}$.

We can describe the change in θ_1 between hits of the cross-section by the mapping

$$\phi_{n+1} = \phi_n + \omega_1\tau = \phi_n + 2\pi\frac{\omega_1}{\omega_2}, \tag{3.6}$$

where we call $\omega = \frac{\omega_1}{\omega_2}$ the winding number.

Introducing the parameter

$$\rho = \sqrt{2J_1}, \tag{3.7}$$

we have the mapping

$$\rho_{n+1} = \rho_n, \tag{3.8}$$

$$\phi_{n+1} = \phi_n + 2\pi\omega(\rho_n). \tag{3.9}$$

As ρ varies the points in the cross-section will lie on different circles. If ω is a rational number we find that the points will lie on discrete periodic intervals. If ω is irrational the points will densely fill a circle in the cross-section. This is illustrated in figure 3.1.

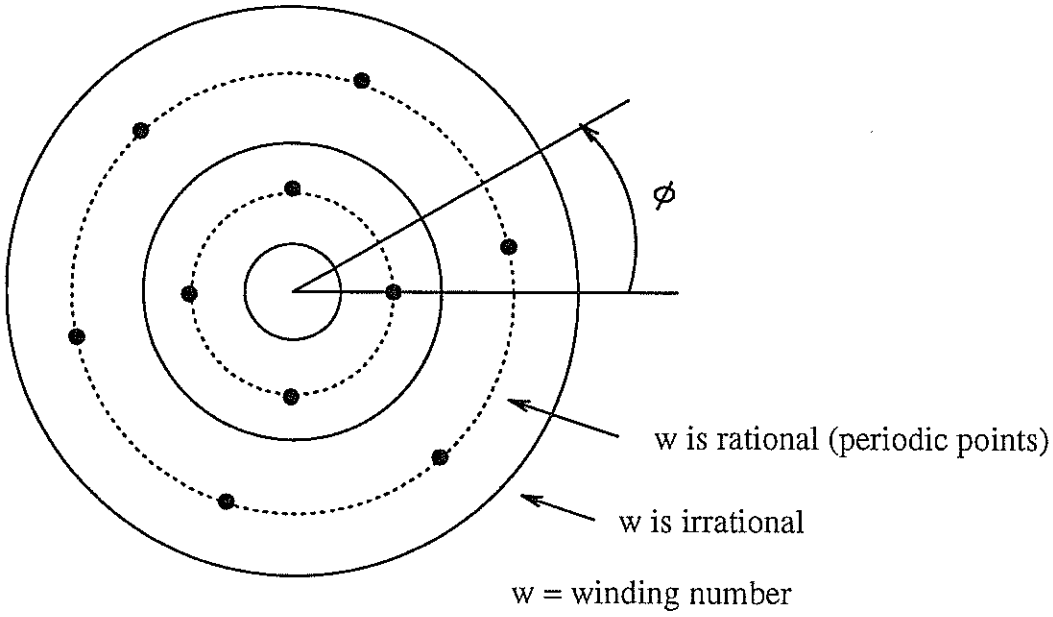

Figure 3.1: The Poincaré section of trajectories' motion on the 2-torus displayed in figure 3.1

Twist maps have a 'twist condition' - a trajectories motion around the origin is a function of its radius, and a further requirement is that

$$\left.\frac{\partial\phi_{n+1}}{\partial\rho_n}\right| \phi_n \neq 0, \tag{3.10}$$

in order that the direction of the twist does not reverse.

We note that as a twist map is a continuous map from a bounded region to a bounded region, there exists a fixed point of the map by the Brouwer Fixed Point theorem. Before we state and prove the Brouwer Fixed Point theorem we need some initial definitions and results from Fixed Point theory and Degree theory [19, 23].

Definition 3.1 Convexivity

A set Ω is convex if for any two points $x_0, x_1 \in \Omega$, $(\lambda x_0 + (1-\lambda)x_1) \in \Omega$ for all $\lambda \in [0,1]$.

Definition 3.2 Brouwer Degree

Let $p \in \mathbb{R}^n$ and $f(x) \neq p$ for all $x \in \partial\Omega$, where $\Omega \in \mathbb{R}^n$ is a set, and $\partial\Omega$ denotes the boundary of Ω. Let $\overline{\Omega}$ denote the closure of Ω. The Brouwer degree associates with each triple (f, Ω, p) an integer $d(f, \Omega, p)$ such that

(1) $d(I, \Omega, p) = \begin{cases} 1 & \text{if } p \in \Omega \\ 0 & \text{if } p \notin \overline{\Omega}, \end{cases}$

(2a) if $K \subseteq \mathbb{R}^n$ is closed and $f(x) \neq p$ for all $x \in K$ then $d(f, \Omega \setminus K, p) = d(f, \Omega_1, p)$. Here $\Omega \setminus K = \{x \in \Omega | x \notin K\}$,

(b) Additivity: if $\Omega = \Omega_1 \cup \Omega_2$, $\Omega_1 \cap \Omega_2 = \emptyset$, and Ω_i are open, then $d(f, \Omega, p) = d(f, \Omega_1, p) + d(f, \Omega_2, p)$,

(3) Homotopy: let $H : [0,1] \times \overline{\Omega} \to \mathbb{R}^n$ be a continuous function and $H(t, x) \neq p$ for all $x \in \partial\Omega$ and each $t \in [0,1]$, then $d(H(t, \cdot), \Omega, p) = \text{constant}$,

(4) $d(f, \Omega, p) = d(f - p, \Omega, 0)$. Here $(f - p)(x) = f(x) - p$.

$B(x_0, r) \subseteq A \subseteq \mathbb{R}^n$ denotes the set $\{x | x \in A, ||x - x_0||_2 < r\}$ where $||\cdot||_2$ denotes the usual euclidean norm: $||y_i||_2 = (\sum_i (y_i)^2)^{\frac{1}{2}}$.

$f \in C^n(A; B)$ denotes a function $f : A \to B$ whose *zero*th, first, second, third,..., and nth order partial derivatives are continuous. If n is not stated we take $n = 0$.

Definition 3.3 Retraction

Let $A \subseteq \mathbb{R}^n$. A function $R \in C(\mathbb{R}^n; A)$ is called a retraction of $\mathbb{R}^n$ onto A if $R(x) = x$ for all $x \in A$.

Theorem 3.1 If $A \subseteq \mathbb{R}^n$ is closed and convex then there exists a retraction $R \in C(\mathbb{R}^n; A)$.

Theorem 3.2 Brouwer fixed point theorem

Let $A \subseteq \mathbb{R}^n$ be closed, convex and bounded, and $f \in C(A; A)$. Then there exists a fixed point $x_0 \in A$ of f, that is, there is $x_0 \in A$ such that $f(x_0) = x_0$.

Proof As A is bounded, there exists $r > 0$ such that $A \subseteq B(0, r)$. Also, as A is closed and convex there exists a retraction $R \in C(\mathbb{R}^n; A)$.

Let $G(x) = f(R(x))$. We note that G is a continuous function as it is the composition of two continuous functions. G is defined for all $x \in \mathbb{R}^n$, and $R(x) = x$ for all $x \in A$ which implies that $G(x) = f(x)$ for all $x \in A$ and thus G is a continuous extension of f from A to $\mathbb{R}^n$.

Now $G : \overline{B(0, r)} \to A \subseteq \overline{B(0, r)}$. We want to show that $G(x) = x$ for some $x \in B(0, r)$, that is for some $x \in A$, since $G : \mathbb{R}^n \to A$. We want $G(x) = f(x) = x$,

in which case x is the required fixed point of g and we have a fixed point of the twist map.

Now $x = G(x) \equiv f(x) = x - G(x) = 0$, and we want to compute $d(f, B(0,r), 0)$.

Let $H(t,x) = x - tG(x)$ be a homotopy. Now, either there exists a solution on the boundary of Ω in which case we have found our fixed point, or there does not, in which case we wish to show that there is a homotopy. So let us assume now that there is not a fixed point on the boundary of Ω. We now use a homotopy to show that there must be a fixed point in Ω.

Now if $H(1,x) = x - G(x) = 0$ for some $x \in \partial B(0,r)$, then $x - G(x) = 0$ has a solution and we have found our fixed point. So let us assume $H(1,x) = x - G(x) \neq 0$ for all $x \in \partial B(0,r)$.

Consider $0 \leq t < 1$. Assume $H(t,x) = 0$ for some $x \in \partial B(0,r) \equiv x = tG(x)$.

This implies that $\Omega = ||x|| = t||G(x)|| < r$, since $||G(x)|| \leq r$, and $0 \leq t < 1$. Thus $H(t,x) \neq 0$ for all $t \in [0,1]$, and $x \in \partial B(0,r)$.

Now clearly H is continuous, which implies that H is a homotopy. Thus

$$\begin{aligned} d(H(\cdot,x), B(0,r), 0) &= \text{constant}, \\ \Rightarrow d(H(1,x), B(0,r), 0) &= d(H(0,x), B(0,r), 0), \\ \Rightarrow d(x, B(0,r), 0) &= d(x - G(x), B, 0), \\ \Rightarrow x - G(x) &= 0 \end{aligned}$$

has a solution $x \in B(0,r)$.

Thus there exists a fixed point of the function, and thus we have shown that every twist map has at least one fixed point.

3.4 Perturbed Twist Maps

We look at the generalised perturbed twist map [13]

$$J_{n+1} = J_n + \epsilon f(J_{n+1}, \theta_n), \tag{3.11}$$

$$\theta_{n+1} = \theta_n + 2\pi\alpha(J_{n+1}) + \epsilon g(J_n, \theta_n), \tag{3.12}$$

where f, g are periodic in θ. The transformation from the nth co-ordinates to the $n+1$st co-ordinates are generated by Hamilton's equations, and thus the map is area-preserving. The generating function

$$F_2 = J_{n+1}\theta_n + 2\pi\mathcal{A}(J_{n+1}) + \epsilon\mathcal{G}(J_{n+1}, \theta_n), \tag{3.13}$$

generates the perturbed twist map, with

$$\alpha = \frac{d\mathcal{A}}{dJ_{n+1}}, \tag{3.14}$$

$$f = -\frac{\partial \mathcal{G}}{\partial \theta_n}, \tag{3.15}$$

$$g = \frac{\partial G}{\partial J_{n+1}}. \tag{3.16}$$

From the foregoing, we can see that

$$\frac{\partial f}{\partial J_{n+1}} + \frac{\partial g}{\partial \theta_n} = 0, \tag{3.17}$$

and thus the perturbed twist map is area preserving.

If we take f to be independent of J, and let $g \equiv 0$, then the perturbed twist map takes the form of a radial twist mapping

$$J_{n+1} = J_n + \epsilon f(\theta_n), \tag{3.18}$$

$$\theta_{n+1} = \theta_n + 2\pi\alpha(J_{n+1}). \tag{3.19}$$

Linearizing about a period 1 fixed point $J_{n+1} = J_n = J_0$, where $\alpha(J_0)$ is an integer, for a nearby action

$$J_n = J_0 + \Delta J_n, \tag{3.20}$$

and substituting a new action

$$I_n = 2\pi\alpha' \Delta J_n, \tag{3.21}$$

converts the radial twist mapping to the generalised standard mapping

$$I_{n+1} = I_n + K f'(\theta_n), \tag{3.22}$$

$$\theta_{n+1} = \theta_n + I_{n+1}, \pmod{2\pi}. \tag{3.23}$$

We call

$$K = 2\pi\alpha'\epsilon f'_{max}, \tag{3.24}$$

the stochasticity parameter, and

$$f' = \frac{f}{f_{max}}, \tag{3.25}$$

is the jump in the action normalised to a maximum of 1. The generalised standard map is locally equivalent (in J) to any radial twist map. If we set

$$f' = \sin\theta_n, \tag{3.26}$$

the generalised standard mapping becomes the Chirikov-Taylor (standard) map

$$I_{n+1} = I_n + K\sin\theta_n, \tag{3.27}$$

$$\theta_{n+1} = \theta_n + I_{n+1}, \tag{3.28}$$

which has been the subject of much research in the transition to chaos in Hamiltonian systems.

Before we consider the standard map we examine its derivation from two models.

3.5 Derivation of the Standard Map

We derive the standard map by firstly examining aspects of the Duffing system, and secondly examining a periodically kicked rotor with one degree of freedom.

3.5.1 The Duffing system

The standard map can be derived from the Duffing system [21].

The Duffing Hamiltonian has the form

$$H = H_0 + \epsilon q\cos\omega_0 t + \phi, \tag{3.29}$$

where

$$H_0 = \frac{p^2}{4} - 2q^2 + q^4, \tag{3.30}$$

and ϕ is an arbitrary phase.

We derive the standard map by taking a map corresponding to this Hamiltonian, the whisker map; a twist map that maps the change in energy of an orbit in the neighbourhood of the separatrix of a hyperbolic point for each period of its motion.

The whisker map is

$$\omega_{n+1} = \omega_n + \epsilon\pi\omega_0\mathrm{sech}\left(\frac{\omega_0\pi}{2\sqrt{2}}\right)\sin\phi_n, \tag{3.31}$$

$$\phi_{n+1} = \phi_n + \frac{\omega_0}{\sqrt{2}}\ln\frac{64}{\omega_{n+1}}. \tag{3.32}$$

In the separatrix region the whisker map represents the behaviour of trajectories fairly well, provided that the width of the separatrix is not too great. The whisker

map has an infinite number of fixed points, with the lth fixed point given by the requirement

$$2\pi l = \frac{\omega_0}{\sqrt{2}} \ln \frac{64}{\omega_f^l}, \tag{3.33}$$

where ω_f^l is the energy associated with the lth fixed point.

We can examine the behaviour of trajectories near a fixed point by linearizing the energy about the lth fixed point. We define a dimensionless energy

$$I_n = -\frac{\omega_0}{\sqrt{2}\omega_f^l}(\omega_n - \omega_f^l). \tag{3.34}$$

Linearizing about the fixed point ω_f^l, we obtain the mapping

$$I_{n+1} = I_n - K \sin \phi_n, \tag{3.35}$$

$$\phi_{n+1} = \phi_n + I_{n+1}, \tag{3.36}$$

where

$$K = \frac{\epsilon \pi \omega_0^2}{\sqrt{2}\omega_f^l} \operatorname{sech}\left(\frac{\omega_0 \pi}{2\sqrt{2}}\right), \tag{3.37}$$

which leads us to the standard map.

3.5.2 A Kicked Rotor

We can secondly derive the standard map by examining a Hamiltonian describing a rotor with one degree of freedom being periodically kicked by a time periodic position dependent forcing term modelled by a dirac delta function. This material is drawn from Zaslavsky et al [28].

The Hamiltonian which describes the motion is

$$H = H_0 - K \cos\theta \sum_{n=-\infty}^{\infty} \delta\left(\frac{t}{T} - n\right), \tag{3.38}$$

where the unperturbed Hamiltonian H_0 is

$$H_0 = \frac{I^2}{2}, \tag{3.39}$$

and the perturbation is a periodic sequence of kicks with period

$$T = \frac{2\pi}{\mu}. \tag{3.40}$$

As we can write

$$\sum_{n=-\infty}^{\infty} \delta\left(\frac{t}{T} - n\right) = \sum_{n=-\infty}^{\infty} \cos\left(2\pi n \frac{t}{T}\right), \tag{3.41}$$

equation 3.41 can be rewritten

$$H = \frac{1}{2}I^2 - K\cos\theta \sum_{m=-\infty}^{\infty} \cos m\mu t. \tag{3.42}$$

We have

$$\dot{I} = -K\sin\theta \sum_{m=-\infty}^{\infty} \delta\left(\frac{t}{T} - n\right), \tag{3.43}$$

$$\dot{\theta} = I, \tag{3.44}$$

and between two kicks of the system we have

$$I = c, \tag{3.45}$$

$$\theta = It + d, \tag{3.46}$$

where c, d are constants.

At each kick, θ is constant and I changes by $-K\sin\theta$ so we have

$$I_{n+1} = I_n - K\sin\theta_n, \tag{3.47}$$

$$\theta_{n+1} = \theta_n + I_{n+1} \pmod{2\pi}, \tag{3.48}$$

$$\tag{3.49}$$

which is merely the standard map.

3.6 The Standard Map

We have seen how the standard map can be derived from the motion of a kicked rotor, and from the Duffing system. If we set $K = 0$ in the standard map, we have an integrable twist map, and the phase space in Action-Angle co-ordinates (I, θ) is similar to figure 3.1, if we treat the distance of a point from the centre of the region in figure 3.1 as corresponding to the action in the standard map, and if we think of the angle in figure 3.1 as corresponding to the angle co-ordinate in the standard map. We find that for rational values of the action we obtain periodic orbits that densely fill the phase space, and for irrational values of the action, the orbit densely fill out a line of constant action.

If we perturb the system by setting $K \neq 0$, $K \ll 1$, we obtain an enormously complicated structure. For each rational value of the action, we find that the periodic orbits in the unperturbed case are now chains of elliptic and hyperbolic periodic

points. Resonances surround the elliptic points and the separatrices of the hyperbolic points surround the resonances. For each irrational value of the action there exists a surface that is topologically equivalent to the lines in the corresponding non-perturbed standard map. For $K \neq 0$ we refer to these lines as KAM tori, after the KAM theorem, and we note the KAM tori are perturbed by the resonances. A phase plane diagram for $K = 0.4$ is shown in figure 3.2.

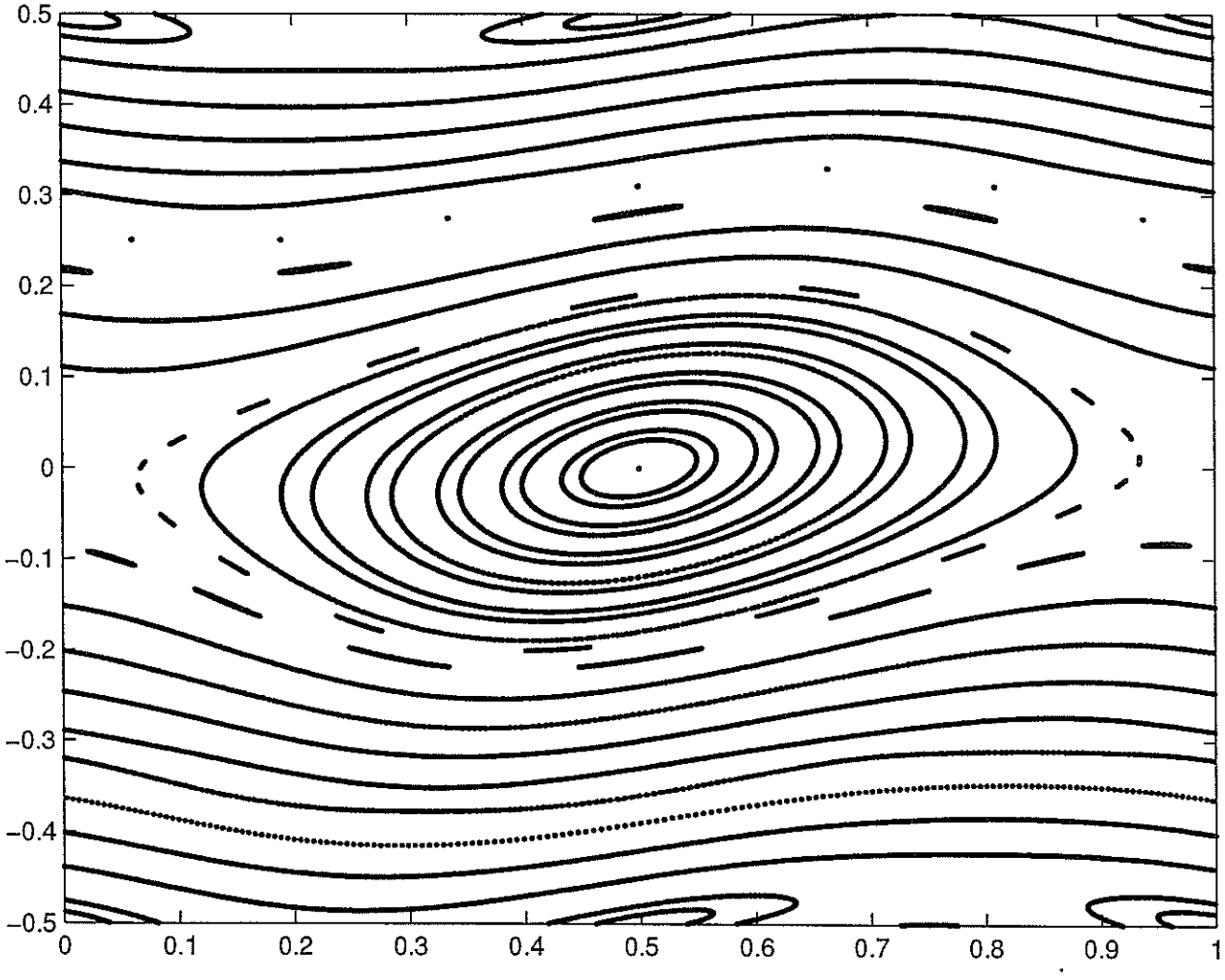

Figure 3.2: Phase plane diagram for the standard map, $K = 0.4$

The Poincare-Birkhoff theorem guarantees the existence of two intersecting curves that surround each chain of periodic points. The curves intersect heteroclinically, and the dynamics is chaotic in the vicinity of their crossing at the hyperbolic points. We can say that a Bernoulli shift consisting of a bi-infinite string of characters can be embedded in the vicinity of the hyperbolic points.

Phase plane diagrams for the cases $K = 0.8, K = 0.971635406, K = 1, K = 1.5$, and $K = 3.0$ are shown in figures 3.3, 3.4, 3.5, 3.6, and 3.7 respectively.

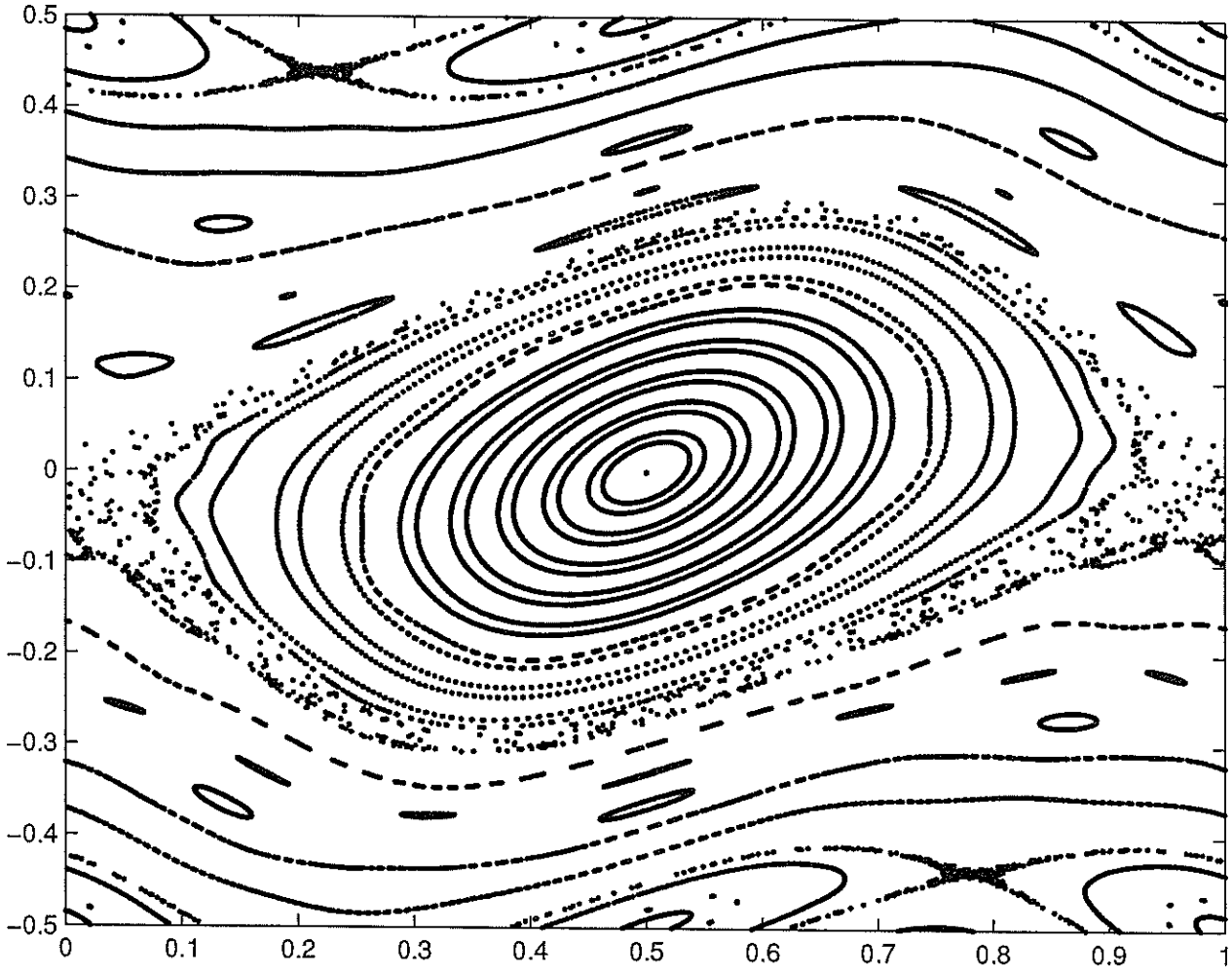

Figure 3.3: Phase plane diagram for the standard map, $K = 0.8$

As K increases from 0 to 0.971635406 increasing numbers of KAM tori are destroyed by the island chain resonances. For a given KAM tori, there is a certain value of K for which the structure of the KAM torus is transformed from being topologically identical to a line, to being a cantor set. We call the destroyed KAM torus a cantorus.

From Meiss [17], we can say the the cantorus is a nonempty, perfect, totally disconnected, and compact set. Denoting the cantorus by $\mathcal{Q}$,

(i) by perfect we mean that for all $x_0 \in \mathcal{Q}, \lim_{i\to\infty} x_i = x_0$, where all $x_i \in \mathcal{Q}$,

(ii) totally disconnected means that for any $x, y \in \mathcal{Q}$, where $x \neq y$, there exists a closed ball enclosing x, and a disjoint closed ball enclosing y, such that $\mathcal{Q}$ equals the union of all such balls,

(iii) $\mathcal{Q}$ is compact merely means that every sequence in $\mathcal{Q}$ has a convergent subsequence.

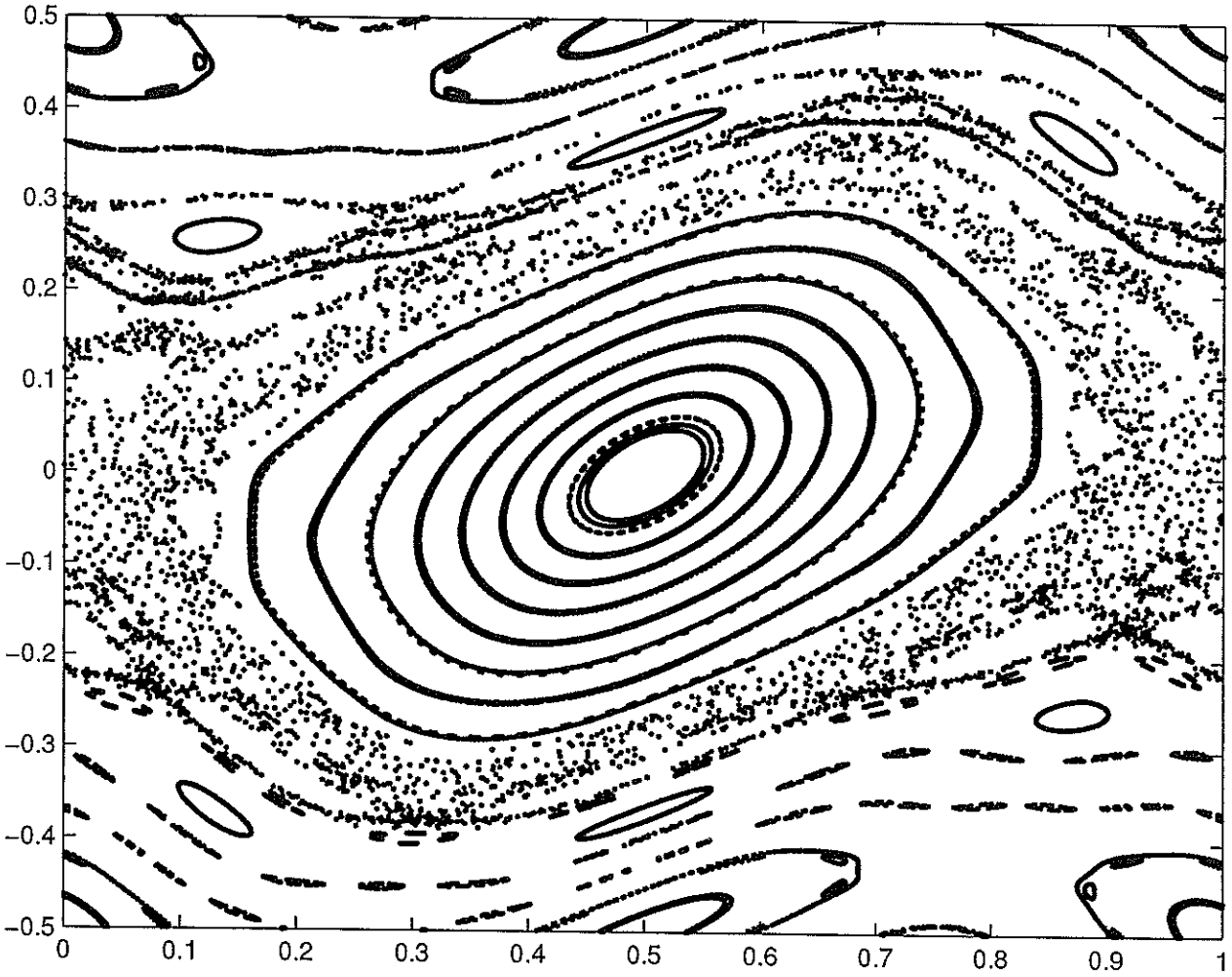

Figure 3.4: Phase plane diagram for the standard map, $K = 0.971653406$

KAM tori bound trajectories in phase space. When a KAM torus turns into a cantorus it still partially bounds trajectories, as the cantorus contains an uncountable number of points.

When $K \approx 0.971635406$ every KAM torus has turned into a cantorus, and thus a trajectory that starts in a chaotic region of the phase space can, in principle, traverse any other chaotic region in the phase space.

An example of cantori bounding the orbit generated by 5000 iterations of one initial condition through phase space is shown in figure 3.8.

As K increases, we find that the elliptic periodic points become unstable and bifurcate, and for large K we are left with a phase space in which there is a 'stochastic sea' of apparently fractal dimension within which is a countable infinity of unstable periodic points and the remains of the cantori.

An important point to be aware of is how the computer generated phase space

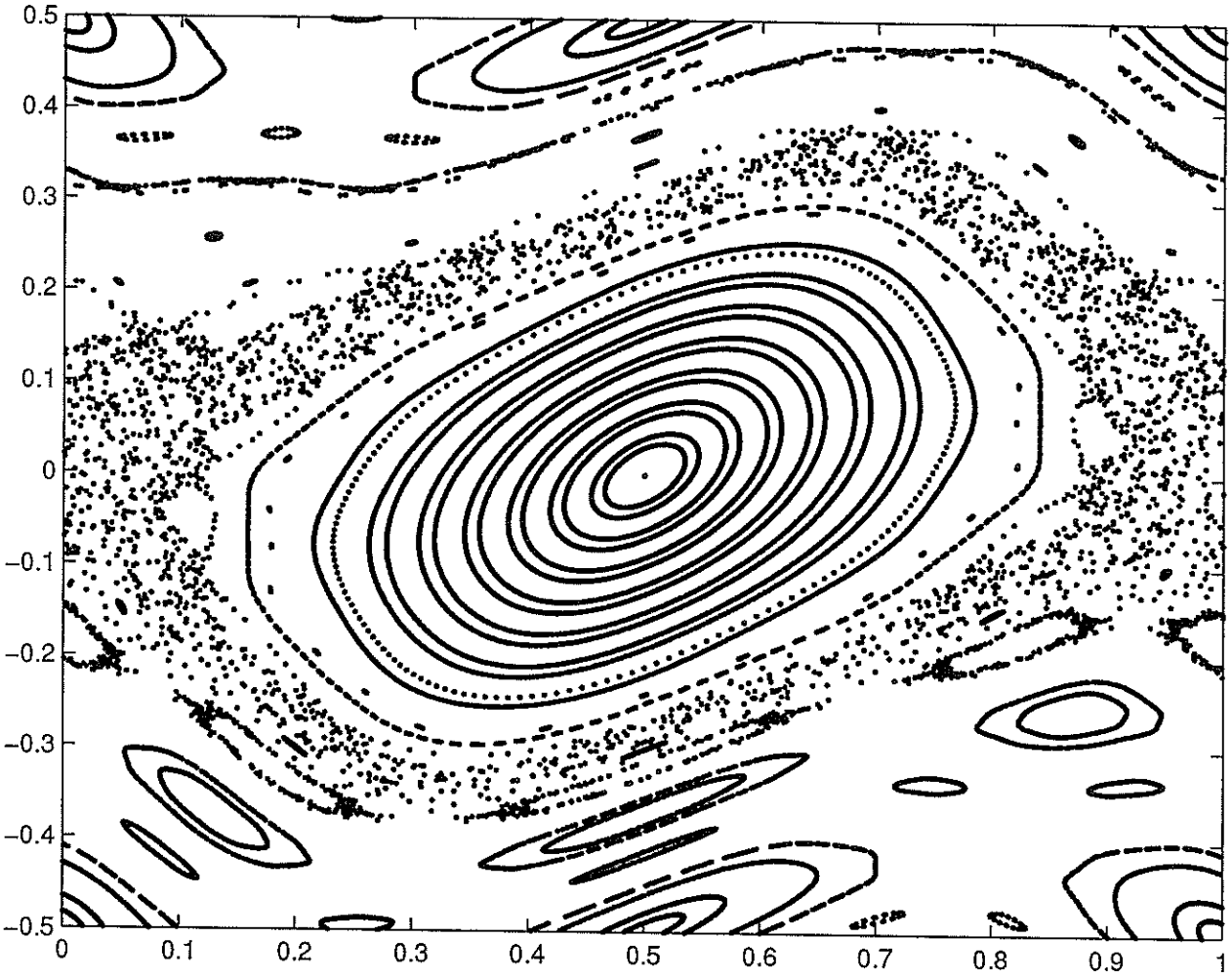

Figure 3.5: Phase plane diagram for the standard map, $K = 1.0$

diagram corresponds to the 'true' phase space plot. As computers deal with finite decimals, we obtain approximations to 'real' orbits of the system. This problem is addressed by the shadowing lemma [13].

Lemma 3.1 Shadowing lemma

Given an orbit which is corrupted by a small amount of noise such that

$$||x_{k+1} - f(x_k)|| < \delta, 0 \leq k \leq N-1, \tag{3.50}$$

for all points on the orbit up to $N-1$, where $x'_{k+1} = f(x_k)$ is the noiseless orbit, then there exists $\epsilon > 0$ such that a noiseless orbit can be found,

$$y'_{k+1} = f(y'_k), \tag{3.51}$$

such that

$$||y'_k - x_k|| \leq \epsilon, 0 \leq k \leq N-1, N \to \infty, \tag{3.52}$$

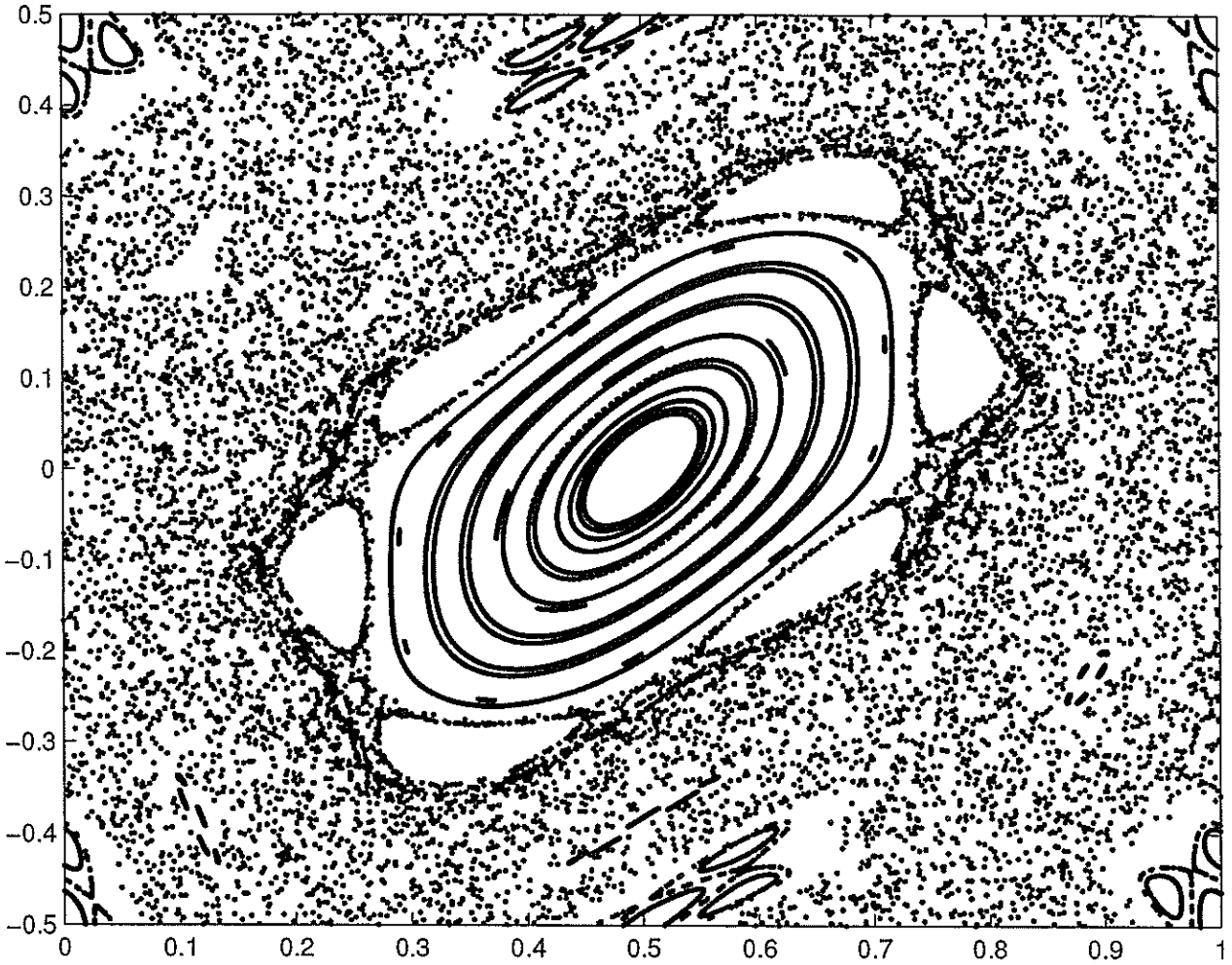

Figure 3.6: Phase plane diagram for the standard map, $K = 1.5$

that is, the shadowing orbit always remains within ϵ of a noisy orbit.

3.7 KAM Theory

One of the problems in classical mechanics that had remained unsolved for hundreds of years was the solution of the n-body problem. The $n-$body problem asks for given initial positions and momentums of n bodies ($n \geq 3$), subject to interactions amongst themselves modeled by a central force (typically gravity), what is the closed solution for their positions and momentums for all time. Poincaré showed in a competition in the late 1800's that it was not possible to obtain solutions in closed form, as the infinite series which represented the solution in general diverged, thus suggesting that the solutions were in principle unpredictable. In the last few decades, the KAM theorem, which proved the existence of predictable solutions to the general

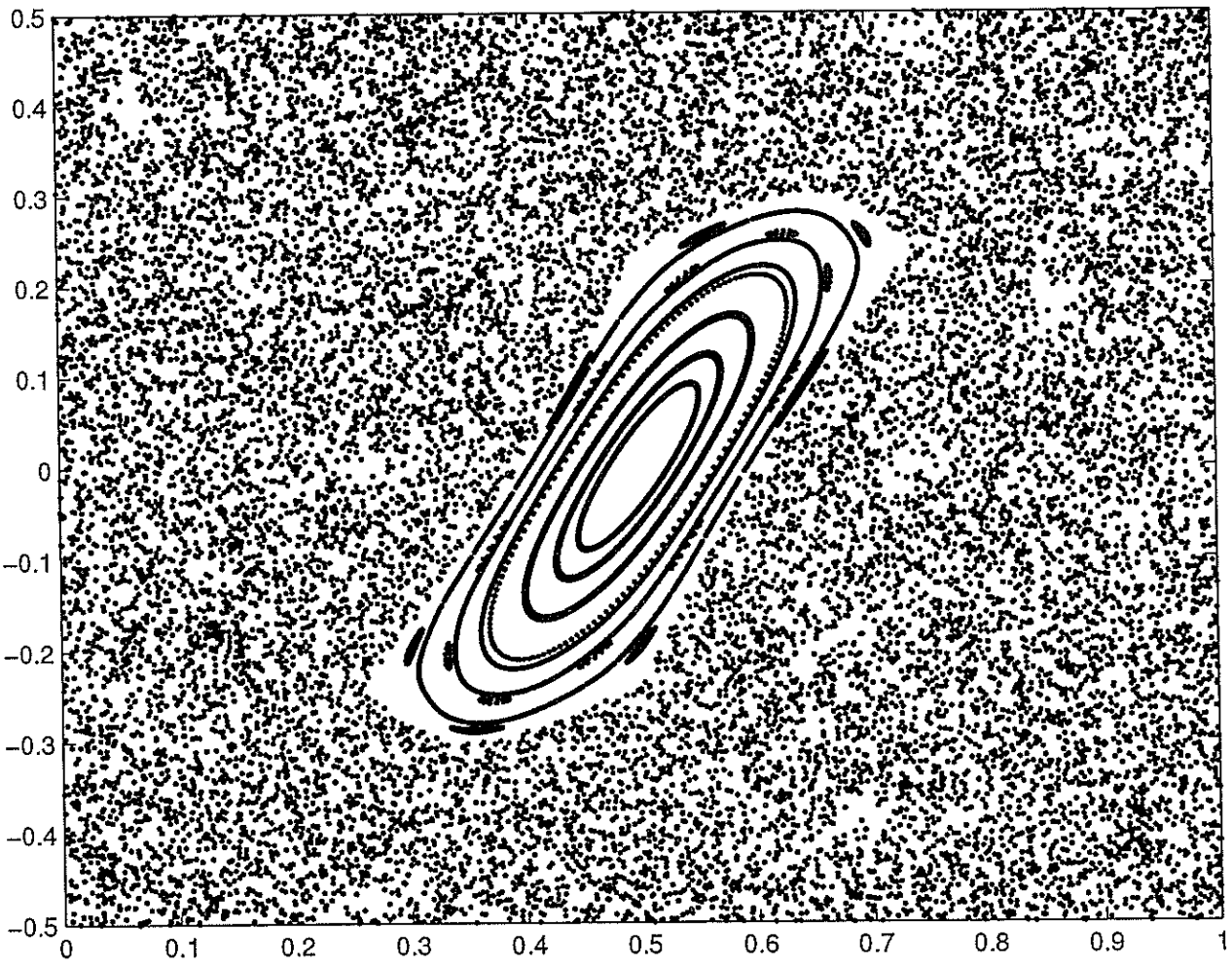

Figure 3.7: Phase plane diagram for the standard map, $K = 3.0$

problem of an integrable dynamical system subject to small perturbations in certain regions of the phase space, was developed, and has proved useful in understanding certain aspects of the behaviour of dynamical systems. The KAM theorem is difficult to understand, and for the interested reader an English translation of Kolmogorov's original paper may be found in [10]. In the following we state the KAM theorem without proof.

Theorem 3.3 KAM Theory for Analytic Hamiltonian Systems

Let

$$H(I, \theta, t) = H_0(I) + \epsilon H_1(I, \theta, t), \tag{3.53}$$

where H is an analytic Hamiltonian system with N degrees of freedom, $I \in \mathbb{R}^n, \theta \pmod{2\pi} \in \mathrm{T}^N, H_0(I)$ is an analytic, integrable, and non-degenerate Hamiltonian, $\epsilon H_1(I, \theta, t)$ is an analytic perturbation of period 2π, and ϵ is a small parameter.

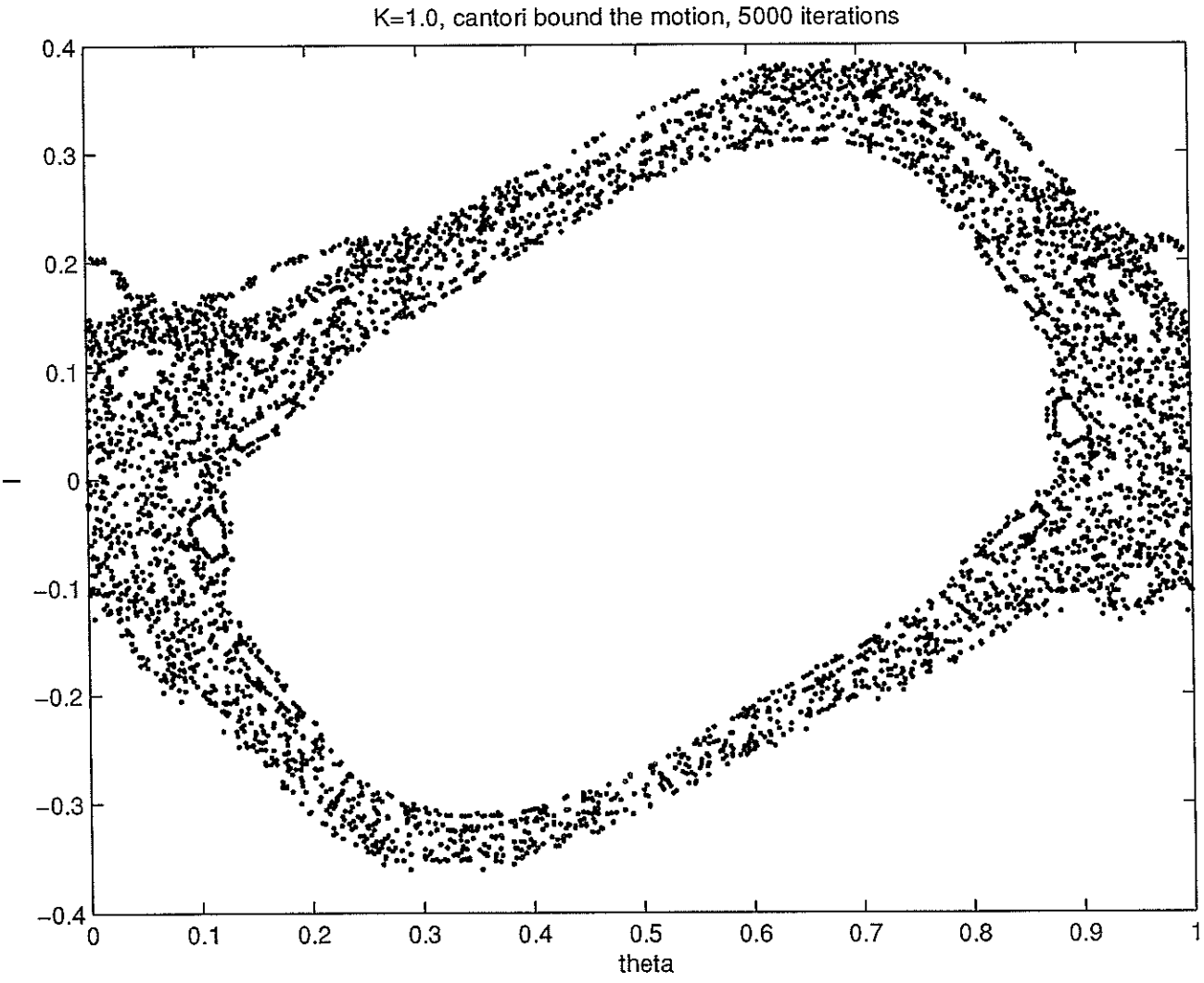

Figure 3.8: An example of cantori bounding the orbit of one initial condition, with $K = 1.0$

For sufficiently small perturbations, all invariant tori with 'sufficiently irrational' frequencies r persist, although distorted, and the set of the union of these tori has non-zero measure. The measure of the complement of this set is proportional to the size of the perturbation.

The requirement that $H_0(I)$ is non-degenerate is

$$\left|\frac{\partial^2 H}{\partial I^2}\right| \neq 0, \tag{3.54}$$

that is, the frequencies of the unperturbed system r, are independent.

The condition that the frequencies be 'sufficiently irrational' is that

$$|m.r| \geq C|m|^{-\tau}, \tag{3.55}$$

$$\forall m \in \mathbb{Z}^N \setminus \{0\}, \tag{3.56}$$

where C is a constant that depends on the nonlinearity of the unperturbed Hamiltonian H_0, and τ is dependent on the number of degrees of freedom of the system.

Theorem 3.4 KAM Theory for Maps

Let a twist map be j times differentiable, and

$$\int_0^{2\pi} f(I,\theta)d\theta = 0. \tag{3.57}$$

Define

$$|f|_j = \sup_{m+n\leq j} \left| \frac{\partial^{m+n} f}{\partial x^m \partial g^n} \right|. \tag{3.58}$$

If $|f|_j$ and $|g|_j$ is sufficiently small then all rotational invariant circles with winding number satisfying the Diophantine condition

$$|m\omega - n| > Km^{-\alpha}, \tag{3.59}$$

for all $m, n \in \mathbb{Z} \setminus \{0\}$, and some $\alpha \geq 1$ persist.

We now examine a small amount of number theory to further our consideration of the conditions in the KAM theory.

3.7.1 Continued Fractions

We may represent any number $r \in \mathbb{R}$ by a sequence of numbers $[a_0, a_1, \ldots]$ where

$$r = a_0 + \cfrac{1}{a_1 + \frac{1}{a_2 + \cdots + \frac{1}{a_n + \cdots}}}. \tag{3.60}$$

The continued fraction expansion of an irrational number is infinite and unique while the expansion for a rational number is finite and not unique: note that the continued fraction expansion $[a_0, a_1, \ldots, a_n], a_i > 0$ for $i \geq 1$, is equivalent to the expansion $[a_0, a_1, \ldots, a_n - 1, 1]$, where $a_n \neq 1$ unless $n = 0$.

We say that a convergent of a given continued fraction expansion is the rational approximated by the continued fraction expansion corresponding to the first m elements of the original fraction expansion where $m \leq n$,

$$\frac{b_m}{d_m} = [a_0, a_1, \ldots, a_m], \tag{3.61}$$

where b_m and d_m are coprime.

We note that the continued fraction expansion is strongly convergent, that is, for any ϵ, there exists p such that

$$|d_m r - b_m| < \epsilon, \forall m \geq p. \tag{3.62}$$

The convergents are known to be the best approximants, that is to say, given $\frac{b}{d}$ to be a convergent of r, then every $\frac{b'}{d'}$, where $d' \leq d$, is further from r in the sense that

$$|d'r - b'| < |dr - b|. \tag{3.63}$$

We say that every convergent is 'close' to its frequency r in the sense that the following equation is satisfied

$$|dr - b| < \frac{C}{d}, \tag{3.64}$$

where $C = 1$. When $C = \frac{1}{2}$, every rational that satisfies this equation is convergent, while for $C < \frac{1}{\sqrt{5}}$ and certain r, there are only finitely many convergents that satisfy the equation.

We say that irrationals with small continued fraction elements are difficult to approximate. Numbers of a 'constant type' are defined to be those numbers for which there exists $e \in \mathbb{R}$ where $a_m < e$, for all m. The set of these numbers are those that satisfy the Diophantine condition when $\tau = 1$.

The Diophantine condition is that there exists $C > 0$ such that $\forall (b, d) \neq (0, 0); b, d \in \mathbb{Z}$,

$$|dr - b| > \frac{C}{d^\tau}, \tag{3.65}$$

for some

$$\tau \geq 1. \tag{3.66}$$

Now let $D_\tau(C)$ be the set of r that satisfy the above equation. Given small enough $C, D_\tau(C) \neq \emptyset$, for any $\tau > 1$ the measure of $D_\tau(C) \to 1$ as $C \to 0$.

The set of Diophantine numbers D_τ is the union of $D_\tau(C)$ for all $C > 0$.

The noble numbers are those whose continued fraction representation is of the form

$$[a_0, a_1, \ldots, a_n, 1, 1, 1, \ldots], \tag{3.67}$$

where $a_i \in \mathbb{Z}$, and $i \in 0, \ldots, n$. The noble numbers are difficult to approximate given the strings of 1's in the continued fraction representation.

The noblest number has the continued fraction representation

$$[1, 1, 1, \ldots], \tag{3.68}$$

and is called the golden mean (γ). The golden mean is the larger of the solutions of the equation $\gamma^2 = \gamma + 1$ and has the value

$$\gamma = \frac{1 - \sqrt{5}}{2}. \tag{3.69}$$

As an aside, we note that the number with the continued fraction representation

$$[2, 2, 2, \ldots], \tag{3.70}$$

is called the *silver mean.*

The golden mean has particular application to the standard map as the KAM torus with winding number equal to the golden mean is the last KAM torus to survive under nonzero and increasing K.

3.7.2 Farey Tree

We can organise each rational using the Farey tree. The Farey tree is generated by taking a pair of rationals

$$\frac{m}{n}, \frac{m'}{n'}, \tag{3.71}$$

where m, m', n, n' are in lowest terms, and where

$$mn' - nm' = 1, \tag{3.72}$$

that is, the numbers are neighbours.

We generate the first level of the tree by

$$\frac{m''}{n''} = \frac{m + m'}{n + n'}. \tag{3.73}$$

$\frac{m''}{n''} = \frac{m+m'}{n+n'}$ is called the mediant of $\frac{m}{n}$ and $\frac{m'}{n'}$, and $\frac{m''}{n''}$ is a neighbour of $\frac{m}{n}$ and $\frac{m'}{n'}$. We note that both m'' and n'' are co-prime.

The second level of the Farey tree is generated by finding the mediants of $\frac{m''}{n''}$ with each of its parents. In a similar way we can generate the Farey tree to any desired level.

We can generate all positive rationals by taking the initial rationals

$$\frac{0}{1}, \frac{1}{0}, \tag{3.74}$$

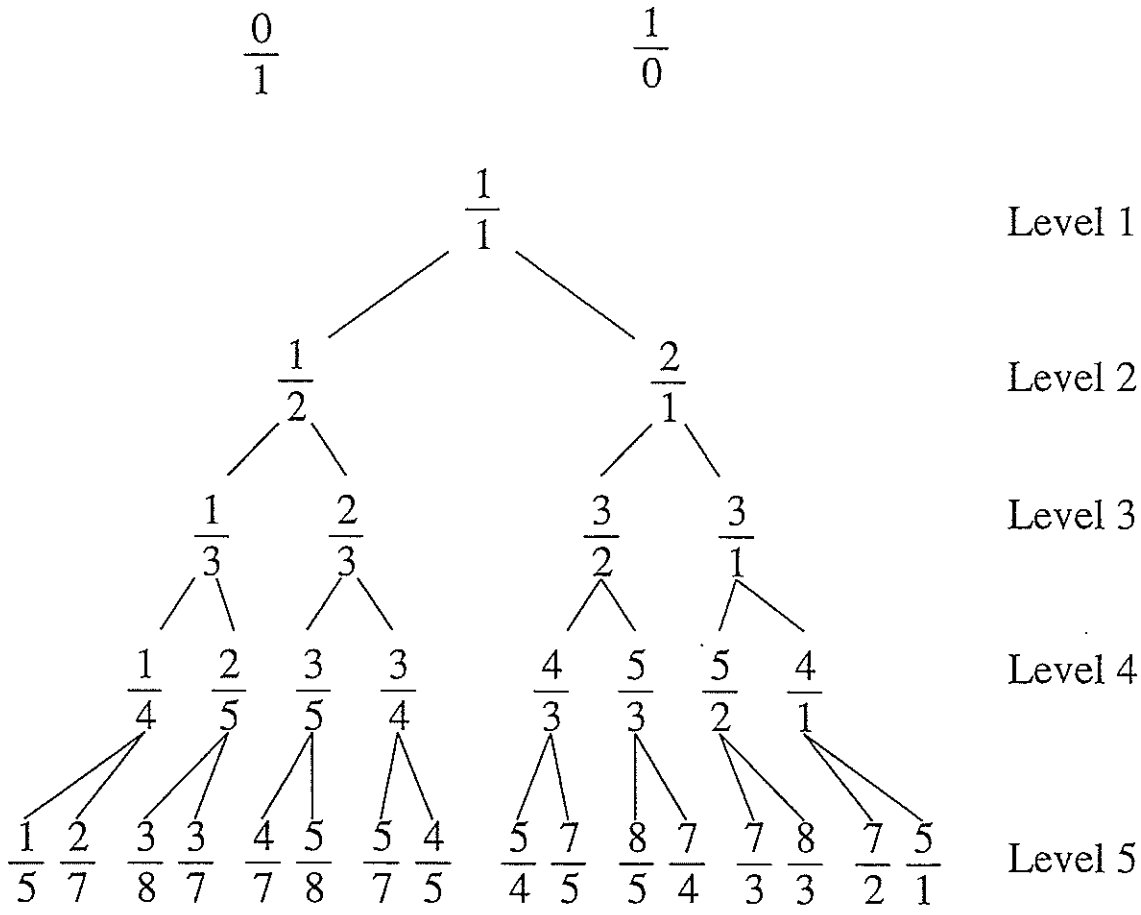

Figure 3.9: The first five levels of the Farey tree

as indicated in figure 3.9.

The Farey path for a number is the path taken in the Farey tree from $\frac{1}{1}$ to the specified number expressed in the form LLRLRRLRRL. For example, the Farey path for $\frac{4}{7}$ is LRLL. Each rational number has a unique Farey path, and the Farey path for an irrational is infinite. Infinite Farey paths that end in a string of L's or R's correspond to irrationals that converge to rationals. Numbers represented by a Farey path that ends in a string of ...RLRLRL... are the noble numbers. We expect that the golden mean can be represented by the Farey path LRLRLRLRLRLRLR...

An interesting relationship between the Farey tree and the continued fraction representation of a number is that the number $n = p/q$ appears on the ith level of the Farey tree if the elements of the continued fraction representation $p/q = [a_0, a_1, a_2, \ldots, a_n]$ sum to i, that is

$$i = \sum_{j=1}^{n} a_j. \tag{3.75}$$

The Farey tree approximates to a number (generated by truncating the Farey tree at any given level) appear to converge more slowly than the continued frac-

tion convergents. The best approximates to a number appear in the Farey tree approximates, along with many other rationals.

3.7.3 Higher Dimensional Number Theory

The previous consideration of the continued fraction and Farey path representation of numbers is only directly of relevance to dynamical systems with one degree of freedom. In chapter 4 we will consider a Hamiltonian system with 2 degrees of freedom and thus we should examine some analogues of the above number theory to such systems.

Two Dimensional Farey Tree

In dynamical systems with two degrees of freedom the idea corresponding to the winding number in a one degree of freedom system is the two component winding number. We wish to generate a sequence of pairs of rationals with the same denominator $(a/b, c/b)$ that converge to a pair of irrationals, (ω_1, ω_2). We can associate with each pair of rationals a 3−vector

$$(\omega_1, \omega_2) = \left(\frac{a}{b}, \frac{c}{b}\right) \rightarrow (a, c, b), \tag{3.76}$$

and we require a method of approximating (ω_1, ω_2) by a similar process to the representation of any real number by a series of rationals, or the approximation of reals by paths on the Farey tree.

Kim and Ostlund [9] considered this problem, and developed the two dimensional Farey tree to represent two component winding numbers. We represent their process graphically in figure 3.10.

We represent pairs of rationals from the first seven levels of the two dimensional Farey tree on the x, y plane in figure 3.11.

3.8 Converse KAM Theory

While we are interested in where KAM surfaces exist bounding or partially bounding trajectories motion through the phase space, we are often interested in knowing where KAM surfaces do not exist, that is, a non-existence criterion. This problem is the province of Converse KAM theory, and various methods have been developed to give estimates of various values of parameters at which KAM surfaces do not exist.

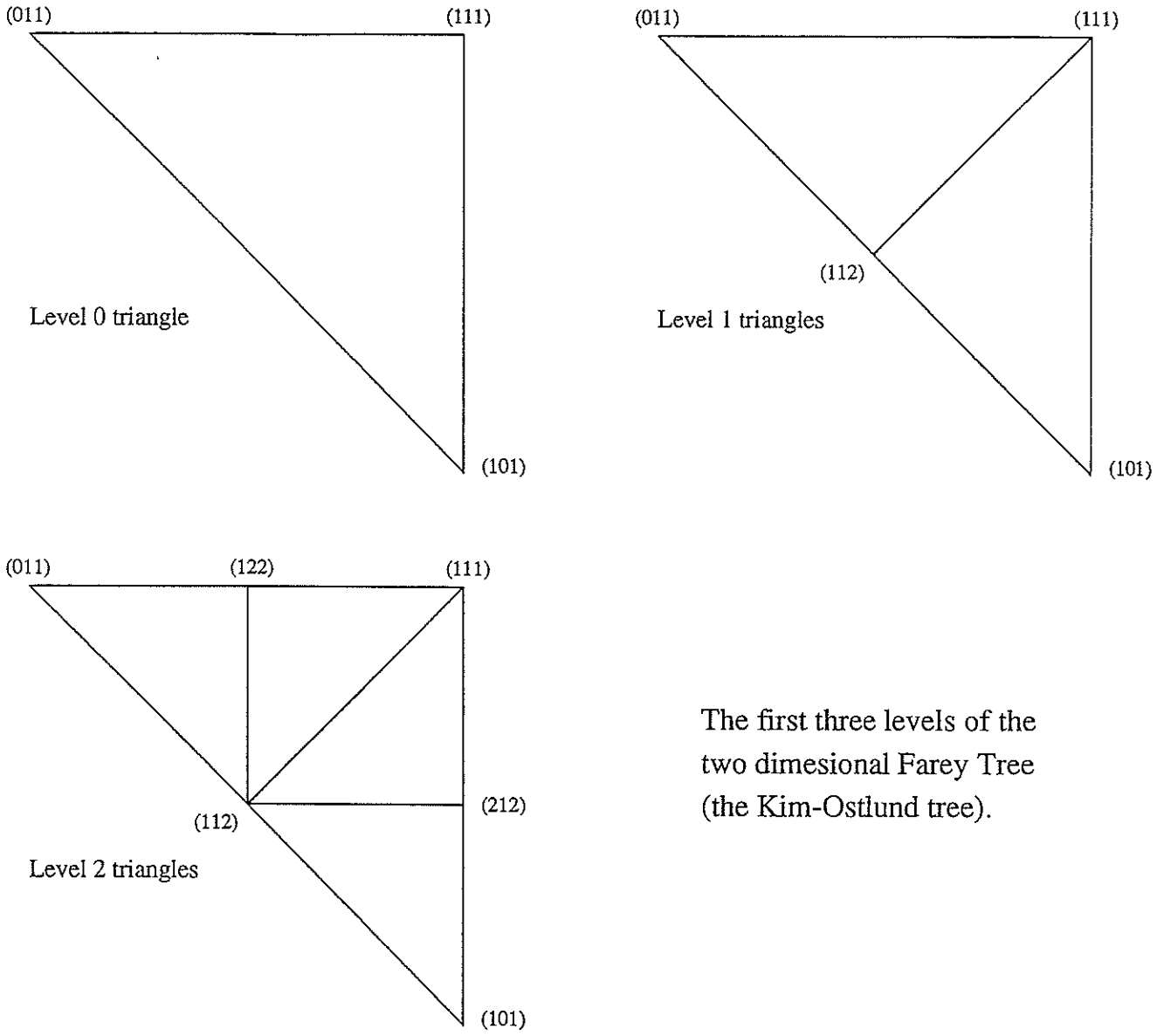

Figure 3.10: Two dimensional Farey tree.

3.8.1 Chirikov Overlap Criterion

A vigorous estimation of when KAM surfaces do not exist was made by Chirikov, in his resonance overlap criteria developed in 1979 [2]. Chirikov considered that if the stochastic separatrix of two resonances overlap then no KAM torus between the resonances can exist. If the separatrix surrounding the primary resonance overlaps itself then no KAM torus in the phase space will exist.

Chirikov approximated the standard map by the pendulum Hamiltonian

$$H = \frac{y^2}{2} + k\cos\theta, \tag{3.77}$$

in the vicinity of two resonance islands. As k varies, the stable manifold of one resonance island intersects the unstable manifold of the other island in a heteroclininc

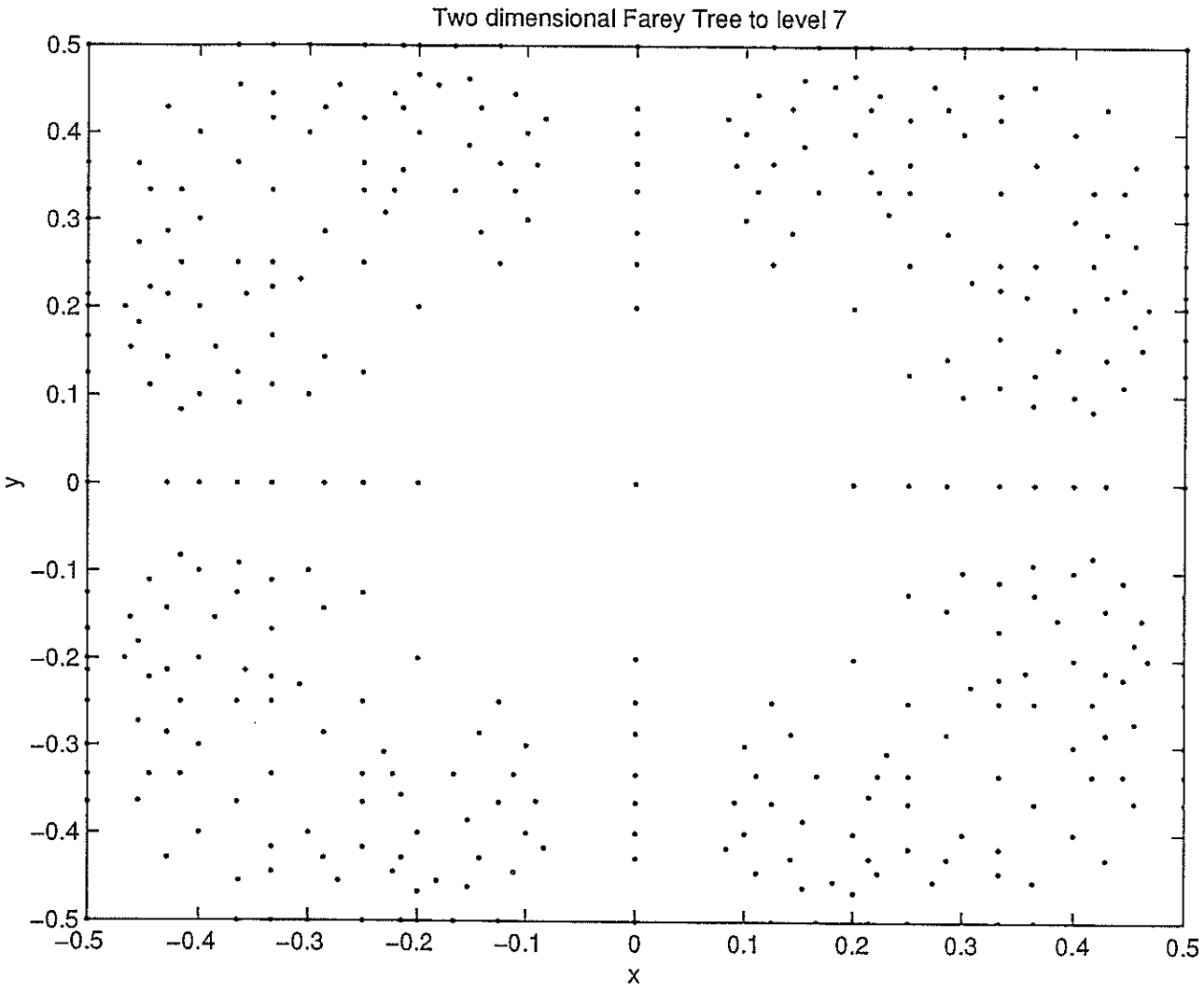

Figure 3.11: The first seven levels of the two dimensional Farey tree

intersection, and there cannot be any KAM tori between these islands. This method results in an approximation of k which may be improved if higher order resonances are considered.

3.8.2 Mather's ΔW Criterion

KAM tori bound trajectories motion. Thus, if we examine the flux through periodic orbits the winding numbers of which converge to the irrational winding number of the KAM torus, we can determine if a KAM torus exists with that irrational winding number. If the flux through the period orbits converges to a non-zero number, then there can be no KAM torus with that irrational winding number. The ΔW in the title of the criterion is related to the flux.

Chapter 4

A Coupled Standard Map

The one degree of freedom standard map has attracted a lot of research attention as it displays various aspects of the transition to chaos in many nonlinear dynamical systems as one parameter is varied [13, 20, 21, 28].

Various mathematical models of physical systems can be derived by coupling together standard maps. Froschle [4, 5] introduced a two degree of freedom symplectic map that models the time evolution of elliptic galaxies, a model that has been studied by Kook and Meiss, who examined the periodic orbits of the map, MacKay, Meiss and Stark, who used it to test their non-existence criterion for KAM tori, and Kaneko and Bagley [8], who examined Arnol'd diffusion. Robins [22] examined the application of Greene's residue criterion to Froechle's map.

We introduce a different map that models the interaction of a laser with atoms in a magneto-optical trap. The atoms are cooled, spatially localised in the trap, and periodically kicked by a laser. An introduction to the cooling and localisation of atoms in a magneto-optical trap may be found in [18]. Just as we wish to determine the orbits' rate of transport and the portion of the phase space they can visit in the two dimensional standard map for various values of the stochasticity parameter K, it is of interest to determine the same for orbits in the four dimensional phase space for various values of K and the coupling parameter.

Our four dimensional map is as follows

$$I_{n+1} = I_n + \frac{K}{2\pi}\sin 2\pi\theta_n + \frac{b}{2\pi}\sin \pi\theta_n \cos \pi\psi_n, \tag{4.1}$$

$$\theta_{n+1} = \theta_n + I_{n+1}, \tag{4.2}$$

$$J_{n+1} = J_n + \frac{K}{2\pi}\sin 2\pi\psi_n + \frac{b}{2\pi}\sin \pi\psi_n \cos \pi\theta_n, \tag{4.3}$$

$$\psi_{n+1} = \psi_n + J_{n+1}, \tag{4.4}$$

where we often take $\theta, \psi \pmod 1$, and for convenience in plotting phase space diagrams, $I, J \pmod 1$ as well.

This map is volume preserving, as the Jacobian is

$$\mathcal{J} = \begin{pmatrix} 1 & K\cos 2\pi\theta_n + \frac{b}{2}\cos\pi\theta_n\cos\pi\psi_n & 0 & -\frac{b}{2}\sin\pi\theta_n\sin\pi\psi_n \\ 1 & 1 + K\cos 2\pi\theta_n + \frac{b}{2}\cos\pi\theta_n\cos\pi\psi_n & 0 & -\frac{b}{2}\sin\pi\theta_n\sin\pi\psi_n \\ 0 & -\frac{b}{2}\sin\pi\psi_n\cos\pi\theta_n & 1 & K\sin 2\pi\psi_n + \frac{b}{2}\cos\pi\psi_n\cos\pi\theta_n \\ 0 & -\frac{b}{2}\sin\pi\psi_n\cos\pi\theta_n & 1 & 1 + K\sin 2\pi\psi_n + \frac{b}{2}\cos\pi\psi_n\cos\pi\theta_n \end{pmatrix},$$

and a straightforward, though time consuming, calculation shows that $\det\mathcal{J} = 1$.

We note that this four dimensional map may be obtained by coupling together two standard maps. In the uncoupled standard map Chirikov numerically determined that the last KAM torus is destroyed for $K \approx 0.989$ [2], and Greene refined this approximation to $K \approx 0.971635406$ using the residue criterion [21]. As KAM tori are the only features of the phase space which bound orbits for all time, an orbit that finds itself in any chaotic region of the phase space will, in principle, be able to visit any other chaotic region of the phase space. The union of the chaotic regions of the phase-space for $K \geq 0.971635406$ has been amusingly and evocatively termed the 'stochastic sea' [20]. For values of K just greater than 0.971635406, the remnants of the destroyed KAM tori, the cantori, still tend to partially restrict transport to other regions of the phase space, and thus orbits may take an incredibly long time, on average, to traverse the stochastic sea.

In order to determine the value of K at which the last KAM torus is destroyed, Chirikov used the fact that if the last KAM torus exists, an orbit that is at some point in time 'above' or 'below' that KAM torus in the phase space will never be able to traverse that KAM torus. For various values of $K \geq 0.989$ Chirikov calculated the average number of iterations of the map numerous initial conditions took to traverse the last surviving KAM torus - the KAM torus with golden mean winding number. If we designate K_{crit} as the value of K at which the last KAM torus is destroyed, and N as the average number of iterations of the map the various initial conditions take to traverse the last surviving KAM torus, then for $K < K_{crit}$, $N = \infty$, and

$$N(K) \to \infty, \tag{4.5}$$

as

$$K \to K_{crit+}. \tag{4.6}$$

Chirikov found that $N(K) \to \infty$ as $K \to 0.989$, and thus concluded that the last KAM torus is destroyed for $K \approx 0.989$. It is likely that K_{crit} is actually an irrational number. We refer the reader to figure 5.3 in Chirikov [2] for a graph of the relationship between N and various values of K in the 2−dimensional standard map.

It is interesting to note from figure 5.3 in [2] that the average number of iterations of the map the numerous initial conditions take to traverse a certain distance in the phase space appears to be a function of the stochasticity parameter K. While the precise meaning of this relationship is not clear, it appears valid to apply this algorithm to other maps to obtain respective realtionships between N and K. We refer to Chirikov's algorithm as a 'characteristic transport time' algorithm.

This characteristic transport time algorithm employed by Chirikov naturally lends itself to application to other maps, and in particular to other maps that appear similar to the two dimensional standard map. We can then naturally employ this algorithm to our four dimensional map to determine how various values of the coupling parameter affect the motion of orbits through the phase space, and for what values of the coupling for various values of K is the last KAM torus destroyed.

We have applied a characteristic transport time algorithm to our four dimensional map and found what appears to be a definite relationship between the average number of iterations numerous (2500) initial conditions take to move a certain distance in the phase space for various values of b for each value of K.

For each value of K and b we started the 2500 initial conditions evenly distributed in the region of the phase space bounded by

$$0.45 \leq \theta, \psi \leq 0.55, \tag{4.7}$$

$$-0.01 \leq I, J \leq 0.01, \tag{4.8}$$

and iterated the map until the orbit corresponding to each initial condition moved beyond the region of the phase space bounded by

$$-0.5 \leq I, J \leq 0.5, \tag{4.9}$$

or expressing it slightly differently,

$$||I, J||_1 > 0.5, \tag{4.10}$$

where $||\cdot||_1$ is the norm defined by $||x_1, x_2, \ldots, x_n||_1 = \max_i |x_1, x_2, \ldots, x_n|$.

We then calculated the average number of iterations of the map that was required for the 2500 initial conditions to satisfy this last condition, and found that there appears to be a fairly strong relationship between N and b for each K.

As an analogy to the two dimensional standard map, if $||I, J||_1 > 0.5$, we know that the orbit will have traversed the last surviving KAM torus and it will be able to traverse, in principle, the entire stochastic sea.

We have applied the characteristic transport time algorithm to our four dimensional map for $K = 1.0$ and $0.01 \leq b \leq 1.00$ to determine whether we can find a definite relationship between N, and b, and we have graphed $\log_{10}(N)$ against b in figure 4.1.

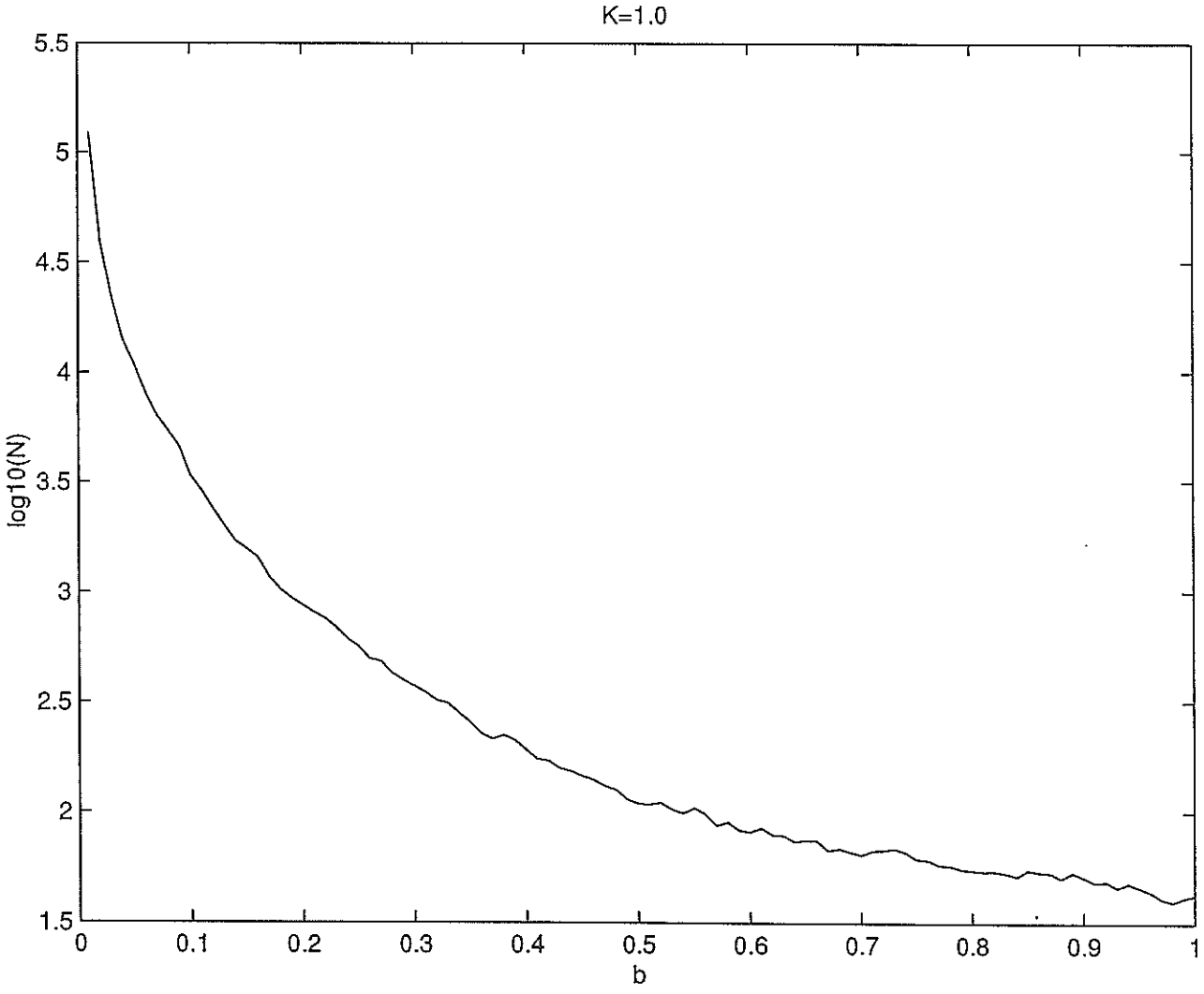

Figure 4.1: 'Characteristic transport times' for 2500 particles vs b

There appears to be a very strong relationship between N and b, and scaling the horizontal axis to $\log_{10}(100b)$, we obtain the interesting graph in figure 4.2.

Using linear regression we have obtained an equation that appears to moderately fit the graph in figure 4.1 of the form

$$\ln(N) = 1.9015 - 0.5290\ln(b), \tag{4.11}$$

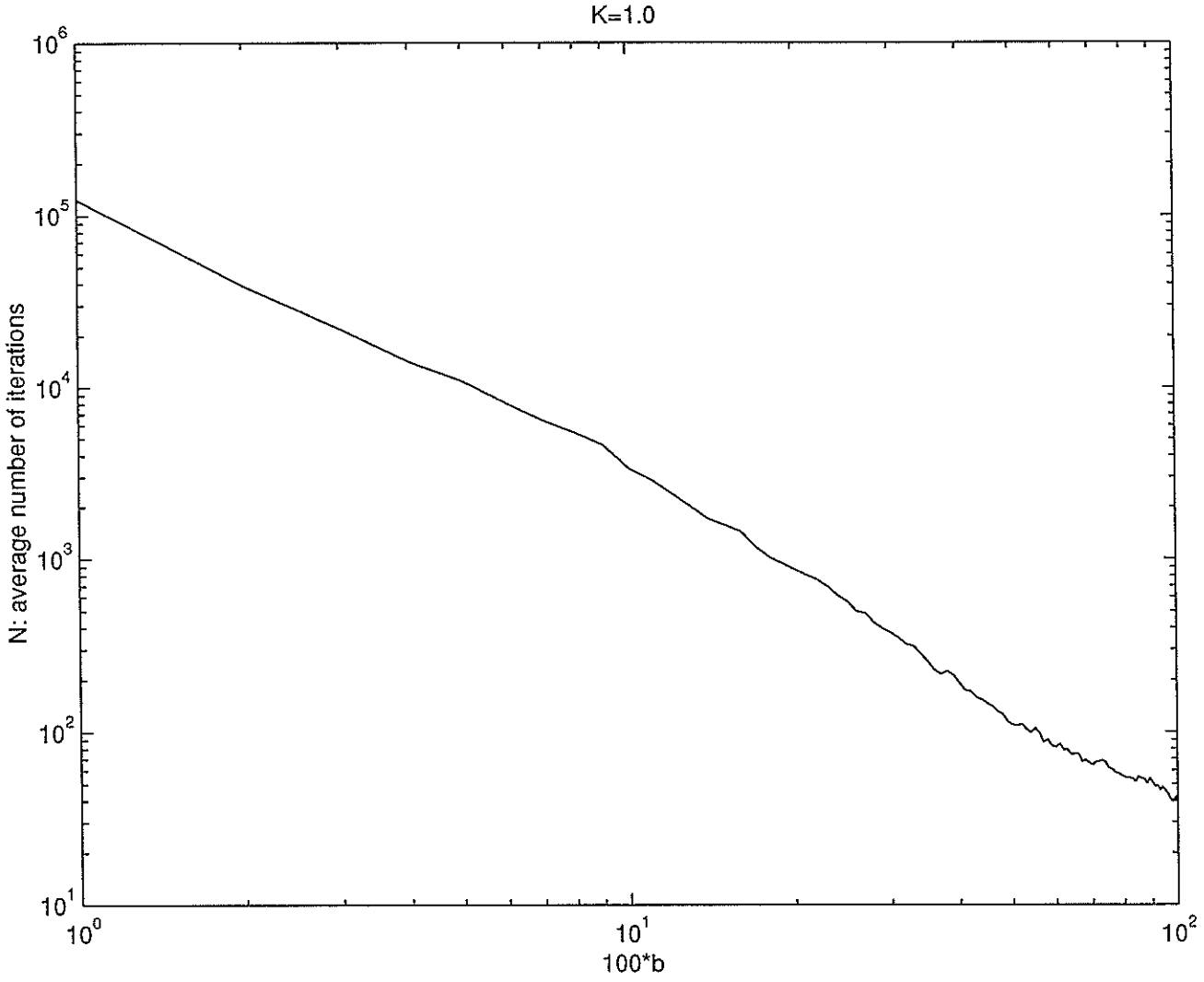

Figure 4.2: 'Characteristic transport times' for 2500 particles vs $\log_{10}(100b)$

and we overlay the graph of this equation on the numerical data in figure 4.3.

To confirm the results shown in figure 4.1 we applied the characteristic transport time algorithm for $1.1 \leq K \leq 2.0$ and $0.01 \leq b \leq 1.00$, the results of which are graphed together with the results for $K = 1.0$ in figure 4.4.

We plot the analogue of figure 4.2 for $1.0 \leq K \leq 2.0$ in figure 4.5.

As $m \to \infty$ (uncountable), where m is the number of initial conditions, and $||b_{i+1} - b_i||_1 \to 0$, we obtain a smooth ($C^r$, where $r \in \mathbb{N}$) curve in the graph in figure 4.1. We give an indication of this by applying a characteristic time algorithm for $K = 2.0$ for 2500 and 5000 initial conditions in figure 4.7 and 4.8, respectively.

We note that all KAM tori have been destroyed for $K \geq 1.0$, and thus the above results give an indication of how rates of transport through the phase space are affected by various values of the coupling b.

We now turn to the problem of the existence of the last KAM torus for $K < K_{crit}$

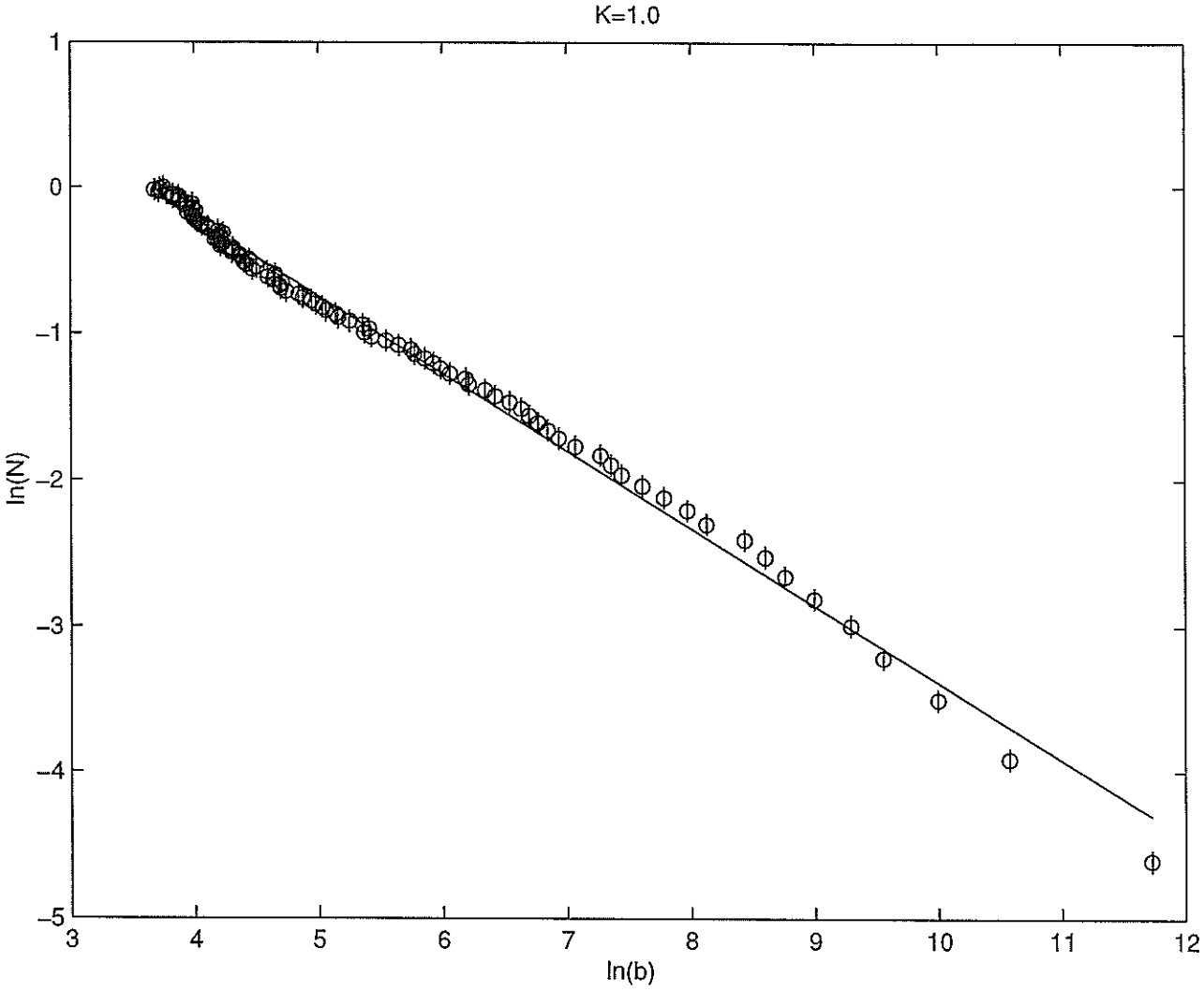

Figure 4.3: Overlay of the equation 4.11 on the numerical data for $K = 1.0$

and nonzero b by attempting to numerically determine when the last KAM torus is destroyed using a characteristic transport time algorithm. It is reasonable to suggest that for each $K < K_{crit}$ there is $b > 0$ for which the last KAM torus is destroyed. We thus expect to obtain plots that are fairly similar to figure 4.1 for any value of $K < K_{crit}$ and b we wish to choose. We give an example of a plot similar to that in figure 4.1 for $K = 0.1, 0.0033 \leq b \leq 0.5000$ in figure 4.8. We expect from the foregoing that there exists a $b_0 > 0$ such that $N = \infty$ for $b < b_0$. Now b_0 may be very small and thus difficult to determine numerically, but we believe that it exists.

Analytic results suggest that whatever value b_0 has, we cannot simply determine it by the relation

$$N(b) \to \infty,$$

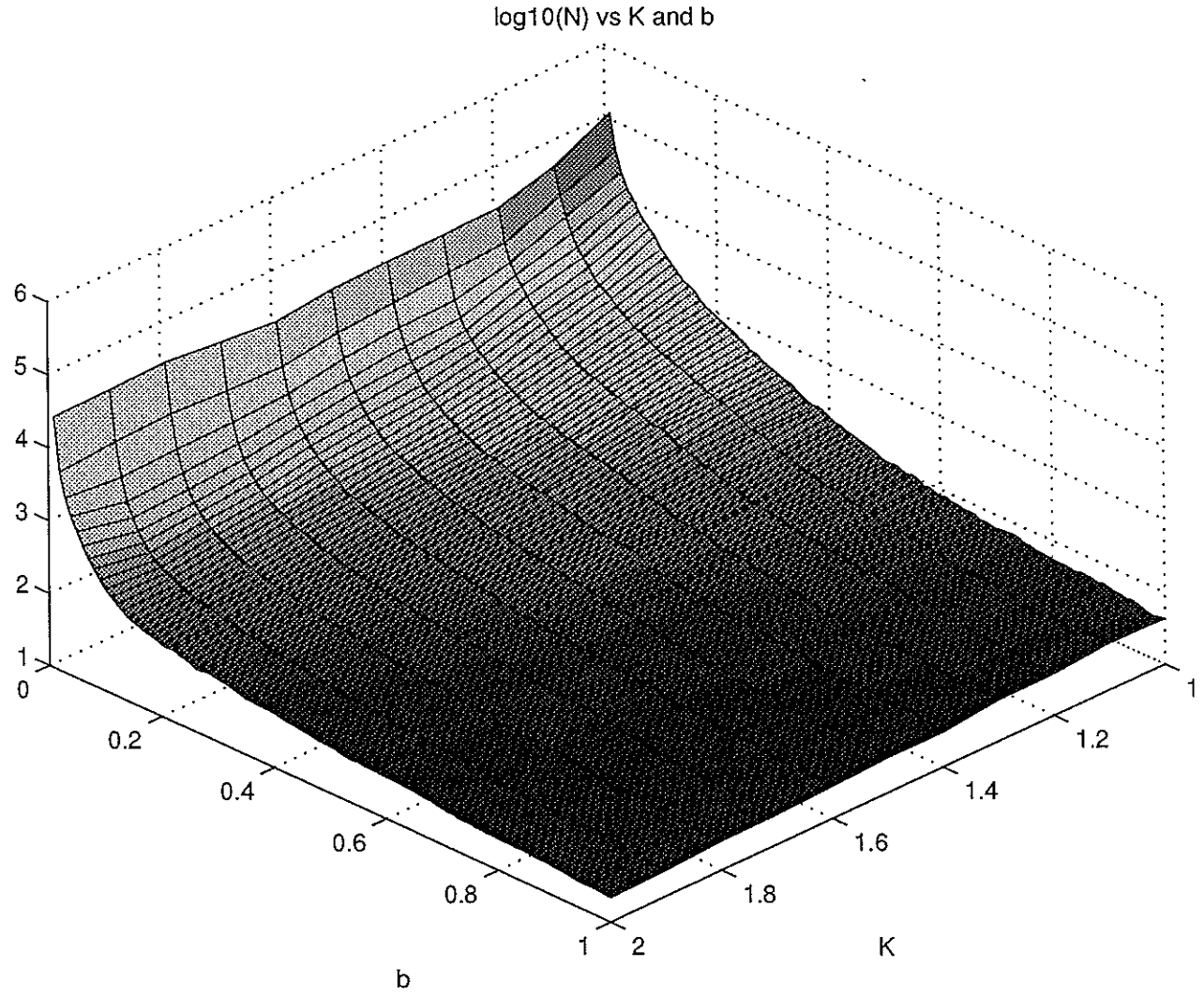

Figure 4.4: 3−dimensional plot of $\log_{10}(N)$ vs K and b

as

$$b \to b_{0+},$$

as there exists another form of transport through the phase space not previously discussed, the 'Arnol'd diffusion' (which will be discussed in chapter 5). This Arnol'd diffusion has the effect on the plot that

$$N(b) < \infty, \tag{4.12}$$

for

$$b > 0. \tag{4.13}$$

As the rate of Arnol'd diffusion appears to be smaller than other forms of transport through the phase space (see chapter 5), we will not be surprised if the 'slope' of the

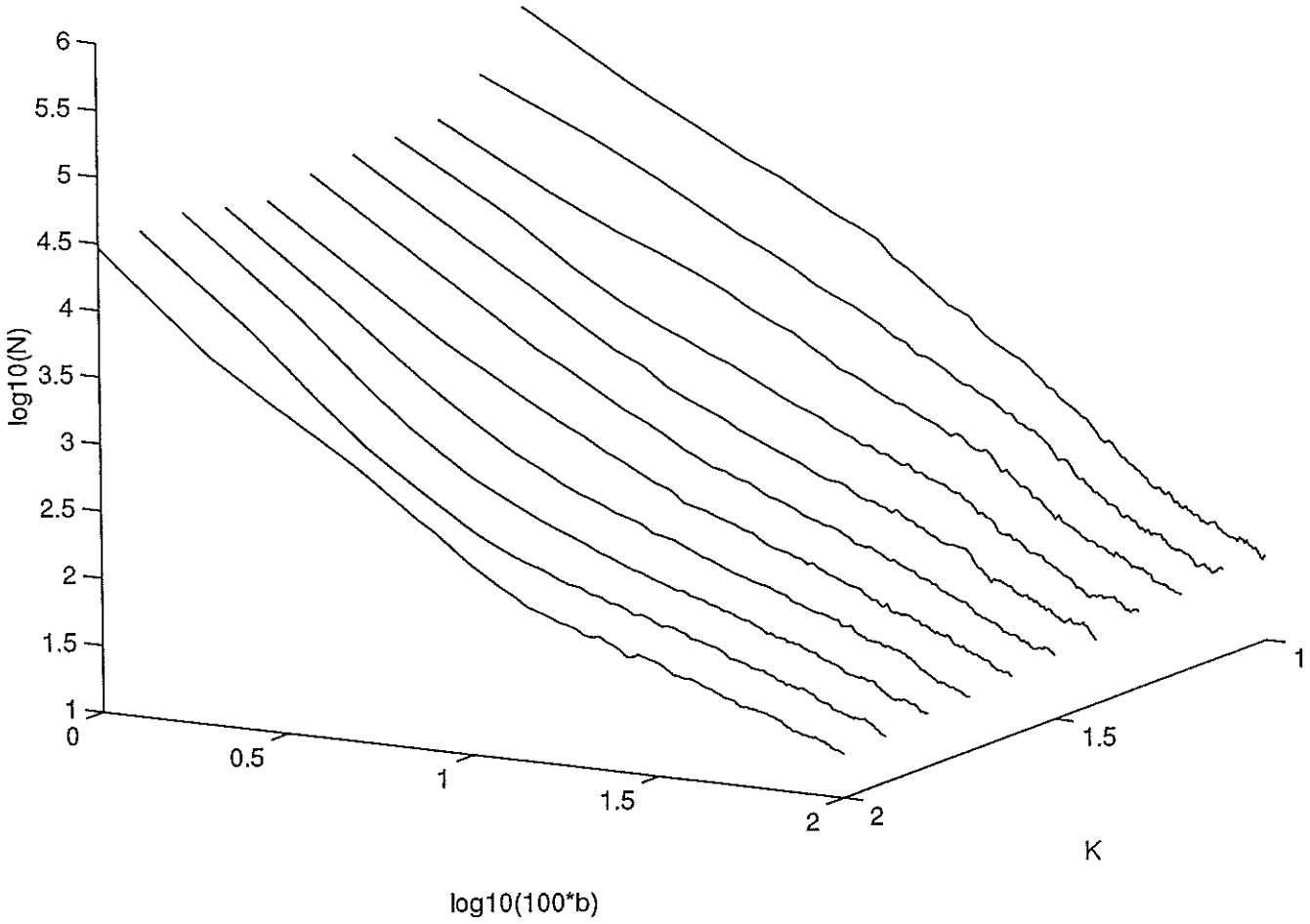

Figure 4.5: 3−dimensional analogue of figure 4.2

data in figure 4.8 appears to change from relatively fast transport rates for $b \geq b_0$ to much slower rates for $b < b_0$.

Applying linear regression, a relation between N and b may be found as follows

$$\ln(N) = 3.2813 - 2.2465\ln(b), \tag{4.14}$$

and this is illustrated in the linear regression fit in figure 4.9.

It is difficult to speculate from figures 4.8 and 4.9 if the last KAM torus is destroyed at any value of $b, 0.0033 \leq b \leq 0.5000$. It could be that the last KAM surface is destroyed at $b \approx 0.0050$. Further work on this required to completely determine the value of b at which the last KAM torus is destroyed.

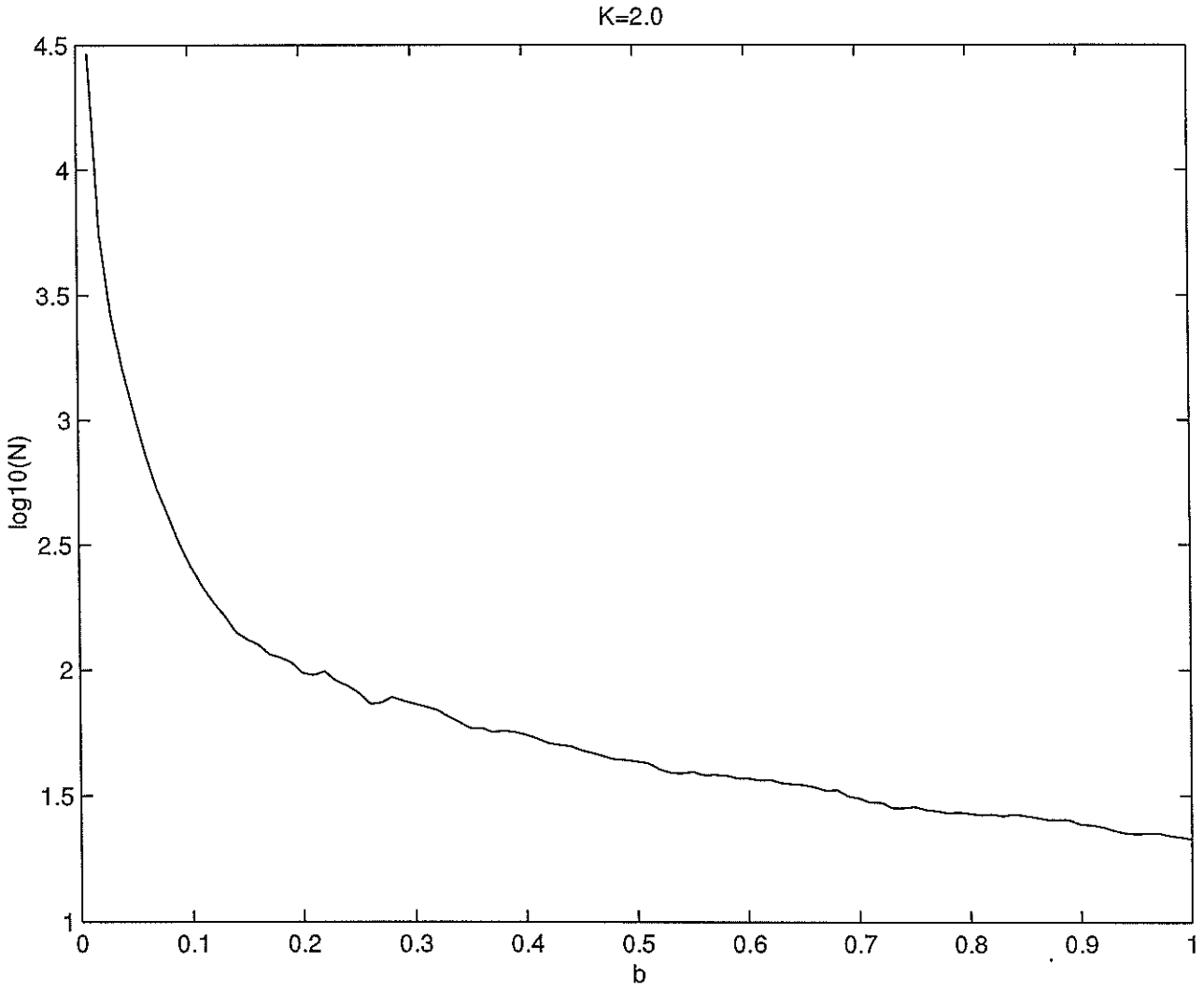

Figure 4.6: Characteristic transport time algorithm for K=2.0, 2500 initial conditions

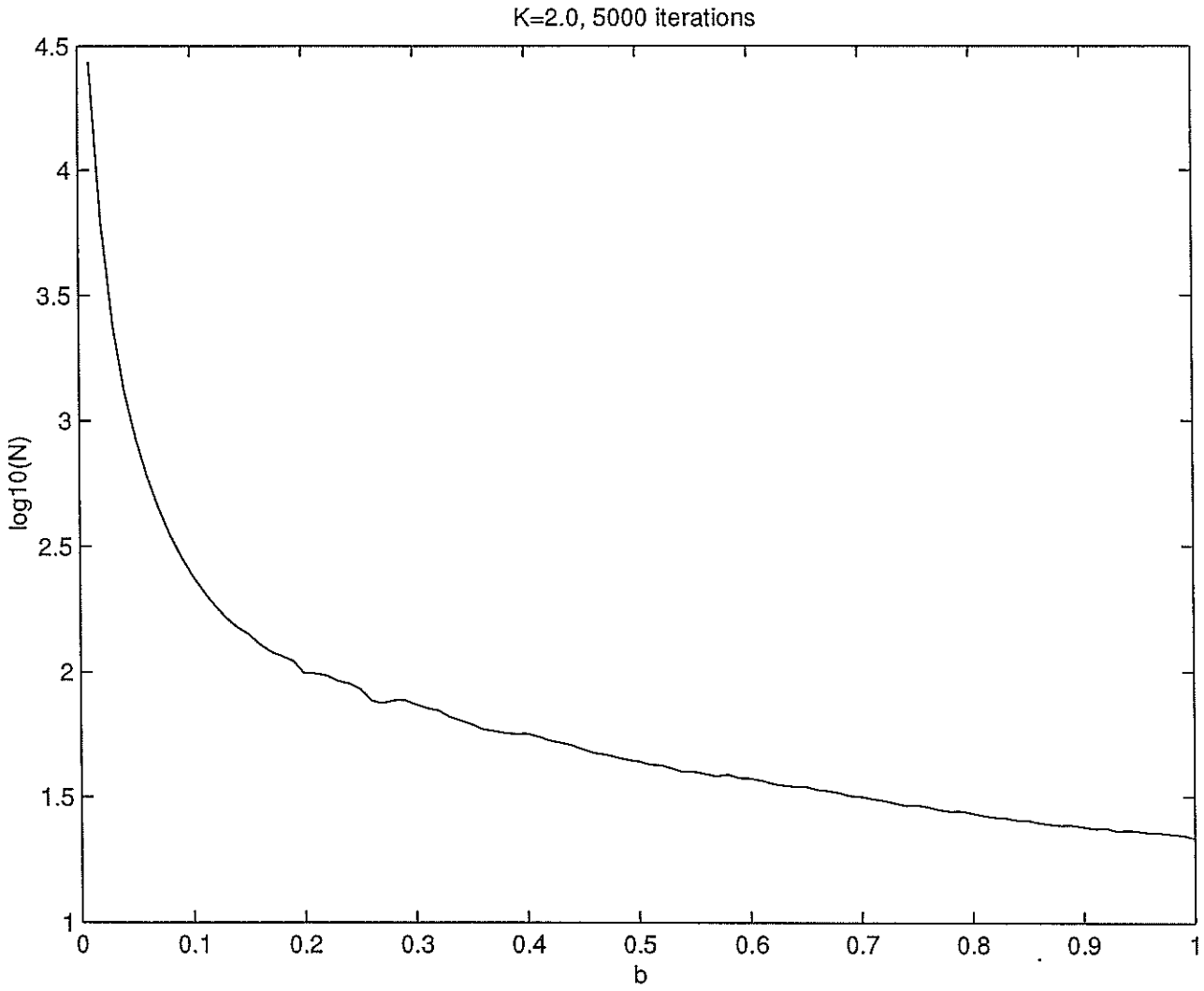

Figure 4.7: Characteristic transport time algorithm for K=2.0, 5000 initial conditions

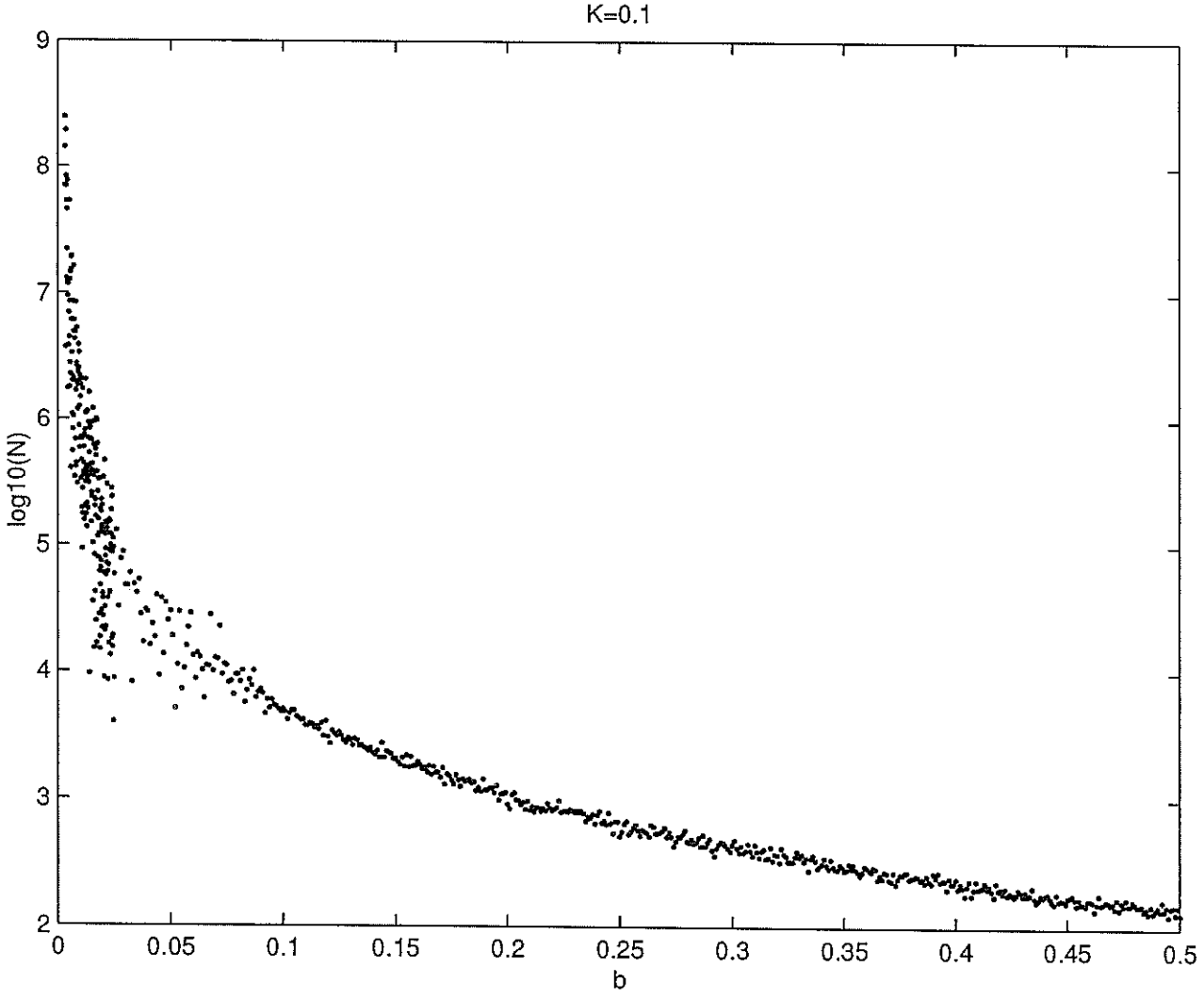

Figure 4.8: Plot of $\log_{10}(N)$ vs b, for $K = 0.1$, and $0.0033 \leq b \leq 0.5000$. 2500 particles were averaged for $0.1000 \leq b \leq 0.5000$, 25 particles were averaged for $0.0500 \leq b \leq 0.1000$, and 1 particle was used for $0.0033 \leq b \leq 0.0500$ as the time required for this algorithm is very large

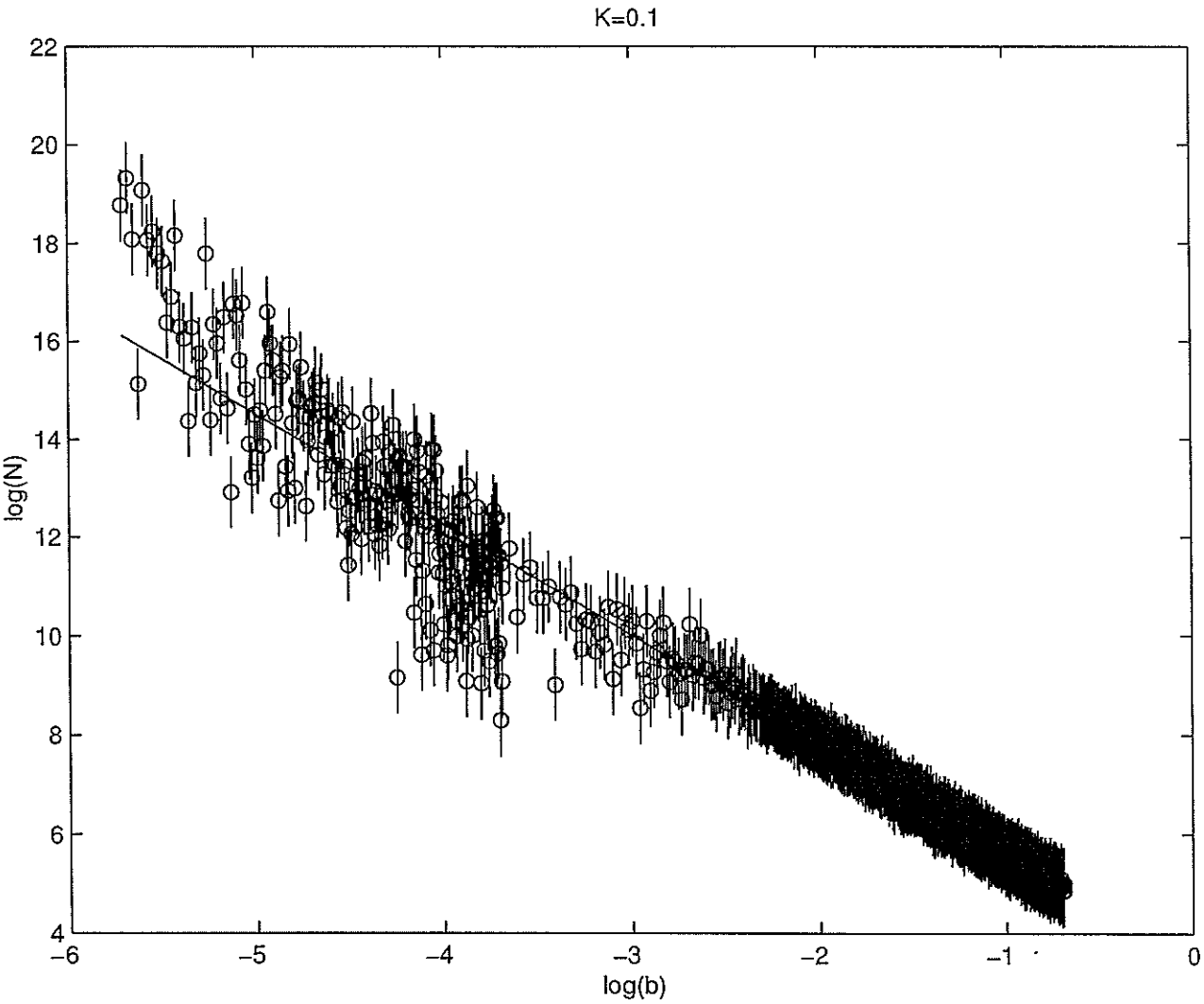

Figure 4.9: Data in figure 4.8 fitted to a curve by linear regression

Chapter 5

Arnol'd Diffusion in a Coupled Standard Map

5.1 Diffusion in Many Degrees of Freedom Hamiltonian Dynamical Systems

A particle's orbit through the phase space of a Hamiltonian system with N degrees of freedom is determined by the structure of the $2N$ dimensional phase space. If the system under consideration is isomorphic to a system of coupled standard maps we can consider the structure of its phase space by analogy and reference to the phase space of the one degree of freedom (uncoupled two dimensional) standard map.

In an integrable N degree of freedom Hamiltonian system we will have a countable collection of periodic orbits densely filling the phase space, and an uncountable collection of $N-$dimensional KAM tori separating the periodic orbits.

If our system is nearly integrable, and satisfies the conditions of the KAM theorem, we will have $N-$dimensional KAM tori, $N-$dimensional cantori, resonances surrounding the periodic orbits, and separatrices surrounding the resonances.

Orbits visit various regions of the phase space as orbits do in the standard map: they traverse the cantori and the separatrices, and get caught in resonances.

There is another avenue by which orbits can visit regions of the phase space - the so-called Arnol'd diffusion. In the $2N$ dimensional phase space regions of the phase space are separated by surfaces of dimensionality $2N-1$. The KAM tori are N-dimensional surfaces and thus, unlike their counterparts in a one degree of freedom system, do not separate regions of the phase space. An orbit may, for all autonomous systems with at least 2.5 degrees of freedom, move in a direction orthogonal to every element of the KAM tori, and thus not be bound by that torus.

By analogy, one dimensional surfaces (lines) in a three dimensional space do not separate regions of the space, and trajectories are free to wander the phase space; this is illustrated in figure 5.1.

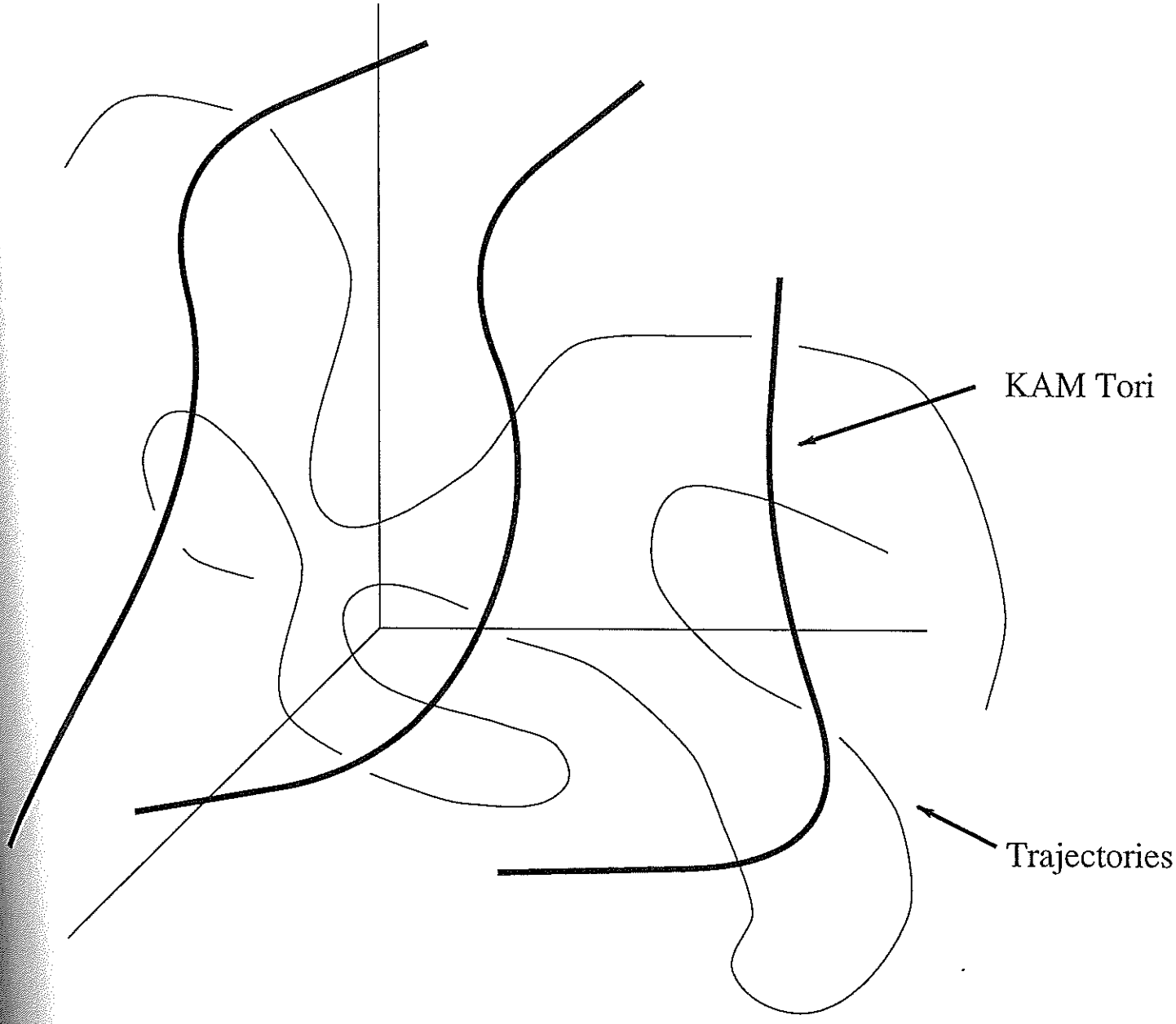

Figure 5.1: Figurative illustration of the idea of Arnol'd diffusion in a 3 dimensional phase space with 1 dimensional KAM tori

In our 4 dimensional map the 2 dimensional KAM tori do not separate regions of the phase space and thus Arnol'd diffusion can occur. We note, however, that the 'characteristic' time for Arnol'd diffusion appears to be of a greater order than for other forms of diffusion, and thus numerical investigations of Arnol'd diffusion may prove difficult [21].

Reichl states that in N-coupled two dimensional standard maps there exists Arnol'd diffusion for $N > 1$ and all nonzero coupling. We are thus motivated to numerically investigate the possibility of Arnol'd diffusion for small K and small coupling in the four dimensional map.

5.2 Possible Arnol'd Diffusion in the Four Dimensional Map

In order to be certain of the nature of certain diffusion through the phase space (that is, whether it is Arnol'd diffusion), we need to be sure of the existence of KAM tori in the relevant regions of the phase space. Only with knowledge of the existence of certain KAM tori can we entertain the possibility of Arnol'd diffusion.

As an example of this problem, we refer to the article of Kaneko and Bagley [8], who claim to demonstrate Arnol'd diffusion in a coupled standard map. However, as Robins [22] points out, they fail to demonstrate the existence of KAM tori, and thus we cannot be sure that their 'Arnol'd diffusion' is actually that.

Interest in the existence of KAM tori has motivated research into various methods by which the existence of these tori can be shown. Robins [22] has examined applying Green's residue criterion in the two dimensional reversible, symplectic twist maps, to four dimensional reversible, symplectic maps and has shown that there is a relationship between the residues associated with various orbits and the Farey-tree approximates to the winding number associated with that periodic orbit.

The KAM theory guarantees the existence of some KAM tori for small enough K and b. Setting $K = 0.001$ in the uncoupled map ensures that KAM tori fill most of the phase space, and we can be confident that an orbit will be trapped between two KAM tori provided that it is sufficiently far from the primary resonance. If we now set $b = 0.001$, we have some interaction between the (I, θ), and (J, ψ) co-ordinates of the particle.

Say we consider the particle in the four dimensional phase space by projecting the (I, θ) co-ordinates onto a plane, and the (J, ψ) co-ordinates onto a different plane. Given the small coupling, we can think of each plane as representing a slightly perturbed standard map.

Now, say the particle is trapped between KAM tori in the (I, θ) and (J, ψ) planes. We may find, due to the interaction between the co-ordinates established by the coupling, that the (I, θ) or (J, ψ) co-ordinates may suddenly 'jump' to a new region in the appropriate plane beyond the KAM tori that previously guided the

orbit.

If we are certain that KAM tori exist in the original region of the plane the orbit traversed, we then have an example of Arnol'd diffusion.

As the KAM theorem guarantees the existence of KAM tori for small enough K, b, we choose K and b to be very small, $K = 0.001, b = 0.001$, and give an example of what may well be Arnol'd diffusion in figures 5.2 and 5.3.

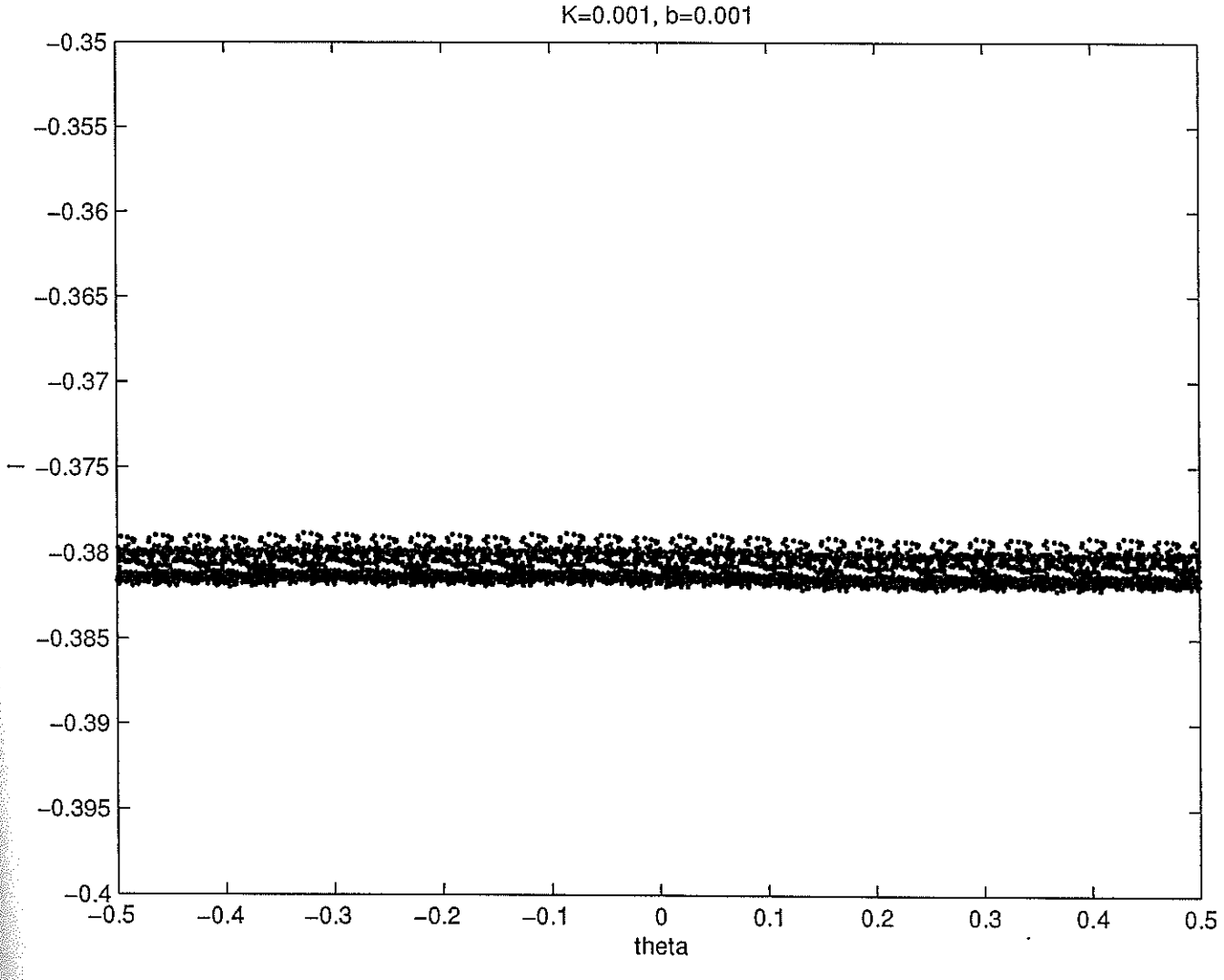

Figure 5.2: Possible Arnol'd diffusion in the I, θ space, 5000 iterations

We know that Arnol'd diffusion has been shown to exist analytically in certain systems. These analyses have shown that Arnol'd diffusion does not occur in random directions, but along resonance channels, the union of which (the Arnol'd web) densely fills the phase space [17, 21, 28].

We thus have the interesting property in our dynamical systems that an orbit can come arbirarily close to any point in the phase space, given enough time. Of course, this 'given enough time' requirement is crucial, as it may be the case that

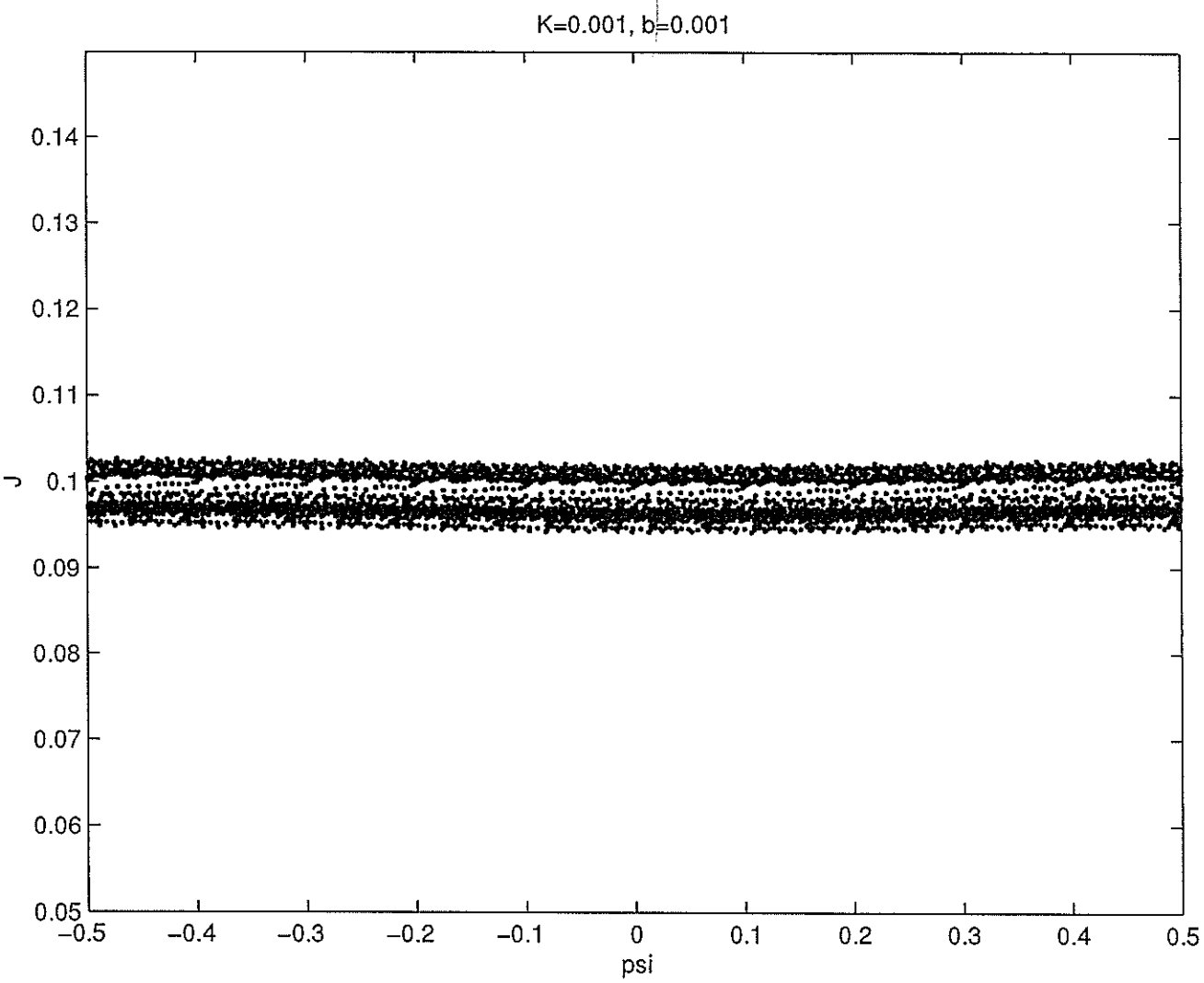

Figure 5.3: Possible Arnol'd diffusion in the J, ψ space, 5000 interations

the 'characteristic transport rates' through the Arnol'd web may be well in excess of the life of the system, in which case such diffusion is of less practical importance than other forms of diffusion.

We note that it is possible to analytically determine the resonance channels, and we determine the primary resonance channels of the Arnol'd web for our map in the next section.

5.3 Calculation of the Primary Resonance Channels in the Arnol'd Web

In this section we follow the method of Reichl [21] to find the primary resonance channels of the Arnol'd web for our four dimensional map.

The Hamiltonian for the coupled map may be written

$$H = \frac{1}{2}I^2 + \frac{1}{2}J^2 + \left(\sum_{M=-\infty}^{\infty} \delta(t-M)\right)\left(\frac{K}{2\pi}(\cos 2\pi\theta + \cos 2\pi\psi)\right) +$$

$$\left(\sum_{M=-\infty}^{\infty} \delta(t-M)\right)\left(\frac{b}{2\pi}(\cos\pi(\theta-\psi) - \cos\pi(\theta+\psi))\right). \tag{5.1}$$

We transform this non-autonomous two degree of freedom system to an autonomous three degree of freedom system by introducing canonical variables $(p, x = t)$ as follows

$$H = \frac{1}{2}I^2 + \frac{1}{2}J^2 + p + \sum_{M=-\infty}^{\infty}\left(\frac{K}{(2\pi)^2}\cos 2\pi(\theta - Mx) + \frac{K}{(2\pi)^2}\cos 2\pi(\psi - Mx)\right) +$$

$$\sum_{M=-\infty}^{\infty}\left(\frac{b}{(2\pi)^2}\cos\pi(\theta - \psi - Mx) - \frac{b}{(2\pi)^2}\cos\pi(\theta + \psi - Mx)\right) = E. \tag{5.2}$$

For small K, b we can approximately locate the primary resonance channels. The unperturbed Hamiltonian is $H_0 = \frac{1}{2}I^2 + \frac{1}{2}J^2 + p = E_0$, which gives rise to a partial energy surface

$$p = E_0 - \frac{1}{2}I^2 - \frac{1}{2}J^2, \tag{5.3}$$

which is a two dimensional surface. The resonance conditions are

$$\dot{\psi} - M\dot{x} = \dot{\theta} - M\dot{x} = \dot{\theta} - \dot{\psi} - M\dot{x} = \dot{\theta} + \dot{\psi} - M\dot{x} = 0. \tag{5.4}$$

For small K and b, $\dot{\theta} \approx \frac{\partial H_0}{\partial I} = I, \dot{\psi} \approx \frac{\partial H_0}{\partial J} = J$, and $\dot{x} \approx \frac{\partial H_0}{\partial p} = 1$. Thus the conditions for the primary resonance channels are $I = M, J = M, I + J = M$, and $I - J = M$.

As M is an integer and $-\infty < M < \infty$, we have a countable infinity of primary resonance channels. Those that appear in the I, J space ($|I, J| \leq 1$) are represented in figure 5.4.

We compare our primary resonance channels with those of the map of Froschle [21] in figure 5.5.

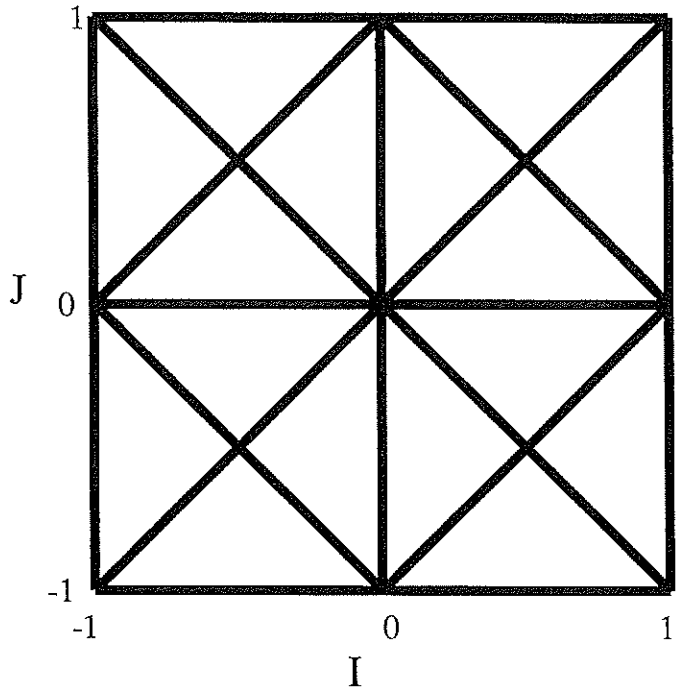

Figure 5.4: Primary resonance channels of the Arnol'd web in the I, J space

Froschle's map is given by the Hamiltonian

$$H = \frac{I^2}{2} + \frac{J^2}{2} + p + \sum_{M=-\infty}^{\infty} \left(\frac{K_1}{(2\pi)^2} \cos\{2\pi(\theta - Mx)\} + \frac{K_2}{(2\pi)^2} \cos\{2\pi(\psi - Mx)\} \right) +$$

$$+ \sum_{M=-\infty}^{\infty} \left(\frac{b}{(2\pi)^2} \cos\left(2\pi\{\theta + \psi - Mx\}\right) \right). \tag{5.5}$$

More analysis reveals the existence of a collection of higher order resonance channels the union of which densely fill the phase space. Meiss [17] states that each resonance is located at the intersection of an infinite number of resonance channels.

The overlay of the Arnol'd web on the already incredibly complicated and detailed fractal structure of the four dimensional phase space challenges our powers of visualisation, and illustrates the complexity of dynamics in our four dimensional map.

5.4 An Analytic Calculation of Arnol'd Diffusion in the Four Dimensional Map

Having now shown an example of potential Arnol'd diffusion in section 5.2, and calculated the primary resonance channels of the Arnol'd web in section 5.3, we now

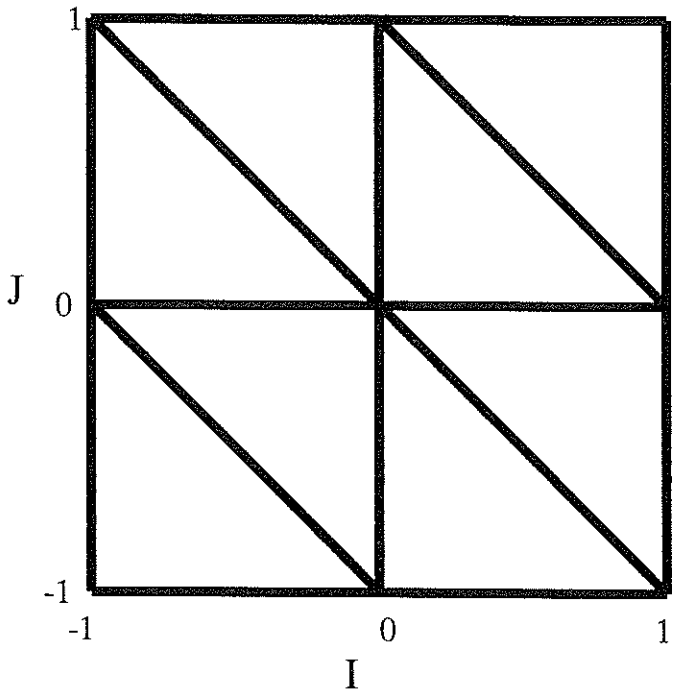

Figure 5.5: The primary resonance channels in Froschle's map

examine some tools that may allow us to analytically find rates of Arnol'd diffusion in the four dimensional map.

Here we examine a model introduced by Lieberman [14], and later used by Wang and Hu [26], and Wood, Lieberman, and Lichtenberg [27]: the stochastic pump model.

In the stochastic pump model it is assumed that the Hamiltonian can be separated into two parts for certain values of the parameters in the map.

Consider small K and b, and consider an orbit trapped between two KAM tori in the (I, θ) space, and within the separatrix surrounding the primary resonance in the (J, ψ). We can approximate the motion of the orbit in the (I, θ) space by

$$I_{n+1} = I_n, \tag{5.6}$$

$$\theta_{n+1} = \theta_n + I_{n+1} \pmod 1. \tag{5.7}$$

Now the above equations are correct for $b = 0$, but for b nonzero, the chaotic motion of the orbit in the separatrix in the (J, ψ) space affects, or 'pumps', the orbit in the (I, θ) space. In a similar manner the orbit in the I, θ space also 'pumps' the orbit in the separatrix, but this effect is very small, and is ignored.

We separate the Hamiltonian for the four dimensional map into two parts: the first describes the motion of a particle on a KAM torus in the (I, θ) space, and the second describes the motion of a particle in the separatrix surrounding the primary resonance in the (J, ψ) space.

Reiterating, our map is

$$\begin{aligned} I_{n+1} &= I_n + \frac{K}{2\pi}\sin 2\pi\theta_n + \frac{b}{2\pi}\sin\pi\theta_n\cos\pi\psi_n, \\ \theta_{n+1} &= \theta_n + I_{n+1}, \\ J_{n+1} &= J_n + \frac{K}{2\pi}\sin 2\pi\psi_n + \frac{b}{2\pi}\sin 2\pi\psi_n\cos\pi\theta_n, \\ \psi_{n+1} &= \psi_n + J_{n+1}. \end{aligned}$$

To illustrate the idea of the stochastic pump model, we let $K = 0.8, b = 0.005$, and start a particle on the KAM torus with golden mean winding number in the I, θ space, and in the separatrix surrounding the primary resonance in the (J, ψ) space. The relevant phase plane diagrams as shown in figures 5.6 and 5.7. The figures graphically display the notion of the chaotic motion of the particle in the separatrix in the (J, ψ) space affecting the motion of the particle in the (I, θ) space. Although $K = 0.8$ is not very small, and will not actually be used, we use it here to illustrate the idea of the stochastic pump model.

We notice that we could place the particle in the (J, ψ) space in a separatrix surrounding a resonance of higher order than the primary resonance: such separatrices are smaller than that surrounding the primary resonance, and the resultant Arnol'd diffusion is smaller as well. Here we only consider the Arnol'd diffusion produced by the particle being in the separatrix surrounding the primary resonance - the so-called thick layer diffusion.

The Hamiltonian for the coupled map is given by equation 5.1. In that Hamiltonian we have $(\theta, \psi, I, J) \in [0, 1)$ and here we transform these variables so that $(\theta, \psi, I, J) \in [0, 2\pi)$. Our Hamiltonian is thus

$$H = \frac{1}{2}I^2 + \frac{1}{2}J^2 + \left(\sum_{M=-\infty}^{\infty}\delta(t-M)\right)(K(\cos\theta + \cos\psi)) +$$

$$\left(\sum_{M=-\infty}^{\infty}\delta(t-M)\right)\left(b\cos\left(\frac{\theta+\psi}{2}\right) - b\cos\left(\frac{\theta-\psi}{2}\right)\right). \tag{5.8}$$

Now making the 'whopping big assumption' (as Lieberman describes it [14]) that we can approximate the Hamiltonian by assuming that the motion across the KAM torus in the (I, θ) space is driven by the chaotic motion of the orbit in the (J, ψ) space, by ignoring the coupling for H_j, and taking only a few terms in the decomposition of the δ function for H_j, we obtain

$$H \approx H_i + H_j,$$

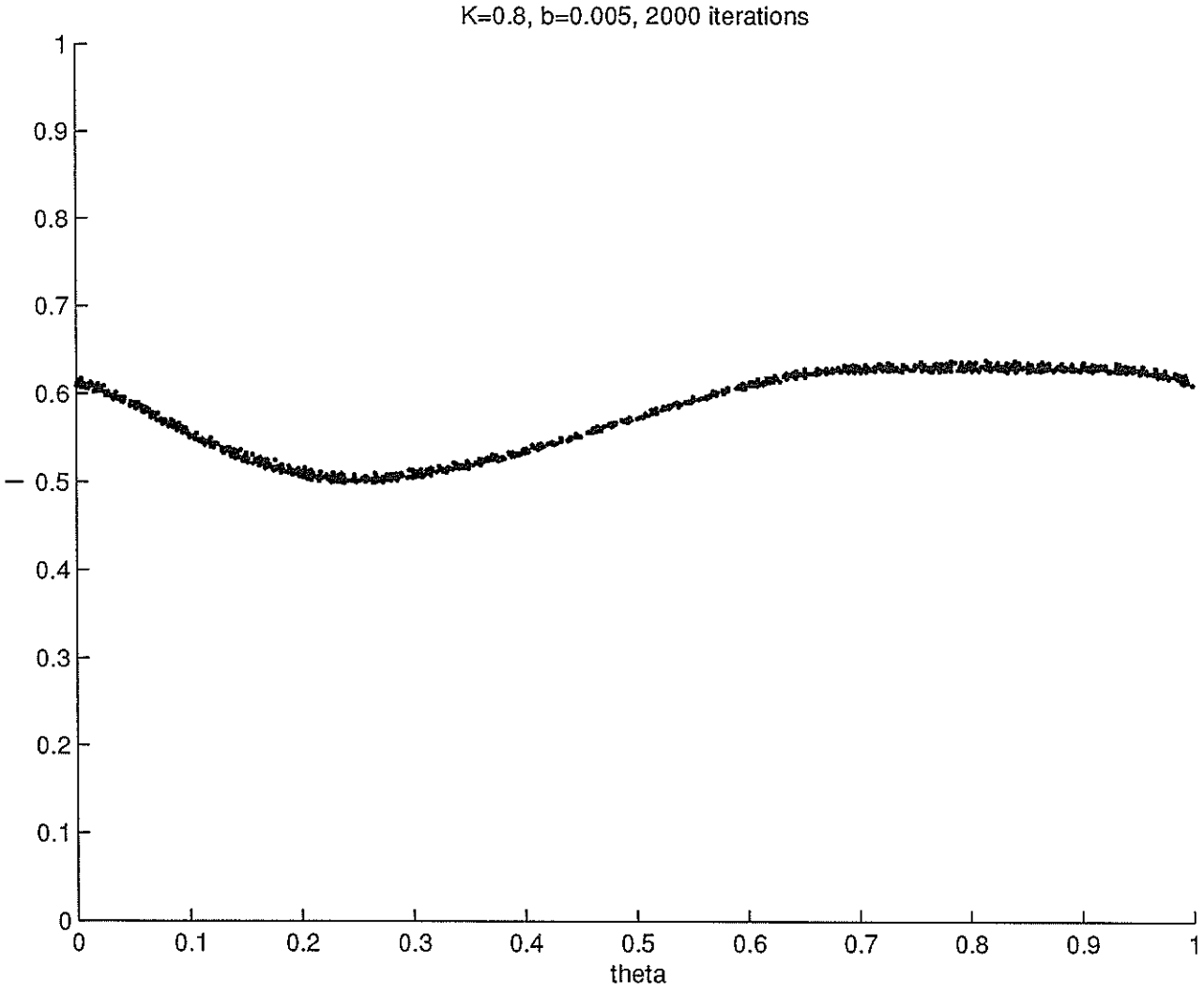

Figure 5.6: Stochastic Pump Model, particles on the KAM torus with golden mean winding number - (I, θ) space

where we note

$$\sum_{M=-\infty}^{\infty} \delta(t - M) = 1 + 2 \sum_{q=1}^{\infty} \cos 2\pi q n, \tag{5.9}$$

$$H_i = \frac{I^2}{2} + K \cos\theta - 2b \left(\cos\left(\frac{\theta - \psi}{2}\right) - \cos\left(\frac{\theta + \psi}{2}\right) \right), \tag{5.10}$$

$$H_j = \frac{J^2}{2} + K \cos\psi + 2K \cos 2\pi n \cos\psi. \tag{5.11}$$

The central part of this model is now considered: to calculate the kicks in I delivered by changes in the (J, ψ) co-ordinates of the orbit per iteration of the map

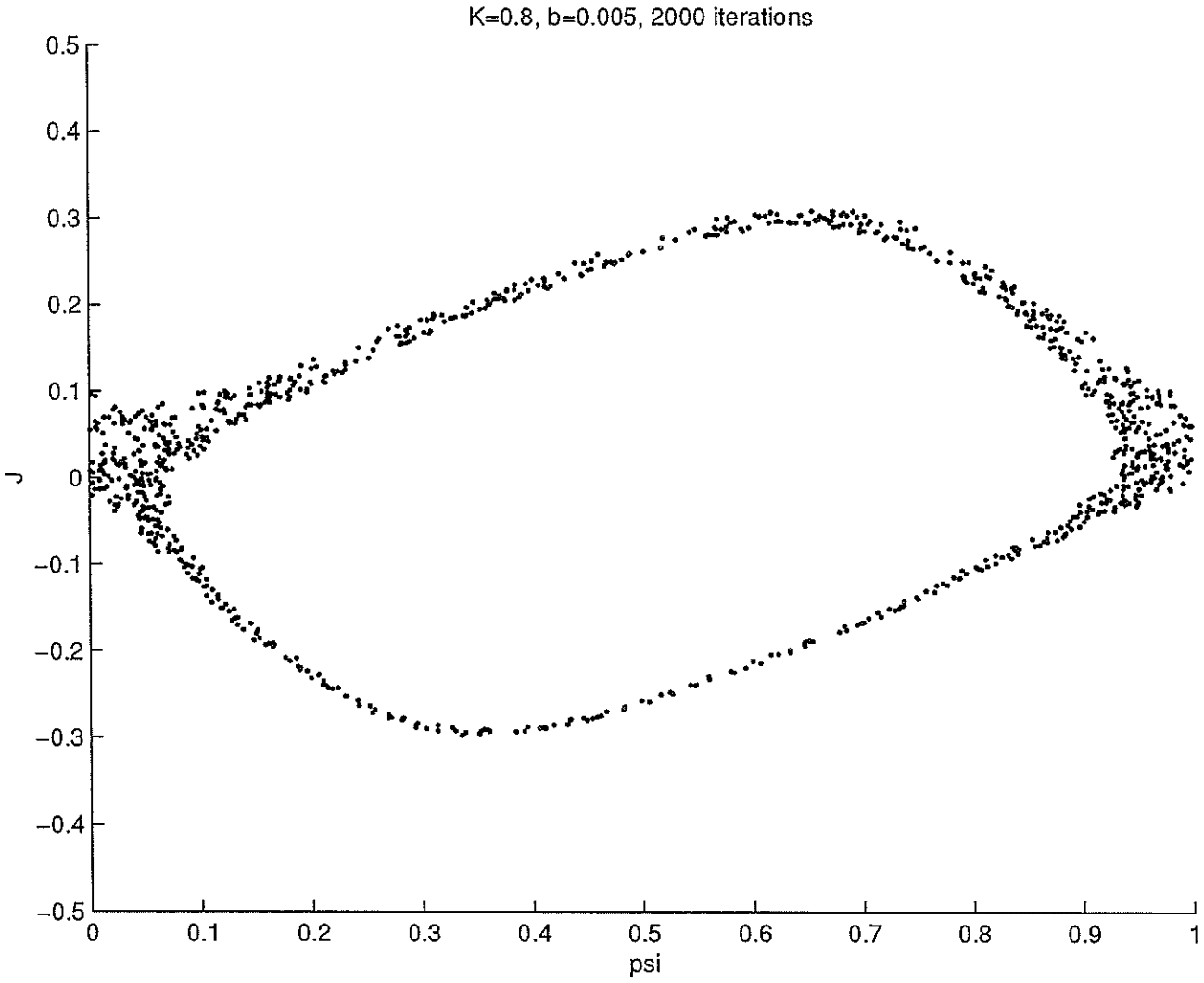

Figure 5.7: Stochastic Pump Model - the pump, (J, ψ) space

we take the derivative of H_i with respect to n

$$\frac{\partial H_i}{\partial n} = \frac{dH_i}{dn} = 2b\frac{d}{dn}\left(\cos\left(\frac{\theta-\psi}{2}\right) - \cos\left(\frac{\theta+\psi}{2}\right)\right) +$$

$$2b\frac{d\theta}{dn}\left(\sin\left(\frac{\theta+\psi}{2}\right) - \sin\left(\frac{\theta-\psi}{2}\right)\right). \tag{5.12}$$

The first part of the derivative contributes nothing over a long period of time so we do not consider it further. For motion on a KAM torus in the (I, θ) space we can assume

$$\theta = \omega_i n + \theta_0, \tag{5.13}$$

where ω_i is the frequency approximately equal to the action (I), and θ_0 is a phase.

We scale the 'time' variable to revolutions of the map: $s = \omega_j n$, and define Q_0

$$Q_0 = \frac{\omega_i}{\omega j} = \frac{\omega_i}{K^{1/2}}. \tag{5.14}$$

We now integrate equation 5.16 as follows

$$\Delta H_i = \int_{-\infty}^{\infty} \frac{dH_i}{dn}\frac{dn}{ds} ds, \tag{5.15}$$

$$= \int_{-\infty}^{\infty} 2b\frac{\omega_i}{\omega_j}\left(\sin\left(\frac{\theta - \psi(s)}{2}\right) - \sin\left(\frac{\theta + \psi(s)}{2}\right)\right) ds, \tag{5.16}$$

$$= 2bQ_0 \int_{-\infty}^{\infty} \left(\sin\left(\frac{\omega_i n + \theta_0 - \psi(s)}{2}\right) - \sin\left(\frac{\omega_i n + \theta_0 + \psi(s)}{2}\right)\right) ds, \tag{5.17}$$

where we note that

$$\psi(s) = 4\arctan(e^s) - \pi, \tag{5.18}$$

describes the motion of an orbit along the separatrix surrounding the primary resonance.

This leads to

$$\Delta H_i = 2bQ_0 \cos\frac{\theta_0}{2}\int_{-\infty}^{\infty} \sin\left(\frac{Q_0 s - \psi(s)}{2}\right) ds + 2bQ_0 \sin\frac{\theta_0}{2}\int_{-\infty}^{\infty} \cos\left(\frac{Q_0 s - \psi(s)}{2}\right) ds +$$

$$2bQ_0 \cos\frac{\theta_0}{2}\int_{-\infty}^{\infty} \sin\left(\frac{Q_0 s + \psi(s)}{2}\right) ds + 2bQ_0 \sin\frac{\theta_0}{2}\int_{-\infty}^{\infty} \cos\left(\frac{Q_0 s + \psi(s)}{2}\right) ds. \tag{5.19}$$

As $\psi(s)$ is an odd function, the first and third of these integrals integrate to zero. The remaining terms are Melnikov-Arnol'd integrals and their evaluation may be derived from Chirikov [2].

The second integral is evaluated to give

$$2bQ_0 \sin\frac{\theta_0}{2}\int_{-\infty}^{\infty} \cos\left(\frac{Q_0 s - \psi(s)}{2}\right) ds = 2bQ_0 \sin\frac{\theta_0}{2}\int_{-\infty}^{\infty} \cos\left(\frac{\psi(s) - Q_0 s}{2}\right) ds,$$

$$= 2bQ_0 \sin\frac{\theta_0}{2}\frac{2\pi e^{\frac{Q_0\pi}{4}}}{\sinh\frac{Q_0\pi}{2}}, \tag{5.20}$$

and the fourth integral may be evaluated to give

$$2bQ_0 \sin\frac{\theta_0}{2}\int_{-\infty}^{\infty} \cos\frac{(Q_0 s + \psi(s))}{2} ds = -2bQ_0 \sin\frac{\theta_0}{2}\frac{2\pi e^{\frac{-Q_0\pi}{4}}}{\sinh\frac{Q_0\pi}{2}}. \tag{5.21}$$

We thus have

$$\Delta H_i = bQ_0 4\pi \sin\frac{\theta_0}{2}\frac{\sinh\frac{Q_0\pi}{4}}{\sinh\frac{Q_0\pi}{2}}. \tag{5.22}$$

Squaring ΔH_i and averaging over θ_0 gives

$$\langle(\Delta H_i)^2\rangle = 8\pi^2 Q_0^2 b^2 \frac{(\sinh\frac{Q_0\pi}{4})^2}{(\sinh\frac{Q_0\pi}{2})^2}. \tag{5.23}$$

The above equation gives the change in H_i over one characteristic half period of the (J,ψ) map. We determine the diffusion coefficient D by dividing $\langle(\Delta H_i)^2\rangle$ by double the average number of iterations in this half period,

$$\mathrm{T}_j = \frac{1}{\omega_j}\ln\left|\frac{32e}{\omega_1}\right|, \tag{5.24}$$

where $\omega_1 = \Delta H/H_{separatrix}$ is the relative energy of the edge of the stochastic region,

$$\omega_1 = 8\pi\left(\frac{2\pi}{K^{1/2}}\right)^3 e^{-\pi^2/(K^{1/2})}. \tag{5.25}$$

Using $\Delta H_i = I\Delta I$, the diffusion distance in the action is

$$\Delta I_{rms} = \left(\langle(\Delta I)^2\rangle n\right)^{\frac{1}{2}} = \frac{(\langle(\Delta H_i)^2\rangle n)^{\frac{1}{2}}}{2\mathrm{T}_j I}, \tag{5.26}$$

$$= \frac{2\pi b K^{1/4} n^{1/2} Q_0 \sinh(\pi Q_0/4)}{I(\frac{3}{2}\ln K + (\pi^2/K^{1/2}) - 4.27)^{1/2}\sinh(\pi Q_0/2))}. \tag{5.27}$$

In Froschle's 4−dimensional map the corresponding diffusion distance in the action is

$$\Delta I_{rms} = \frac{4\pi\mu K_j^{1/4} n^{1/2} Q_0^2 \sinh(\pi Q_0/2)}{I(\frac{3}{2}\ln K_j + (\pi^2/K_j^{1/2}) - 4.27)^{1/2}\sinh\pi Q_0}, \tag{5.28}$$

and we immediately note that the essential difference between this diffusion distance and the diffusion distance in our map is that ours involves the term Q_0 while in Froschle's map equation 5.28 involves the term Q_0^2. Noting that

$$Q_0 = \frac{\omega_i}{K_j^{1/2}}, \tag{5.29}$$

where K_j in our map simply reduces to K, we have for $K \ll 1$,

$$K^{-1/2} \ll K^{-1}, \tag{5.30}$$

and thus, generally,

$$Q_0 < Q_0^2. \tag{5.31}$$

The rate of thick-layer diffusion in our map is much smaller than that in Froschle's map - the coupling term in our map is $b(\cos(\theta+\psi)/2 - \cos(\theta-\psi)/2)$, and the coupling term in Froschle's map is $b\sin(\theta+\psi)$. These differences are noticeable in figures 5.4 and 5.5 respectively. The symmetries present in our map appear to cause a dramatically lower rate of Arnol'd diffusion.

5.5 Numerical Exploration of the Stochastic Pump Model

We now turn our attention to a numerical exploration of thick-layer diffusion in our four dimensional map.

Following Wood, Lichtenberg and Lieberman [27] we started 100 orbits on the KAM torus with golden mean (γ) winding number in the (I,θ) space, and in the separatrix surrounding the primary resonance in the (J,ψ) space. The coupling between the co-ordinates in the (I,θ) and (J,ψ) spaces ensures that the chaotic motion of the particle in the separatrix in the (J,ψ) space affects its motion in the (I,θ) space. We place the particles in the (I,θ) space so that $\theta \in (0, 0.001 \times 2\pi]$.

Our interest is directed towards how 'far' in the action the 100 particles move under the iteration of the map. To examine this, we iterated the map for various values of K and b, and after each iteration of the map calculated the root mean square of the difference in the particles' action and γ.

We start this analysis with the coupling set to 0 and K small: $b = 0, K = 0.01$.

As we are only interested in the (I,θ) space the four dimensional map becomes the two dimensional standard map (scaling $I, \theta \in [0, 2\pi]$)

$$I_{n+1} = I_n + K\sin\theta_n \tag{5.32}$$

$$\theta_{n+1} = \theta_n + I_{n+1}, \pmod{2\pi} \tag{5.33}$$

Setting $\Gamma = 2\pi\gamma$, the first co-ordinates of the hundred points will be

$$I_0 = \Gamma, \tag{5.34}$$

$$\theta_0 = \epsilon, \tag{5.35}$$

where $\epsilon \in (0, 0.001 \times 2\pi]$. After the first iteration of the map we have

$$I_1 = \Gamma + K\sin\epsilon \approx \Gamma + K\epsilon, \tag{5.36}$$

$$\theta_1 = \epsilon + \Gamma + K\sin\epsilon \approx \epsilon + \Gamma + K\epsilon \pmod{2\pi}, \tag{5.37}$$

as ϵ, K are small, and $\sin v \approx v$ for v small ($v \ll 1$).

We note that after the first iteration of the map the maximum difference in action and $I_1 - \Gamma$ is

$$\sup\Delta I_1 = I_1 - \Gamma = K\epsilon \approx 6.28 \times 10^{-5} \tag{5.38}$$

and the particles spread out in the angle co-ordinate by a maximum of

$$\sup\Delta\theta_1 = K\epsilon \approx 6.28 \times 10^{-5} \tag{5.39}$$

We note from figure 5.8 that the root mean square of $I_1 - \Gamma$ for $K = 0.01, b = 0$, at the first iterate of the map appears to be approximately 7×10^{-5} which correlates to some extent with the above.

As $I_{n+1} = I_{n+1}(I_n, \theta_n)$, the spreading out of the particles in the angle co-ordinate θ_n will be fed non-linearly into I_{n+1}, and we expect I_{n+1}, θ_{n+1} to have a range of values for the 100 different particles after each iteration of the map.

After the 2nd iteration of the map

$$\begin{aligned}
I_2 &= \Gamma + K\epsilon + K\sin(\epsilon + \Gamma + K\epsilon), && (5.40)\\
\theta_2 &= 2\Gamma + 2K\epsilon + \epsilon + K\sin(\epsilon + \Gamma + K\epsilon), \quad (\mathrm{mod}\ 2\pi), && (5.41)\\
\Rightarrow I_2 &= \Gamma + K\epsilon + K(\sin(\epsilon + K\epsilon)\cos\Gamma + \sin\Gamma\cos(\epsilon + K\epsilon)) && (5.42)\\
I_2 &\approx \Gamma + K\epsilon + K\epsilon\cos\Gamma + K\sin\Gamma, && (5.43)\\
\theta_2 &\approx 2\Gamma + 2K\epsilon + \epsilon + K\epsilon\cos\Gamma + K\sin\Gamma. && (5.44)
\end{aligned}$$

Thus

$$I_2 - \Gamma = K\epsilon(1 + \cos\Gamma) + K\sin\Gamma \approx K\sin\Gamma \approx 6.75 \times 10^{-3}. \tag{5.45}$$

We can see that in the expression for $I_2 - \Gamma$ the term $K\sin\Gamma$ dominates.

The maximum spread in the action will be

$$\begin{aligned}
\sup\Delta I_2 &\approx K\epsilon(1 + \cos\Gamma), && (5.46)\\
\sup\Delta\theta_2 &\approx K\epsilon(2 + \cos\Gamma) + \epsilon. && (5.47)
\end{aligned}$$

It is evident that the terms I_{n+1}, θ_{n+1} quickly become complicated after only a few iterations of the map, even if we ignore very small terms.

The third iteration of the map yields

$$\begin{aligned}
I_3 &= \Gamma + K\epsilon + K\epsilon\cos\Gamma + K\sin(2\Gamma + 2K\epsilon + \epsilon + K\epsilon\cos\Gamma + K\sin\Gamma),\\
&= \Gamma + K\epsilon + K\epsilon\cos\Gamma + K\sin\Gamma + \sin(2\Gamma + K\epsilon\cos\Gamma + K\sin\Gamma)\cos(2K\epsilon + \epsilon)) +\\
&\quad K(\sin(2K\epsilon + \epsilon)\cos(2\Gamma + K\epsilon\cos\Gamma + K\sin\Gamma),\\
&\approx \Gamma + K\epsilon + K\epsilon\cos\Gamma + K\sin\Gamma + K\epsilon\cos(2\Gamma + K\epsilon\cos\Gamma + K\sin\Gamma) +\\
&\quad K\sin(2\Gamma + K\epsilon\cos\Gamma + K\sin\Gamma),
\end{aligned}$$

and

$$\theta_3 \approx 2\Gamma + 2K \sin \Gamma. \tag{5.48}$$

Thus

$$I_3 \approx \Gamma + K\epsilon + K \sin \Gamma + K \sin 2\Gamma, \tag{5.49}$$

and we can see that we can obtain a general linearised expression for $I_n - \Gamma$

$$I_n - \Gamma \approx \epsilon K + K(\sin \Gamma + \sin 2\Gamma + \sin 3\Gamma + \ldots + \sin n\Gamma). \tag{5.50}$$

Undertaking numerical calculations, we plot the root mean square of the distance in action from the golden mean KAM torus for $K = 0.01, b = 0.00$, with 20000 iterations in figure 5.8.

We also plot the maximum distance in the action from the golden mean for each of the first 2000 iterations for $K = 0.01, b = 0.00$ in figure 5.9.

Further iteration of the map (not shown here) reveals that the root mean square oscillates slowly around its value after 20000 iterations. We can interpret this bound on the root mean square as the trapping of the orbits by the KAM tori. We now introduce coupling into our calculations, setting $b = 0.001 = K/10$, and plotting the data in figure 5.10. It appears that the introduction of small but not insignificant coupling acts as a perturbation to the original system - the general shape of the plot remains similar, but we note that the orbits appear to move farther in the action after fewer iterations, than with no coupling. With no coupling the distance moved is at a peak after $\approx 1.2 \times 10^4$ iterations at a value of $\approx 1.2 \times 10^{-3}$. With $b = 0.001$, the distance moved has a peak after 0.6×10^4 iterations with a value of $\approx 1.5 \times 10^{-3}$.

We have applied the algorithm for $K = 0.01, b = 0.0015$, and the results are shown in figure 5.11.

Repeating the algorithm for $K = 0.01, b = 0.002$ in figure 5.12, we note that doubling the strength of b from figure 5.10 has somewhat increased its perturbing effect.

We can see in figure 5.13 that setting the coupling to half the value of the stochasticity parameter: $b = 0.005, K = 0.01$, appears to cause significant change in the behaviour of trajectories. They appear to move much farther much sooner than previously.

We can conclude from these figures that small coupling acts like a perturbation on the case with no coupling - the overall 'shape' of the plot is maintained. However, when the size of the coupling is of the order of the stochasticity parameter, then something very different occurs, and this change requires further investigation.

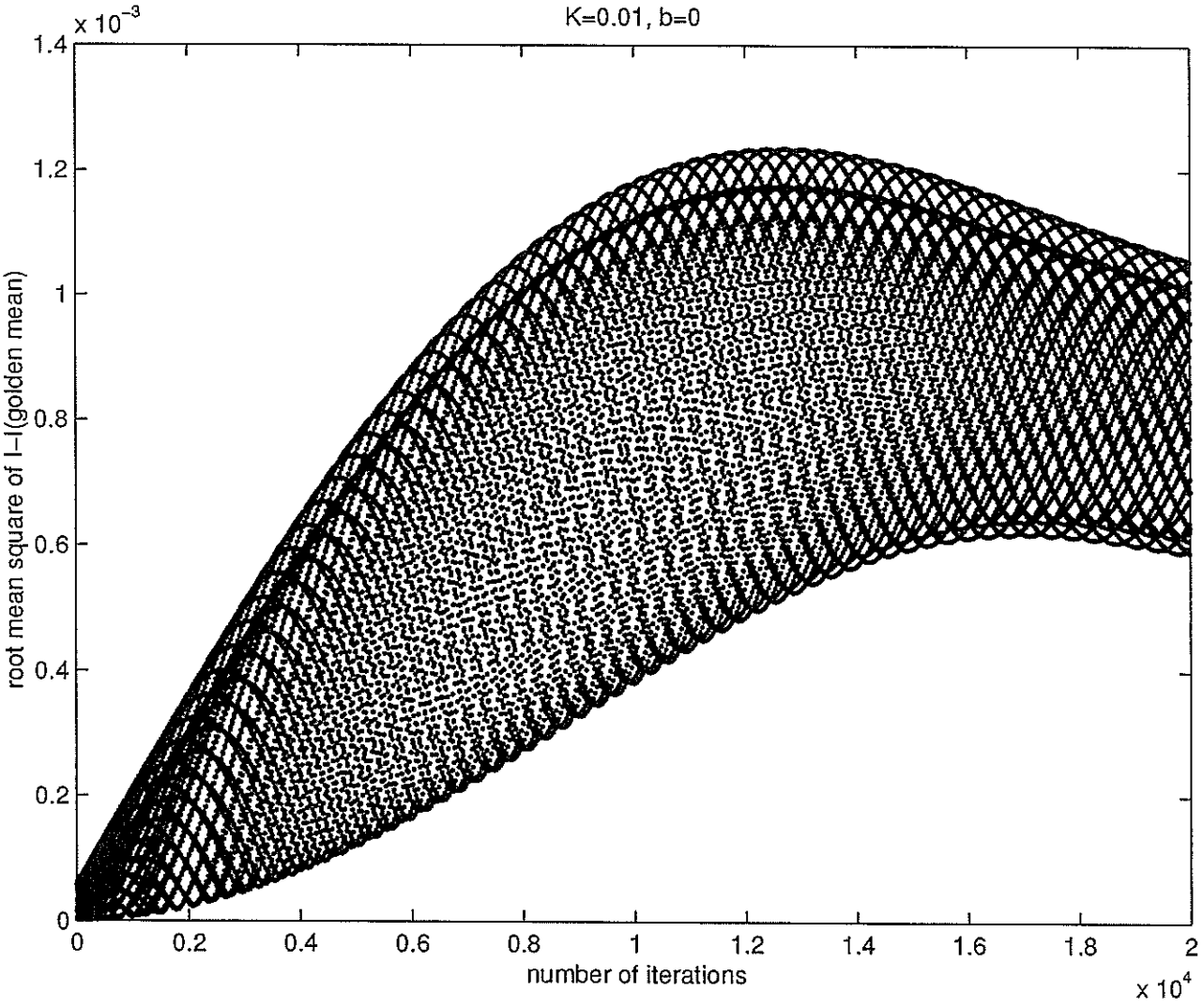

Figure 5.8: Root mean square of the distance in action from the initial action for 100 particles for $K = 0.01, b = 0.00, 20000$ iterations

We now display the results of setting $K = 0.00$, $b = 0.001$ in figure 5.14. In this case our map becomes

$$I_{n+1} = I_n + b \sin\frac{\theta_n}{2}\cos\frac{\psi_n}{2}, \tag{5.51}$$

$$\theta_{n+1} = \theta_n + I_{n+1}, \tag{5.52}$$

$$J_{n+1} = J_n + b \sin\frac{\psi_n}{2}\cos\frac{\theta_n}{2}, \tag{5.53}$$

$$\psi_{n+1} = \psi_n + J_{n+1}. \tag{5.54}$$

Our initial values are

$\theta_0 = \epsilon$,

$I_0 = 2\pi\gamma = \Gamma$,

$\psi_0 \approx \pi$,

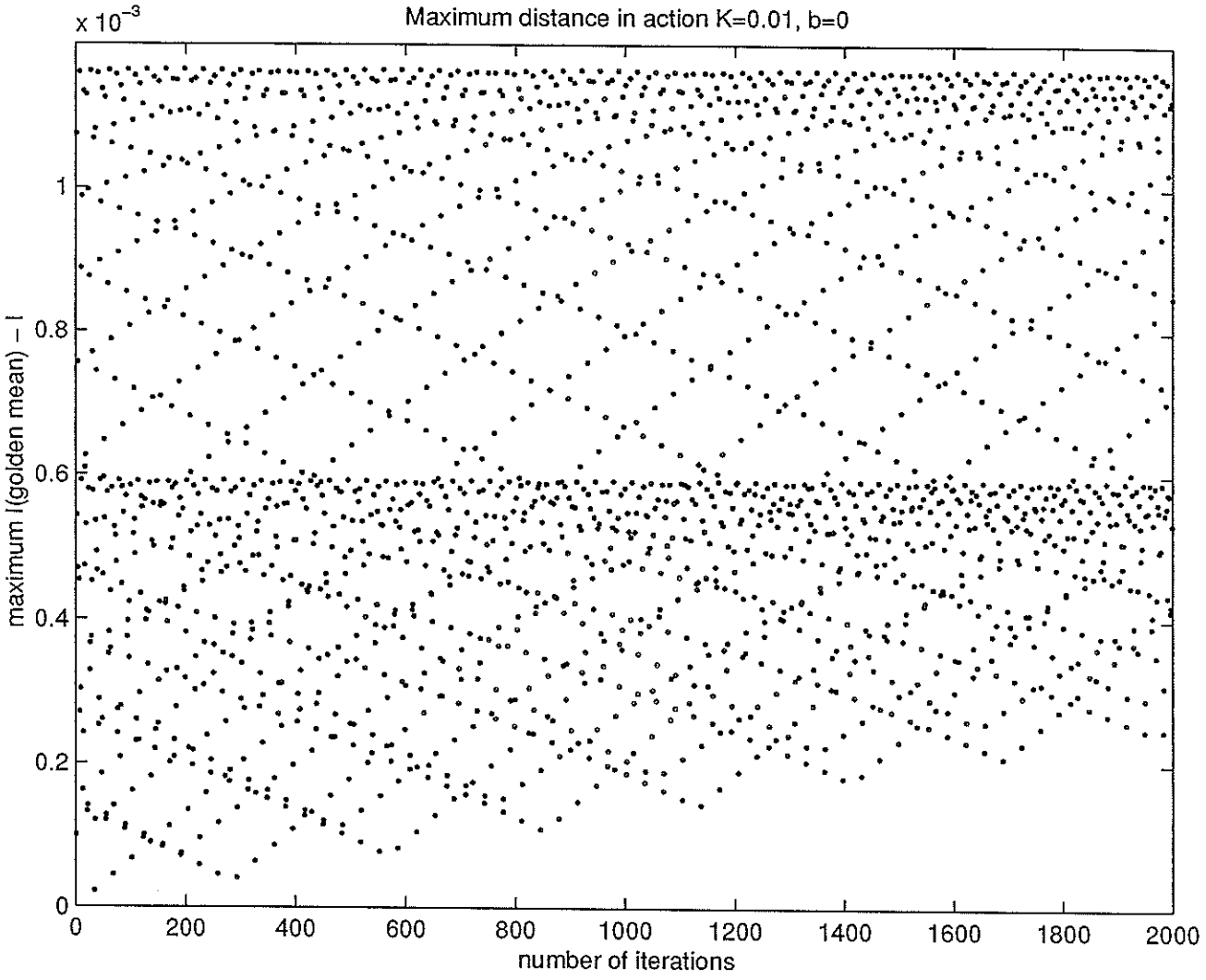

Figure 5.9: Maximum distance in the action from the golden mean KAM torus, 2000 iterations

$J_0 \approx 0$.

After one iteration of the map we obtain

$\theta_1 = \epsilon + \Gamma$,

$I_1 = \Gamma$,

$\psi_1 = \pi + b$,

$J_1 = b$.

After the second iteration of the map we obtain

$\theta_2 = \epsilon + 2\Gamma$,

$I_2 = \Gamma + b \sin\left(\frac{\Gamma+\epsilon}{2}\right) \cos\left(\frac{\pi+b}{2}\right) \approx \Gamma$,

$\psi_2 = \pi + 2b + b \cos\left(\frac{\epsilon+\Gamma}{2}\right) \approx \pi + 2b + b\left(\cos\frac{\Gamma}{2} - \sin\frac{\Gamma}{2}\right)$,

$J_2 = b + b \cos\left(\frac{\epsilon+\Gamma}{2}\right) = b + b\left(\cos\frac{\Gamma}{2} - \sin\frac{\Gamma}{2}\right)$.

It is apparent that something very different is occuring in figure 5.14. From the

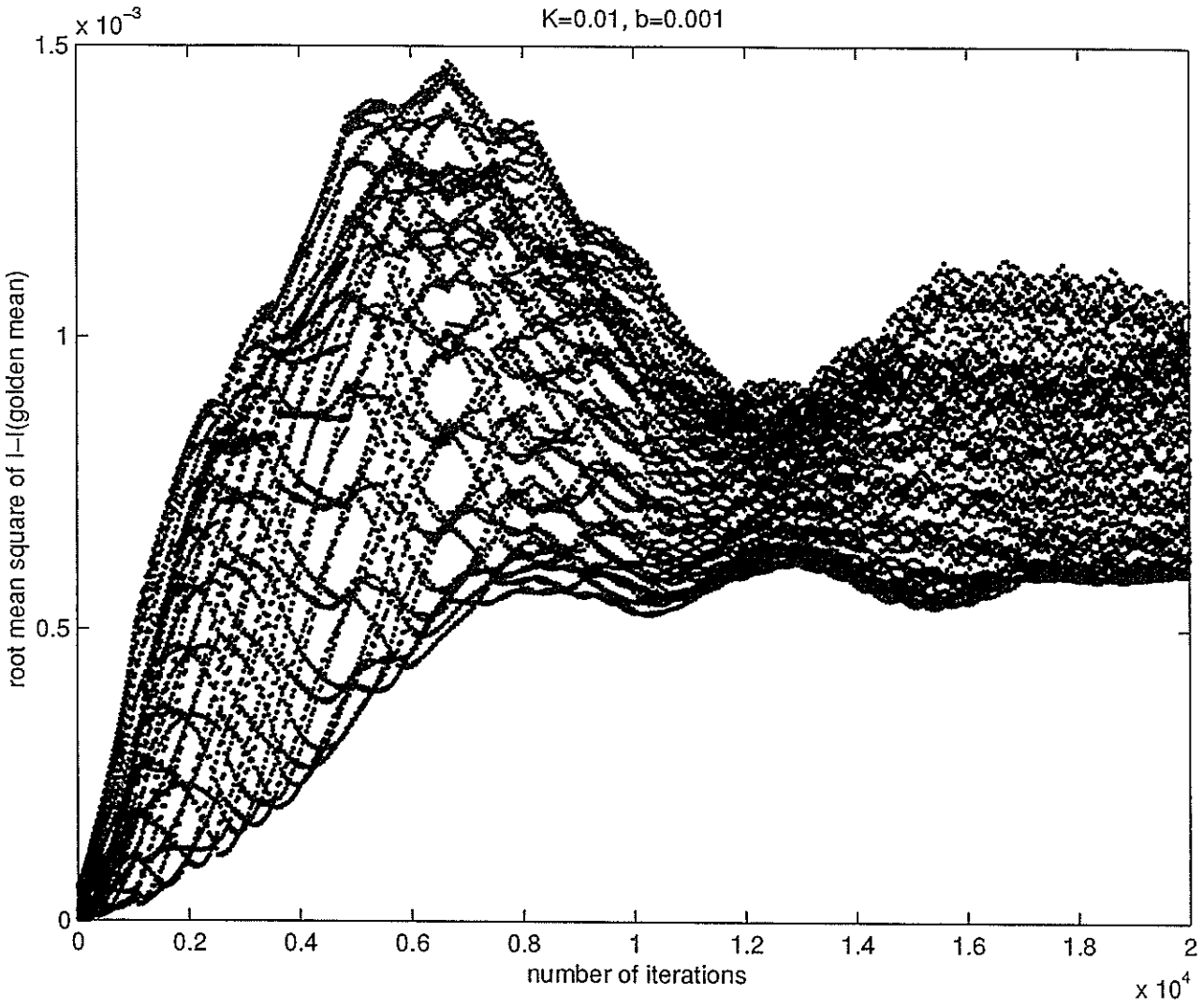

Figure 5.10: Root mean square of the distance in action from the initial action for 100 particles for $K = 0.01, b = 0.001, 20000$ iterations

above analytic investigations of the first few iterations of the four dimensional map, we can see that $I = \Gamma$ for a while, until the pertubations tend to take over and our approximation is inaccurate. From the plot we can see that $I = \Gamma$ for approximately 100 iterations of the map.

In figure 5.15 we show the same figure as in 5.14 but we undertook 20000 iterations of the map.

For interest we plot in figure 5.16 the maximum distance in the action from the golden mean KAM torus for figure In this subsection we have outlined numerical investigations of the stochastic pump model and have conducted some preliminary analytic and numerical calculations concerning the same. This model has been used by many researchers to numerically investigate Arnol'd diffusion.

From the numerics, it appears that introducing small coupling does not (in the

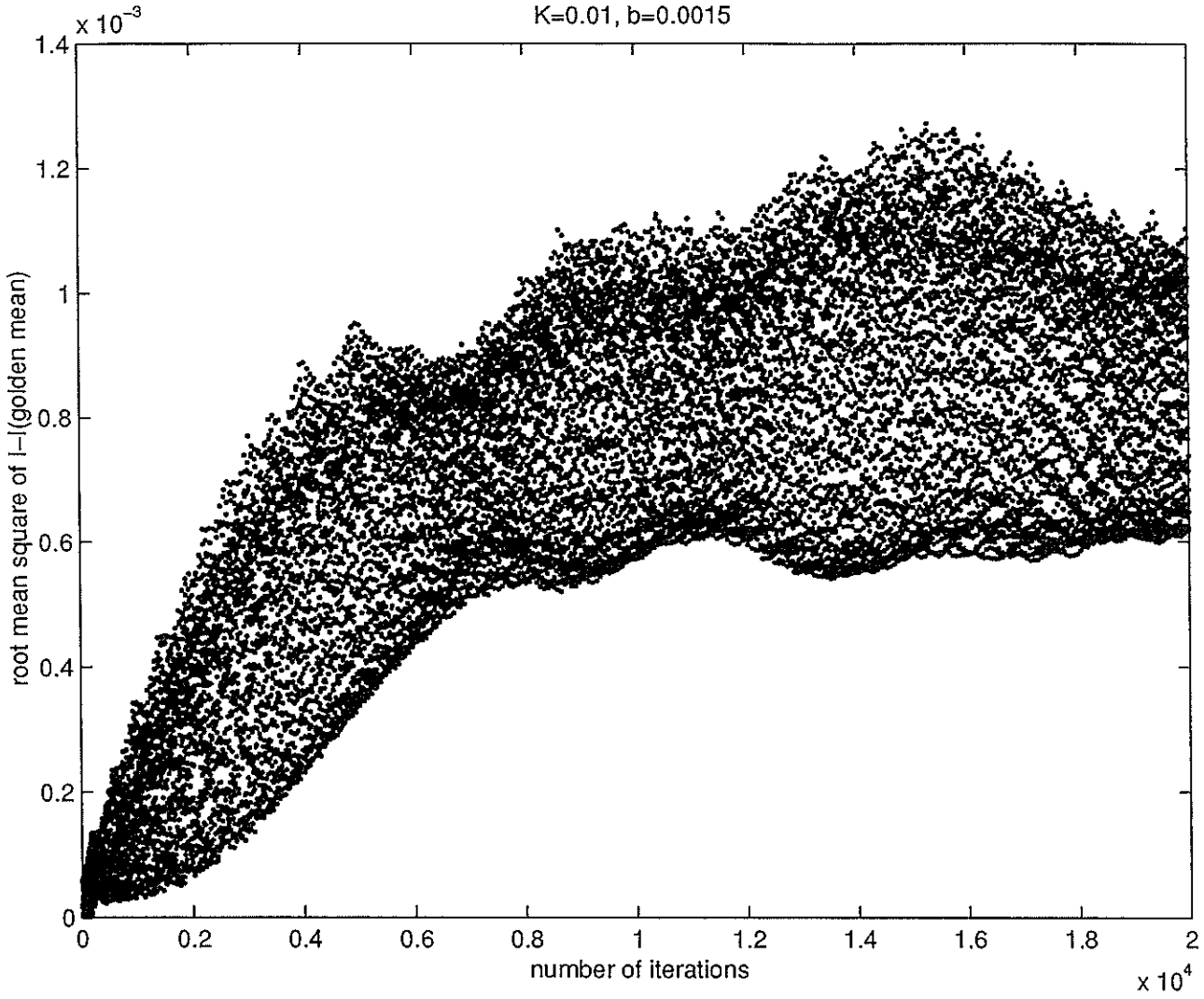

Figure 5.11: Root mean square of the distance in action from the initial action for 100 particles for $K = 0.01, b = 0.0015, 20000$ iterations

short term) dramatically alter the behaviour of trajectories in the system.

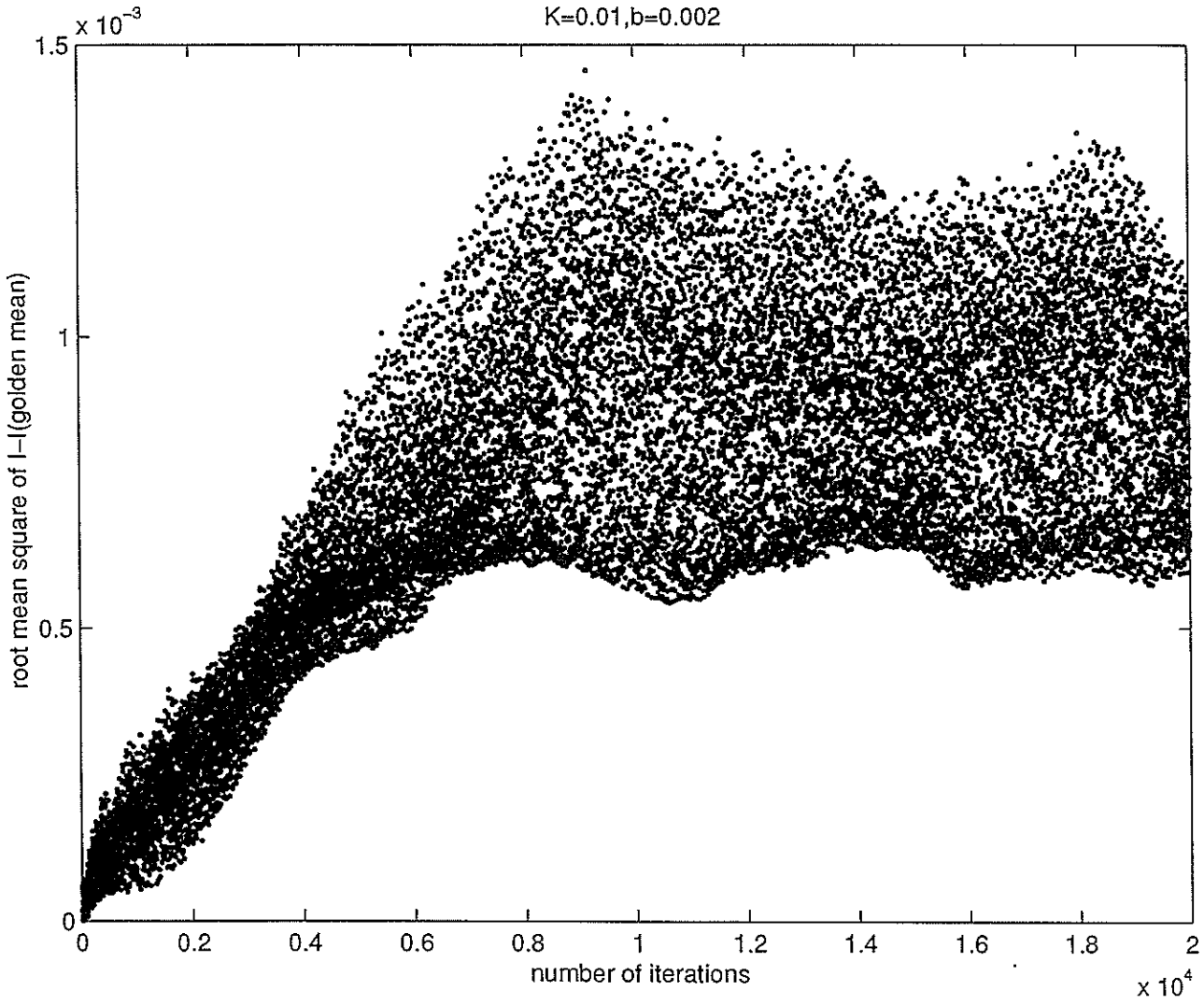

Figure 5.12: Root mean square of the distance in action from the initial action for 100 particles for $K = 0.01, b = 0.002, 20000$ iterations

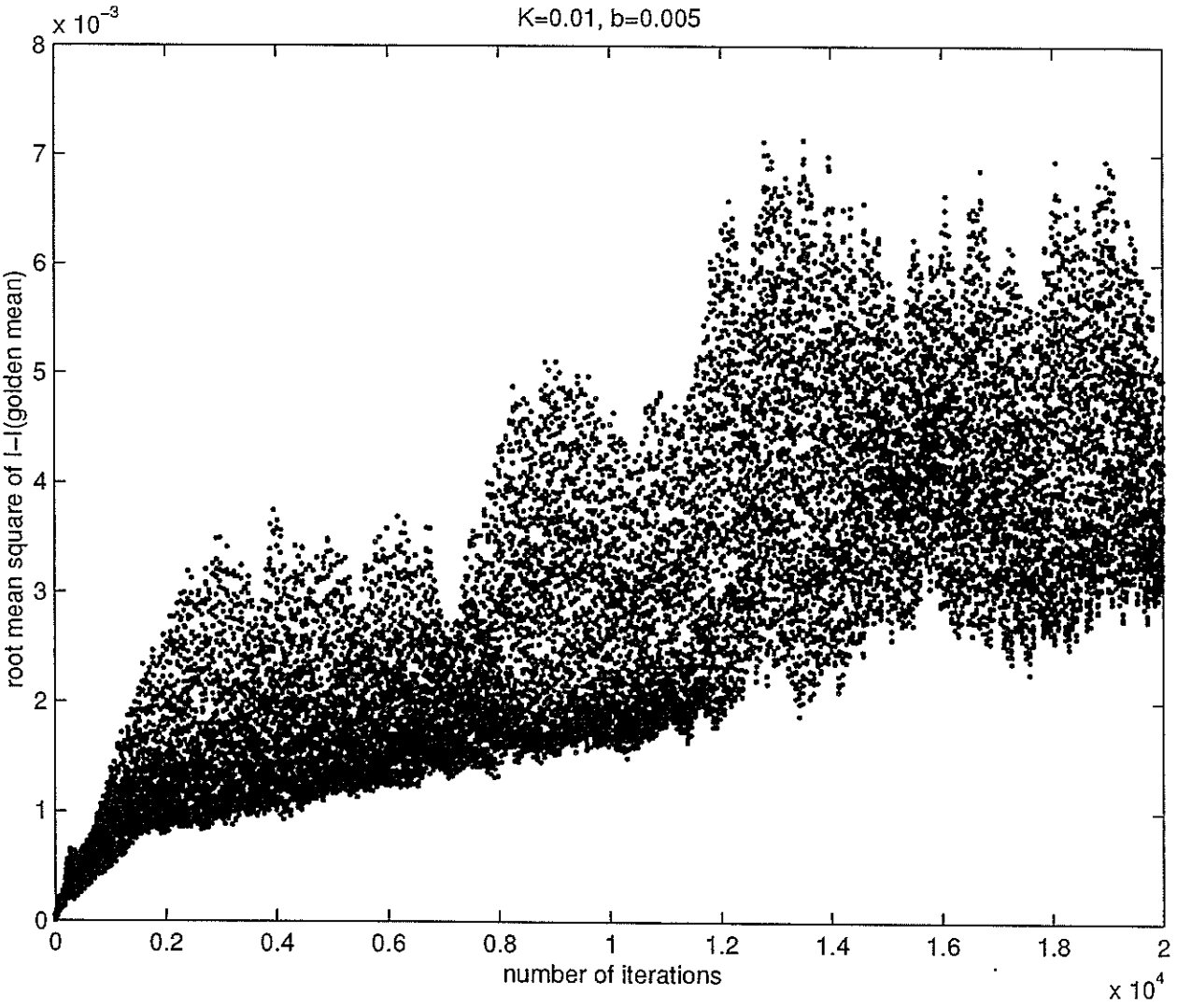

Figure 5.13: Root mean square of the distance in action from the initial action for 100 particles for $K = 0.01, b = 0.005, 20000$ iterations

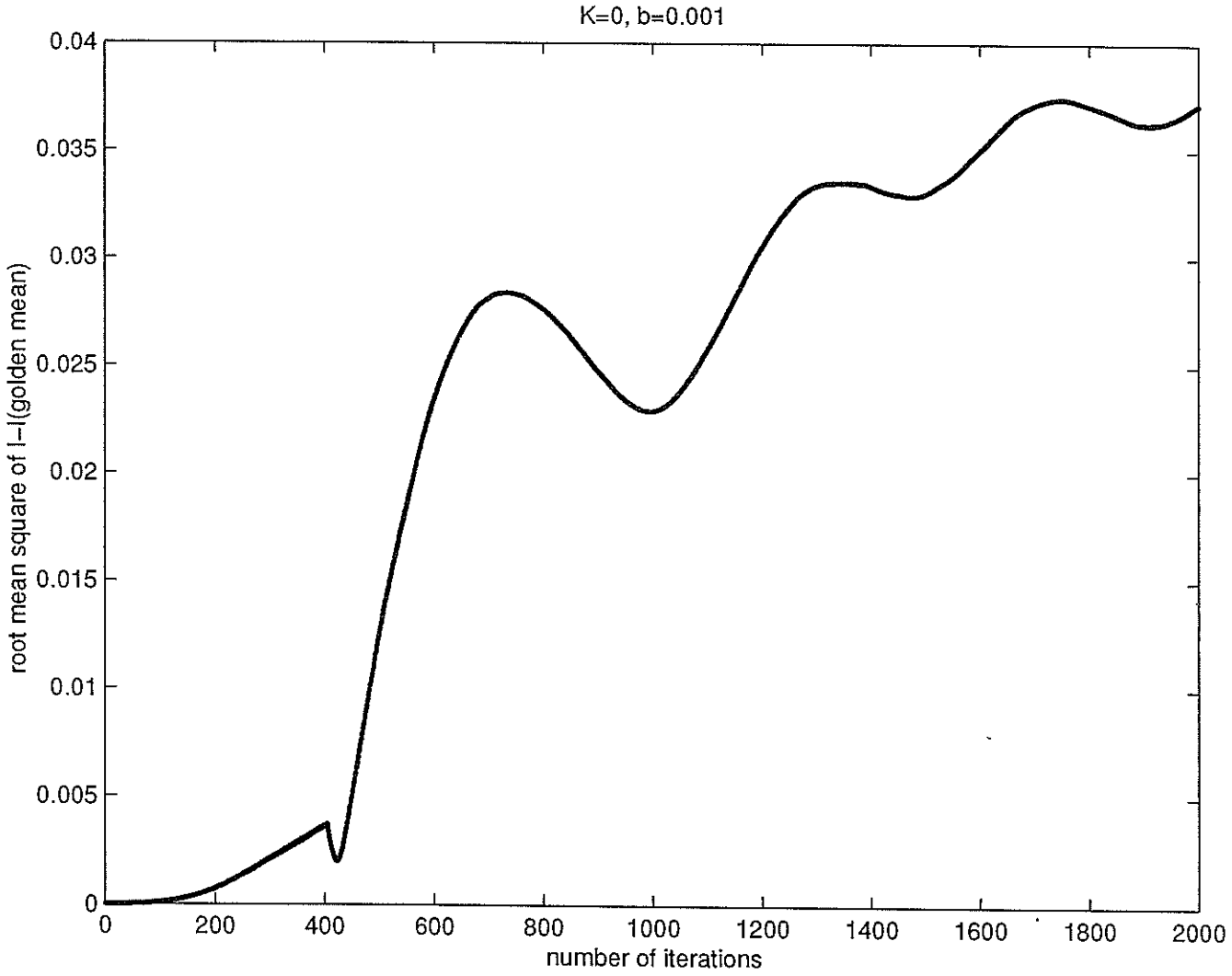

Figure 5.14: Root mean square, K=0, b=0.001

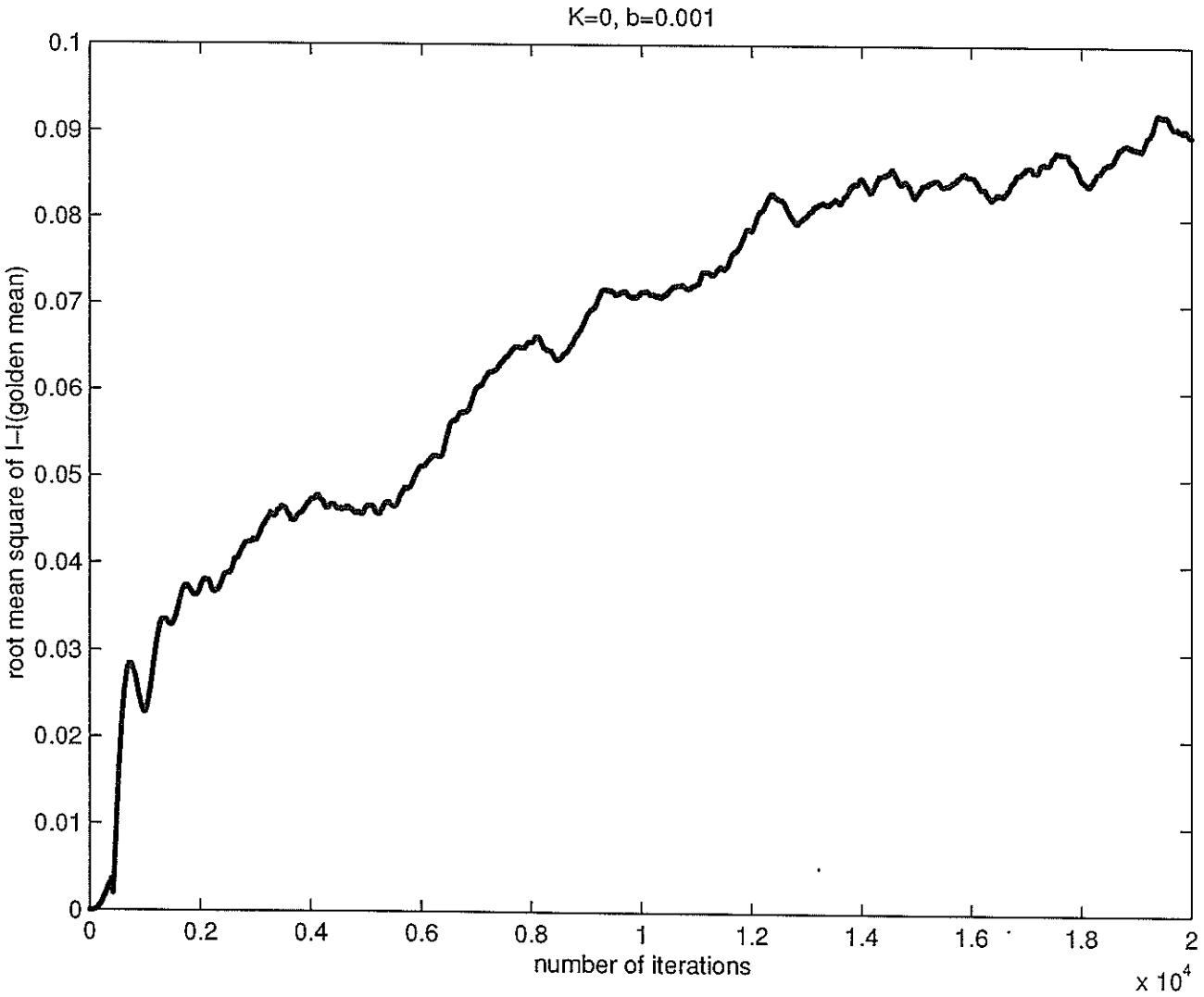

Figure 5.15: Root mean square, K=0, b=0.001

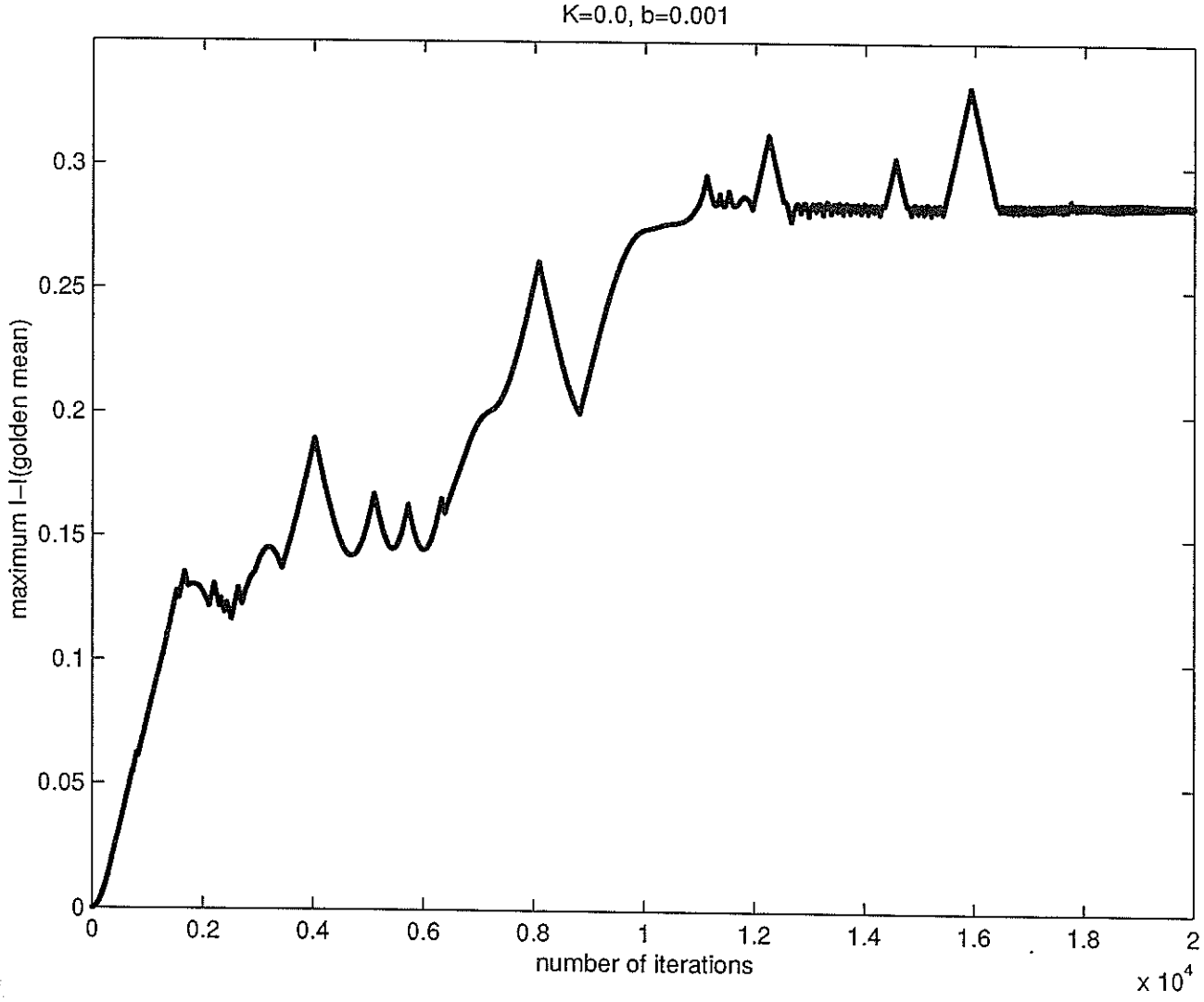

Figure 5.16: Maximum distance in the action from the KAM torus with golden mean winding number, K=0, b=0.001

Chapter 6

Conclusion

In this thesis we have been concerned with the Hamiltonian formulation of dynamics and chaos. After reviewing the relevant theory on Hamiltonian dynamics, we introduced the standard map and the KAM theorem, both of which are essential to the study of a two degree of freedom coupled map we introduce to model the interaction of atoms with a laser in a magneto-optical trap. We examined the rates of transport of orbits through our coupled standard map, and then examined a particular form of transport: Arnol'd diffusion. We analytically showed that the rate of transport resulting from the Arnol'd diffusion is less significant in our map than in other coupled maps that have been considered [26, 27].

We have shown that in our map an approximate power law relationship holds between the rate of transport of collections of orbits through the phase space and the value of the stochasticity and coupling parameters. We also find that the rate of Arnol'd diffusion is less significant than other forms of transport.

The work in this thesis leads to several questions, which could be investigated in the future:

(i) When is the last KAM torus destroyed for various values of K and b?

(ii) What is the detailed behaviour of orbits in our four dimensional map?

(iii) How does the coupled map behave as the value of the coupling parameter approaches the value of the stochasticity parameter?

This thesis, has, perhaps, contributed in some small way, to the general understanding of chaos in Hamiltonian dynamical systems and the the role of Arnol'd diffusion in many degrees of freedom Hamiltonian dynamical systems.

Bibliography

[1] V.I. Arnol'd, ed. *Dynamical Systems V.* Encyclopaedia of Mathematical Sciences, Volume 5, Springer-Verlag, New York, 1991.

[2] B.V. Chirikov. *A Universal Instability of Many-Dimensional Oscillator Systems.* Physical Reports, Volume 52, p. 265-379, 1979.

[3] R.L. Dewar, and J.D. Meiss. *Flux-Minimizing Curves for Reversible Area-Preserving Maps.* Physica D, Volume 57, p. 476-506, 1992.

[4] C. Froschle. *Numerical Study of a Four-Dimensional Mapping.* Astron. and Astrophysics, Volume 16, p. 172-189, 1972.

[5] C. Froschle and J.P. Scheidecker. *Numerical Study of a Four-Dimensional Mapping II.* Astron. and Astrophysics, Volume 22, p. 431-436, 1973.

[6] P. Glendinning. *Stability, Instability and Chaos.* Cambridge University, U.K., 1994.

[7] H. Goldstein. *Classical Mechanics.* Addison-Wesley, Massachusetts, 1950.

[8] K. Kaneko, and R.J. Bagley. *Arnol'd Diffusion, Ergodicity and Intermittency in a Coupled Standard Mapping.* Physics Letters, Volume 110A, no. 9, p. 435-440, 1985.

[9] S. Kim, and S. Ostlund. *Simultaneous Rational Approximations in the Study of Dynamical Systems.* Physical Review A, Volume 34, no. 4, p.3426-3434, 1986.

[10] A.N. Kolmogorov. *Preservation of Conditional Periodic Movements with Small Change in the Hamilton Function,* in H. Bai-Lin, ed., *Chaos II.* World Scientific, Singapore, 1990.

[11] A.R. Kolovsky. *Number of Degrees of Freedom for a Thermostat.* Physical Review E, Volume 50, p. 3569-3576, 1994.

[12] H. Kook, and J.D. Meiss. *Periodic Orbits for Symplectic maps.* Physica D, Volume 35, p. 65-86, 1989.

[13] A.J. Lichtenberg and M.A. Lieberman. *Regular and Chaotic Dynamics.* 2nd edition, Springer-Verlag, New York, 1992.

[14] M.A. Lieberman. *Arnold Diffusion in Hamiltonian Systems with Three Degrees of Freedom.* in *Nonlinear Dynamics.*, Ed. R.H.G. Helleman, p. 119-142, New York Academy of Sciences, New York, 1980.

[15] E.N. Lorenz. *Deterministic Nonperiodic Flow,* in H. Bai-Lin, ed., *Chaos II.* World Scientific, Singapore, 1990.

[16] R.S. Mackay. *A Criterion for Non-existence of Invariant Tori for Hamiltonian Systems.* Physica D, Volume 36, p 64-82, 1989.

[17] J.D. Meiss. *Symplectic Maps, Variational Principles, and Transport.* Reviews of Modern Physics, Volume 64, no. 3, p. 795-848.

[18] G.J. Milburn. *Quantum Technology.* Allen and Unwin, Sydney, 1996.

[19] Non-Linear Analysis (MP479) Lecture Notes. University of Queensland, 1st Semester, 1997.

[20] S.N. Rasband. *Chaotic Dynamics of Nonlinear Systems.* Wiley, New York, 1990.

[21] L.E. Reichl. *The Transition to Chaos, In Conservative Classical Systems: Quantum Manifestations.* Springer-Verlag, New York, 1992.

[22] V. Robins. *Periodic Orbits and Invariant Tori in Symplectic Maps.* Honours Thesis, Australian National University, 1994.

[23] E.H. Rothe. *Introduction to Various Aspects of Degree Theory in Banach Spaces.* American Mathematical Society, Rhode Island, 1986.

[24] D. Ruelle. *Elements of Differentiable Dynamics and Bifurcation Theory.* Academic Press, London, 1989.

[25] A.J. Scott. *Chaos in a 2D Dissipative Map.* Honours Thesis, University of Queensland, 1997.

[26] G.R. Wang, B. Hu, and S.G. Chen. *Arnold Diffusion in a Four-Dimensional Standard Map.* Physics Letters A, Volume 151, no. 1,2, p. 37-42, 1990.

[27] B.P. Wood, A.J. Lichtenberg, and M. A Lieberman. *Arnold Diffusion in Weakly Coupled Standard Maps.* Physical Review A, Volume 42, no. 10, p. 5885-5893, 1990.

[28] G.M. Zaslavsky, R.Z. Sagdeev, D.A Usikov, and A.A. Chrenikov. *Weak Chaos and Quasi-Regular Patterns.* Cambridge University, 1991.